GDSA Repository Systems Analysis Progress Report

Fuel Cycle Research & Development

S. David Sevougian

Emily R. Stein, Tara LaForce,
Frank V. Perry, Thomas S. Lowry,
Leigh Cunningham, Michael Nole,
Charles B. Haukwa, Kyung W. Chang,
and Paul E. Mariner

Sandia National Laboratories
April 30, 2019

Sandia National Laboratories

This is a technical report that does not take into account the contractual limitations under the Standard Contract for Disposal of Spent Nuclear Fuel and/or High-Level Radioactive Waste (Standard Contract) (10 CFR Part 961). For example, under the provisions of the Standard Contract, DOE does not consider spent nuclear fuel in multi-assembly canisters to be an acceptable waste form, absent a mutually agreed to contract amendment. To the extent discussions or recommendations in this presentation conflict with the provisions of the Standard Contract, the Standard Contract provisions prevail.

APPENDIX E
NTRD DOCUMENT COVER SHEET[1]

Name/Title of Deliverable/ Milestone/Revision No.	*GDSA Repository Systems Analysis Progress Report*, M2SF-19SN010304051
Work Package Title & Number	GDSA – Repository Systems Analysis – SNL, SF-19SN01030405
Work Package WBS Number	1.08.01.03.04
Responsible Work Package Manager	S. David Sevougian _S. David Sevougian_
	(Name/Signature)
Date Submitted	April 30, 2019

Quality Rigor Level for Deliverable/Milestone[2]	☐ QRL-1 ☐ Nuclear Data	☐ QRL-2	☒ QRL-3	☐ QRL-4 Lab QA Program[3]

This deliverable was prepared in accordance with   Sandia National Laboratories

(Participant/National Laboratory Name)

QA program which meets the requirements of

    ☒ DOE Order 414.1   ☐ NQA-1   ☐ Other

This Deliverable was subjected to:

☒ Technical Review   ☐ Peer Review

Technical Review (TR)	**Peer Review (PR)**
Review Documentation Provided	**Review Documentation Provided**
☐ Signed TR Report or,	☐ Signed PR Report or,
☐ Signed TR Concurrence Sheet or,	☐ Signed PR Concurrence Sheet or,
☐ Signature of TR Reviewer(s) below	☐ Signature of PR Reviewer(s) below
Name and Signature of Reviewers	
Robert J. MacKinnon	
Robert J. MacKinnon _____	_____
_____	_____

NOTE 1: *Appendix E should be filled out and submitted with the deliverable. Or, if the PICS:NE system permits, completely enter all applicable information in the PICS:NE Deliverable Form. The requirement is to ensure that all applicable information is entered either in the PICS:NE system or by using the NTRD Document Cover Sheet.*

- *In some cases there may be a milestone where an item is being fabricated, maintenance is being performed on a facility, or a document is being issued through a formal document control process where it specifically calls out a formal review of the document. In these cases, documentation (e.g., inspection report, maintenance request, work planning package documentation or the documented review of the issued document through the document control process) of the completion of the activity, along with the Document Cover Sheet, is sufficient to demonstrate achieving the milestone.*

NOTE 2: *If QRL 1, 2, or 3 is not assigned, then the QRL 4 box must be checked, and the work is understood to be performed using laboratory QA requirements. This includes any deliverable developed in conformance with the respective National Laboratory / Participant, DOE or NNSA-approved QA Program.*

NOTE 3: *If the lab has an NQA-1 program and the work to be conducted requires an NQA-1 program, then the QRL-1 box must be checked in the work Package and on the Appendix E cover sheet and the work must be performed in accordance with the Lab's NQA-1 program. The QRL-4 box should not be checked.*

ACKNOWLEDGEMENTS

EXECUTIVE SUMMARY

The Spent Fuel and Waste Science and Technology (SFWST) Campaign of the U.S. Department of Energy Office of Nuclear Energy, Office of Spent Fuel and Waste Disposition (SFWD), has been conducting research and development on generic deep geologic disposal systems (i.e., geologic repositories). This report describes specific activities in fiscal year (FY) 2019 associated with FY19 Geologic Disposal Safety Assessment (GDSA) Repository Systems Analysis (RSA) work package within the SFWST Campaign. The overall objective of the GDSA RSA work package is to develop generic deep geologic repository concepts and system performance assessment (PA) models in several host-rock environments, and to simulate and analyze these generic repository concepts and models using the *GDSA Framework* toolkit, and other tools as needed. The specific objectives in FY2019 are to

- Develop and/or augment generic repository reference cases for three liquid-saturated host rock environments: crystalline (e.g., granite), argillaceous (e.g., typical shale or clay), and bedded salt host rocks; and a host rock environment in the unsaturated zone, such as alluvial valley fill.

- Ensure that reference cases include repository concepts and layouts for the disposal of DPC-canisterized pressurized water reactor (PWR) assemblies, including 37-PWR and 24-PWR waste packages, including the possible effects of criticality events on repository performance.

- Perform PA simulations (deterministic and probabilistic) with *GDSA Framework* for the foregoing reference case concepts and models. Analyze and plot the PA simulation results, including uncertainty and sensitivity analyses.

This report describes specific GDSA RSA accomplishments midway through FY 2019, with more comprehensive reference-case updates and PA simulation results to be reported at the end of the FY in a subsequent Level 3 milestone M3SF-19SN010304052, *GDSA Repository Systems Analysis FY19 Update*.

Section 1 of this deliverable is a brief introduction. Section discusses the relationship of reference case models to the overall generic safety case(s). Section 3 discusses improvements to the numerical solvers in PFLOTRAN, needed for modeling the high heat output from dual purpose canister (DPC) waste packages, particularly during two-phase flow, such as might occur in an unsaturated host-rock environment. Multiphase (liquid and gas) flow and transport capabilities in PFLOTRAN (under the "General" flow mode) have been augmented to more efficiently simulate physically complex processes that could occur in unsaturated repositories and/or under conditions of extreme waste package heat production (as could be the case with a 37 PWR configuration). The most significant of these changes involved refactoring of convergence criteria used during each iteration of the Newton-Raphson nonlinear solution search algorithm.

Section 4 develops a technical basis and conceptual model for a reference case repository located in unsaturated alluvial sediments, including initial simulations for a small-scale "sector" model (four disposal drifts each with four waste packages), as well as a "field-scale" repository model (27 drifts with 24 waste packages each). This section presents an update of the unsaturated zone alluvium reference case introduced in Mariner et al. (2018), primarily related to the inclusion of DPC waste packages and their representative higher heat output per package, which results in more severe coupled process effects at early times after repository closure. Preliminary results indicate

that even using a more coarsely discretized numerical grid with simplified two-phase flow parameters, computation time for flow and temperature in the field-scale simulation remains prohibitively long, perhaps due to numerical difficulties of the coupled thermal and fluid flow problem in unsaturated rock. Several avenues will be explored during the remainder of the FY to investigate the long numerical simulation times:

- Have the development team assess whether any changes can be made to GENERAL mode to speed up simulations

- Divide the simulation workflow up into two separate <u>areal-cale</u> simulation models. In this concept:
  - The first model will be a finely gridded domain focusing on the smaller scale ("sector"), and will accurately capture heat, flow, and radionuclide transport near the waste packages. This model would not address issues of far-field flow and transport of radionuclides.
  - The second model will have a relatively coarse and uniform mesh covering the full domain of interest for radionuclide transport. It will be used to assess transport in the subsurface but cannot accurately capture heat and fluid flow in and around the waste packages. Heat and fluid behavior near the repository would have to be checked to be sure that the coarse model captures the same essential features as the fine scale model.

- Divide the simulation workflow up into two separate <u>time-scale</u> simulation models. In this concept the two modeling stages would be on the same mesh, the extent and discretization of which would be suitable for modeling both near repository heat and fluid flow and far field transport of radionuclides. In this concept:
  - The first model would run GENERAL flow mode to compute flow and temperature for the first several hundred years or until the waste packages are relatively cool. This model would likely be very slow and should not be run many times.
  - The second model will restart at the end of the first and be used for radionuclide transport. After the waste packages are relatively cool it should be possible to simulate in RICHARDS mode without incurring much error. This will speed up the longer-term simulations enormously.

Section 5 is an update and adaptation of the bedded salt reference case documented in Sevougian et al. (2016) and other past bedded-salt reference-case simulations between 2012 and 2016, including some early simulation results for disposal of DPC waste packages. This update changes the repository design to accept 24- and 37-PWR DPC's, in a 50/50 split by weight of heavy metal for each canister size. This report details the preliminary simulations of a near-field repository model simulation that have been conducted in anticipation of a full-scale PA simulation that will be documented in a September 27, 2019 M3 deliverable (M3SF-19SN010304052). The work presented here is preliminary and meant to be a precursor to the full-scale salt reference case to be reported in the September 2019 M3 deliverable. The near-field repository model provides expected results for its 50,000-year simulation and provides confidence that the repository conceptual model and numerical design will be suitable for the full-scale PA simulations. However, several important steps need to take place before those simulations can occur, including updates to parameter values and boundary conditions.

Section 6 is an update to the generic shale reference case (Mariner et al. 2017). Section 6.1 describes the methods used to develop a new Geologic Framework Model (GFM) for a representative shale environment and briefly describes the geologic and hydrogeologic features represented in the GFM. A full discussion of the geology and hydrogeology of the region represented by the GFM and the implications for the shale conceptual model is left to a later report. Construction of the GFM is the first step in developing a workflow that consists of constructing the GFM, exporting the relevant features of the GFM for meshing, and using the mesh for flow and transport modeling in PFLOTRAN. This discussion focuses on the mechanics of creating the GFM as the first step of the workflow. The shale GFM described here represents a relatively simple geologic environment of a horizontally layered sedimentary rock sequence consisting predominantly of shale formations interbedded with limestone and sandstone formations. A second goal of the GFM development is to determine the extent to which a generic GFM can be developed using publicly available data. This would be relevant for a future site screening and site evaluation process where existing geologic and hydrogeologic information would be integrated for assessing and screening alternative candidate sites. At the site characterization stage, new data would be collected and incorporated into the GFM.

Section 6.2 documents some near-field simulations with a highly discretized grid in the shale reference case, as a precursor to coupling more detailed process models into *GDSA Framework*. The objective of this study is to investigate the near-field thermal-hydrologic behavior of pore fluids in a geologic repository located in a shale host rock. The focus is on the impact of hydrogeological properties of the engineered buffer and disturbed rock zone (DRZ) on the near-field performance of a typical bentonite back-filled shale repository. Near-field thermal-hydrologic modeling of a geologic repository at finer discretization than comparable site-scale models suggests more localization of thermal effects within the EBS in the high-resolution model as compared to a site-scale model. Furthermore, when sampling on a range of permeabilities and porosities, local pressure buildup that is observed in the reference case is able to dissipate in scenarios with a higher permeability buffer and DRZ. Work will continue on this near-field model for the remainder of FY2019, with a goal of using this domain in a PA-GDSA model (i.e., *GDSA Framework*) to represent near-field thermal-hydrologic-mechanical coupled process effects. Surrogate modeling will be used to couple a mechanical response to thermal loading by linking permeability and porosity with the pressure and temperature distribution in the near-field.

Finally, Section 6.3 describes some very early considerations for a site-scale shale-host-rock reference case that includes DPC disposal. This section presents status on the FY2019 proposed update to the GDSA Shale Reference Case described in Section 4 of Mariner et. al. (2017). This work has only recently begun, so only a very preliminary update is provided here. The comprehensive report on the update will be reported in the September 27, 2019 Level 3 milestone for the FY19 GDSA Repository Systems Analysis work package (SF-18SN01030405), entitled *GDSA Repository Systems Analysis FY19 Update* (M3SF-19SN010304052). The main tasks that will be undertaken in FY2019 are:

(1) Inclusion of 24-PWR and 37-PWR DPC waste packages in the reference case simulations.

(2) An update to the stratigraphic model for a representative shale domain (Perry et al. 2014; Perry and Kelley, 2017)—see Section 6.1.

(3) An update to the numerical model grids and formation properties to incorporate changes

to stratigraphy and repository design needed for DPC waste.

This report fulfills the FY19 GDSA Repository Systems Analysis work package (SF-18SN01030405) Level 2 milestone *GDSA Repository Systems Analysis Progress Report* (M2SF-19SN010304051).

CONTENTS

FIGURES

TABLES

ACRONYMS

CD	Critical Decision
CSNF	Commercial Spent Nuclear Fuel
Dakota	Design analysis toolkit for optimization and terascale applications
DOE	U.S. Department of Energy
DPC	Dual Purpose Canister
DRZ	Disturbed Rock Zone
EBS	Engineered Barrier System
EDZ	Excavated Damage Zone
FEP	Feature, Event, and Process
FY	Fiscal Year
GDSA	Geologic Disposal Safety Assessment
GFM	Geologic Framework Model
HLW	High-Level Radioactive Waste
IAEA	International Atomic Energy Agency
IAPWS	International Association for the Properties of Water and Steam
IRF	Instant Release Fraction
LHS	Latin Hypercube Sampling
MTHM	Metric Tons Heavy Metal
NBS	Natural Barrier System
OoR	Out-of-Reactor
PA	Performance Assessment
PWR	Pressurized Water Reactor
R&D	Research and Development
RD&D	Research, Development, and Demonstration
SFWST	Spent Fuel and Waste Science and Technology
SNF	Spent Nuclear Fuel
TH	Thermal-Hydrologic
THM	Thermal-Hydrologic-Mechanical
UZ	Unsaturated Zone
WF	Waste Form
WIPP	Waste Isolation Pilot Plant
WP	Waste Package

1 INTRODUCTION

The Spent Fuel and Waste Science and Technology (SFWST) Campaign of the U.S. Department of Energy (DOE) Office of Nuclear Energy, Office of Fuel Cycle Technology is conducting research and development (R&D) on geologic disposal of spent nuclear fuel (SNF) and high level nuclear waste (HLW). Two of the highest priorities for SFWST disposal R&D are design concept development and disposal system performance assessment (PA) modeling (DOE 2012, Table 6). These priorities are directly addressed in the SFWST Geologic Disposal Safety Assessment (GDSA) Repository Systems Analysis work package, which is charged with developing a modeling and analysis capability for evaluating disposal system performance for nuclear waste in geologic media. Current disposal options being considered for SNF and HLW include mined repository concepts in bedded salt, argillite (shale), and crystalline rock. An additional option begun last fiscal year (FY) was a potential mined repository in unsaturated alluvium. The generic disposal concepts and associated reference cases that have been developed since 2012 have mostly focused on commercial spent nuclear fuel (CSNF) inventory packaged in smaller waste packages, such as 4-PWR and/or 12-PWR waste packages. However, a greater emphasis is given this year to simulating direct disposal of much hotter waste packages containing dual purpose canisters (DPCs) with 37 pressurized water reactor (PWR) assemblies, as well as 24 PWR assemblies, which now represents a significant fraction of the spent fuel inventory currently being stored at U.S. reactor sites.

This report describes accomplishments for the first half of Fiscal Year 2019 in the development of generic repository reference cases and PA modeling and analysis. Prior development and accomplishments are documented in Mariner et al. (2018), Mariner et al. (2017), Mariner et al. (2016), Mariner et al. (2015), Sevougian et al. (2016), Sevougian et al. (2014), Sevougian et al. (2013), Sevougian et al. (2012), Freeze et al. (2013b), and Vaughn et al. (2013).

The overall objective of the GDSA Repository Systems Analysis work package is to develop generic deep geologic repository concepts and system Performance Assessment (PA) models in several host-rock environments, and to simulate and analyze these generic repository concepts and models using the *GDSA Framework* toolkit, and other tools as needed. The goals in FY19 are to

- Develop and/or augment generic repository reference cases for three liquid-saturated host rock environments: crystalline (e.g., granite), argillaceous (e.g., typical shale or clay), and bedded salt host rocks; and a host rock environment in the unsaturated zone (UZ), such as alluvial valley fill.

- Ensure that reference cases include repository concepts and layouts for the disposal of DPC-canisterized PWR assemblies, including 37-PWR and 24-PWR waste packages, including the possible effects of criticality events on repository performance

- Perform PA simulations (deterministic and probabilistic) with GDSA Framework for the foregoing reference case concepts and models. Analyze and plot the PA simulation results, including uncertainty and sensitivity analyses

This report fulfills the FY19 GDSA Repository Systems Analysis work package (SF-18SN01030405) Level 2 milestone *GDSA Repository Systems Analysis Progress Report* (M2SF-19SN010304051).

Section 2 sets the context for this analysis work within the framework of the safety case and with respect to a multi-decade project. Section 3 discusses improvements to the numerical solvers in PFLOTRAN, needed for modeling the high heat output from DPC waste packages, particularly during two-phase flow, such as might occur in an unsaturated host-rock environment. Section 4 develops a technical basis and conceptual model for a reference case repository located in unsaturated alluvial sediments, first introduced in Mariner et al. (2018), including initial simulations for a small-scale, finely gridded, "sector" model, as well as a more coarsely gridded, "field-scale" repository model. Section 5 is an update of the bedded-salt reference case documented in Sevougian et al. (2016), including some early simulation results for disposal of DPC waste packages. Section 6 is an update to the generic shale reference case presented in Mariner et al. (2017). Section 6.1 documents initial work on developing geologic framework models (GFMs) for the various reference cases, beginning with the shale reference case. Section 6.2 also documents some near-field simulations with a highly discretized grid in the shale reference case, as a precursor to coupling more detailed thermal-hydrologic-mechanical process models into the PA system model *GDSA Framework*. Finally, Section 6.3 describes some very early considerations for a full-scale shale-host-rock reference case that includes DPC disposal.

2   SAFETY CASE AND REFERENCE CASE METHODOLOGY

During the development of a deep geologic repository, the post-closure Performance Assessment or Safety Assessment is a primary component of the post-closure Safety Case (see IAEA 2012, Sec. 4.4), along with the underlying Technical Bases (engineering and scientific knowledge). Figure 2-1 is an illustration of the main components of a safety (or licensing) case. The red-dash boxes highlight the current generic program's emphasis on R&D activities related to the post-closure technical bases (FEPs) and the safety assessment (DOE 2012).
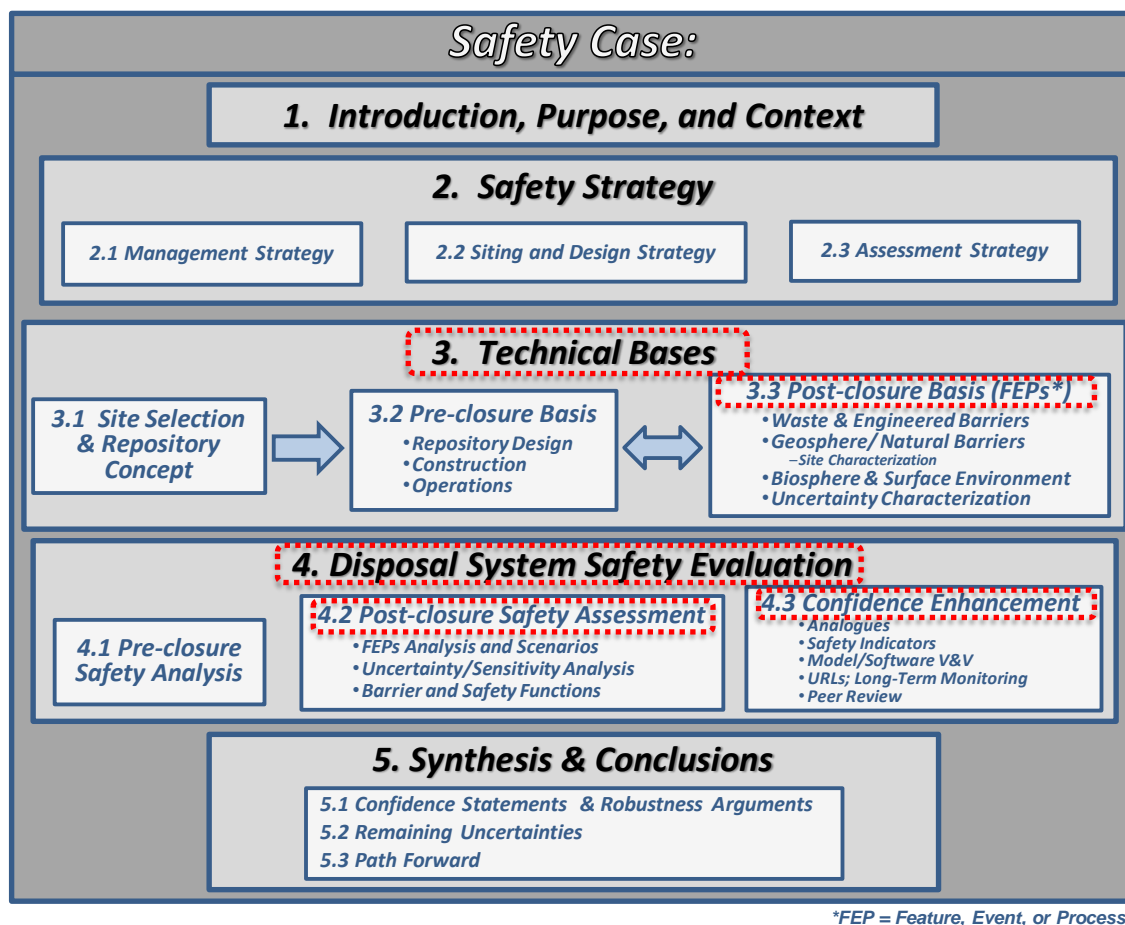
Figure 2-1. Typical components of a deep geologic repository safety case.

Figure 2-2 is a schematic illustration of the progression of these main components of a safety case (the PA and the technical bases) from a generic evaluation phase to a site-specific phase during the typical stages of any geologic disposal project. The maturation of the safety case through these various stages is driven by research, development and demonstration (RD&D) decisions made at key decision points (e.g., Critical Decision (CD) points, as described in DOE 2010), via a formal decision-making process involving major project stakeholders. As of this writing, the U.S. program is at the indicated location on the timeline in Figure 2-2, which corresponds to generic (non-site-specific) RD&D only.
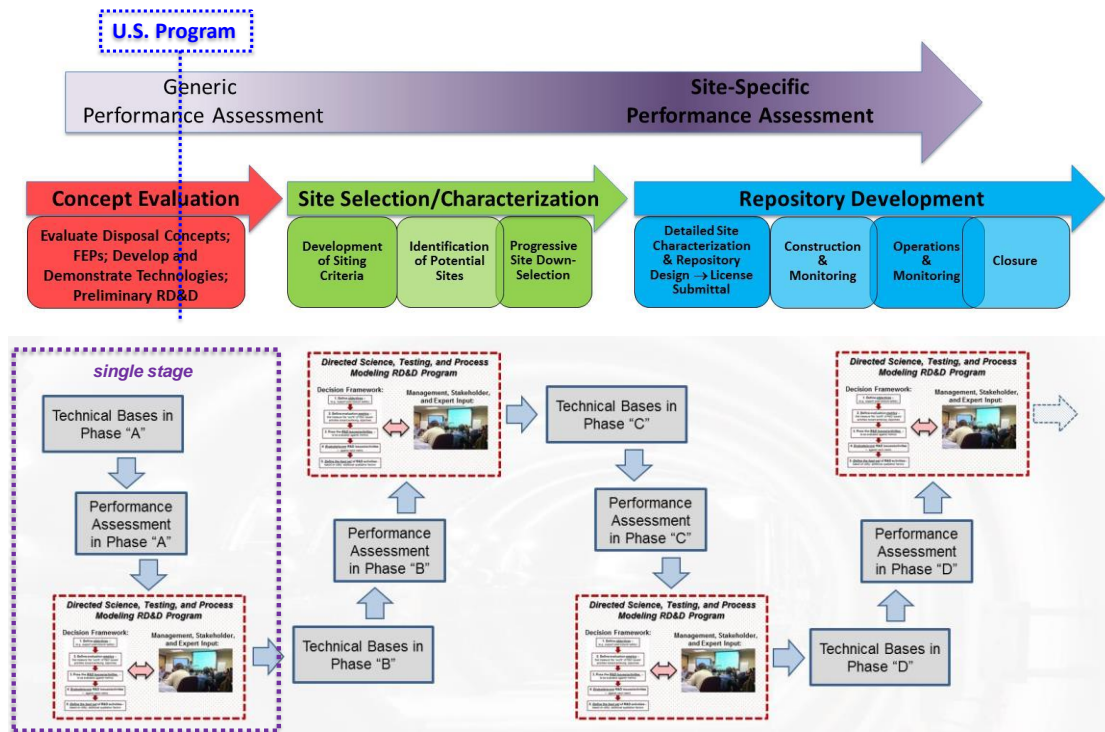
Figure 2-2. Evolution and iteration of the technical bases and performance assessment via RD&D through multiple stages of repository development.

Figure 2-3 shows the information flow during a single stage of a repository program and how the PA model (in the U.S., *GDSA Framework*) is intended to fill a key role in guiding the directed RD&D program. The generic reference cases for potential host-rock geologic environments (argillite, crystalline, bedded salt, and unsaturated alluvium for the current work in the DOE SFWST Campaign) address the key elements of Figure 2-3 outlined by the blue dotted lines, with results of the reference case PA simulations being part of the Safety Assessment Models and Safety Evaluation boxes. This deliverable discusses progress on developing and simulating generic reference case repositories with *GDSA Framework*, updated for direct disposal of DPC inventory and waste packages. The specific reference cases updated here are the argillite (shale), bedded salt, and unsaturated alluvium reference cases (Mariner et al. 2017; Sevougian et al. 2016; Mariner et al. 2018).
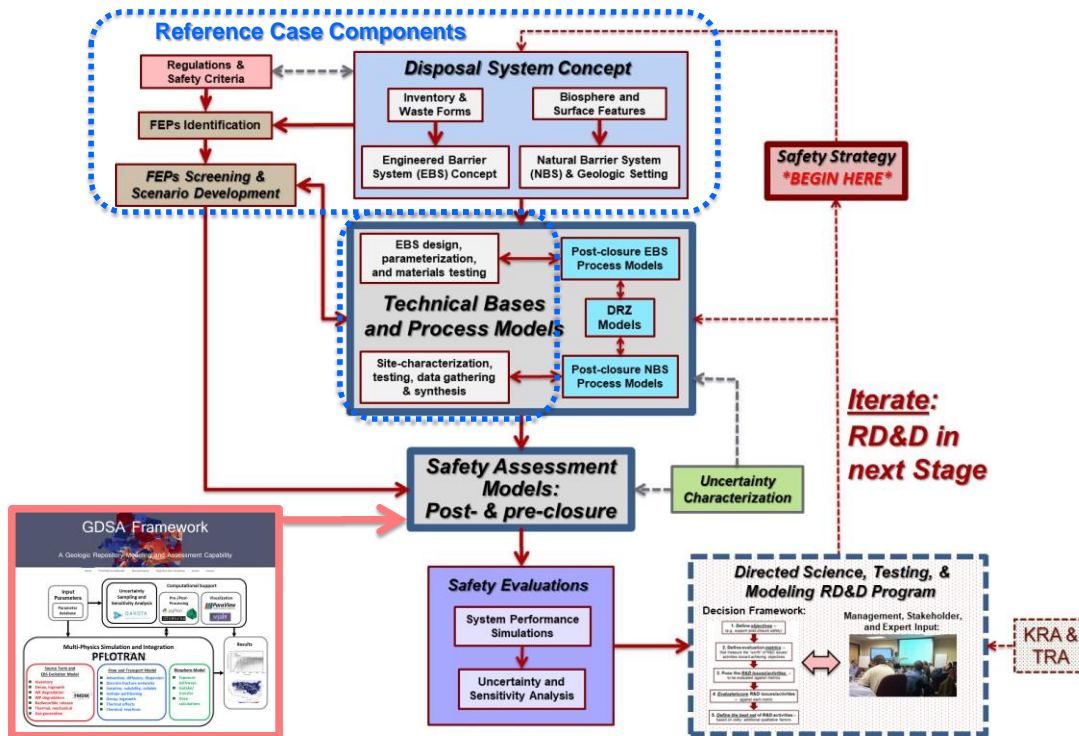
Figure 2-3. Information flow and the role of performance assessment for RD&D prioritization during a single stage of repository development.

3 GDSA FRAMEWORK AND PFLOTRAN UPDATES

3.1 PFLOTRAN Updates

Multiphase (liquid and gas) flow and transport capabilities in PFLOTRAN (under the "General" flow mode) have been augmented to more efficiently simulate physically complex processes that could occur in unsaturated repositories and/or under conditions of extreme waste package heat production (as could be the case with a 37 PWR configuration). The most significant of these changes involved refactoring of convergence criteria used during each iteration of the Newton-Raphson nonlinear solution search algorithm. Additionally, the water equation of state has been updated from International Association for the Properties of Water and Steam (IAPWS) standard IFC67 to standard IF97, which is computationally more efficient and is considered a robust successor to IFC67. Furthermore, additional user-specified options have been added to improve performance and functionality of simulations run in General mode, including implementation of user-prescribed solution dampening, user-imposed state change restrictions, more robust anisotropic permeability scaling, and user-defined heat sources/sinks.

3.1.1 Updated Newton-Raphson Convergence Criteria in General Mode

A Newton-Raphson solution search algorithm addresses the nonlinearities in the system of mass and energy conservation equations that a simulator is trying to solve. The method is said to have converged when mass and energy are considered to have been conserved to an acceptable degree of accuracy. Convergence is approached as the residuals to the governing equations approach zero. The residuals represent the difference between the accumulation/flux terms (LHS) and any sources/sinks (RHS) for each conservation equation at a given iteration of the Newton-Raphson search scheme. The Newton-Raphson search algorithm is kicked off with an initial guess, and the method can be shown to converge quadratically if this initial guess is sufficiently close to the converged solution (Isaacson and Keller 2012). The criteria for what constitute acceptable degrees of convergence can depend on parameter units in the governing equations, as well as on grid discretization.

One criterion for declaring Newton-Raphson convergence is to check whether the Euclidean norm of the residuals and relative changes to the primary variables are both beneath a certain threshold value. For a system of N grid blocks, this would appear as follows:

Residual Euclidean norm:

$$\|\boldsymbol{R}\|_2 = \sqrt{\sum_{i=1}^{N} (R_i^{k+1})^2} \tag{3-1}$$

Primary variable increment Euclidean norm:

$$\left\| \frac{\boldsymbol{x}_{new} - \boldsymbol{x}_{old}}{\boldsymbol{x}_{old}} \right\|_2 = \sqrt{\sum_{i=1}^{N} \left(\frac{x_i^{k+1} - x_i^k}{x_i^k} \right)^2} \tag{3-2}$$

where $\boldsymbol{R}$ is the vector containing a conservation equation residual for each grid block, k is the Newton-Raphson iteration number, and $\boldsymbol{x}$ is the vector of solution values for a given primary variable. Convergence will be considered achieved at the current time step if:

$$\|\boldsymbol{R}\|_2 < \epsilon_1 \tag{3-3}$$

and
$$\left\|\frac{\boldsymbol{x}_{new} - \boldsymbol{x}_{old}}{\boldsymbol{x}_{old}}\right\|_2 < \epsilon_2 \tag{3-4}$$

where ϵ_1 and ϵ_2 are small, pre-determined constants. These criteria must hold true for each governing equation (water mass, air mass, and energy in General mode) and each primary variable (a combination of three of the following: liquid pressure, gas pressure, air partial pressure, aqueous air mole fraction, gas saturation, and temperature). A limitation of this convergence criterion is that the Euclidean norm of the residuals is grid-size dependent. Instead, one could constrain the maximum absolute value of either the residual or the relative update vectors, which is sensitive to large outliers.

PFLOTRAN by default implements Euclidean norm criteria for determining Newton-Raphson convergence. The option to declare convergence on infinity norms has been added as an alternate convergence approach. The infinity norm is used to evaluate the largest absolute value of either a primary variable increment or residual of a given conservation equation. When evaluating the infinity norm on the residual, the residual is normalized by the accumulation term when the accumulation term is greater than 1.

Residual infinity norm:

$$\left\|\frac{\boldsymbol{R}}{\boldsymbol{A}}\right\|_\infty = \max\left(\frac{\boldsymbol{R}^{k+1}}{\boldsymbol{A}^{k+1}}\right) \tag{3-5}$$

Primary variable relative update infinity norm:

$$\left\|\frac{\boldsymbol{x}_{new} - \boldsymbol{x}_{old}}{\boldsymbol{x}_{old}}\right\|_\infty = \max\left(\frac{\boldsymbol{x}^{k+1} - \boldsymbol{x}^k}{\boldsymbol{x}^k}\right) \tag{3-6}$$

where $\boldsymbol{A}$ is the vector of accumulation terms at every grid block for a given conservation equation.

Although the size of the residual will approach zero as the Newton-Raphson iteration converges toward the true solution, a small residual does not necessarily mean the method has reached the true solution. The change in the primary variable increment should approach zero as the method converges, and it will estimate the solution error when the Newton-Raphson method converges quadratically. Convergence is considered achieved when the infinity norms on both the scaled residual and the relative update of the primary variables are reduced below a prescribed tolerance:

$$\left\|\frac{\boldsymbol{R}}{\boldsymbol{A}}\right\|_\infty < \epsilon_3 \tag{3-7}$$

and
$$\left\| \frac{x_{new} - x_{old}}{x_{old}} \right\|_{\infty} < \epsilon_4 \tag{3-8}$$

where ϵ_3 is set to a default value of 1×10^{-5} and ϵ_4 is set to a default value of 1×10^{-3}.

3.1.2 Updated Water Equation of State

The default equation of state for water and superheated steam in PFLOTRAN follows the International Association for the Properties of Water and Steam (IAPWS) standard IFC67. This set of equations of state is now considered obsolete by IAPWS, and currently IF97 is considered an acceptable standard. The IF97 equations (Wagner et al. 2000), as shown in Figure 3-1, for saturation pressure (Region 4), specific volume and specific enthalpy for liquid water (Region 1), and specific volume and specific enthalpy for superheated steam have been implemented (Region 2). This equation of state is valid for temperatures ranging from 273.15 K to 623.15 K when pressures are between 0 Pa and 100 MPa, as well as from 623.15 K to 1073.15 K when pressures are below the boundary between Regions 2 and 3. This range of pressures and temperatures is suitable for most subsurface applications.
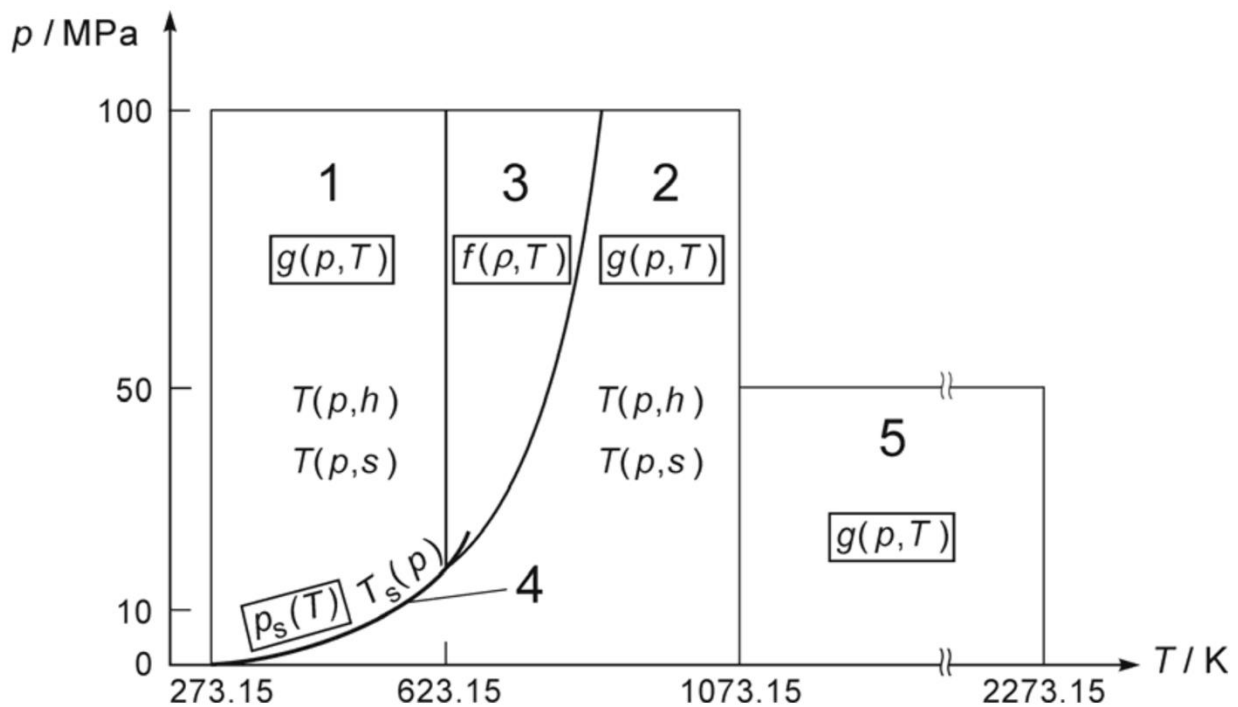
Figure 3-1. Phase diagram regions of IAPWS-IF97 (Wagner et al. 2000).

Analytical derivatives for saturation pressure, specific enthalpy and volume were also calculated for use in PFLOTRAN's analytical Jacobian calculation option, which has been demonstrated to speed up computation time for a wide variety of problems.

3.1.3 Anisotropic Permeability and Unstructured Grids

Laminar porous medium flow is simulated by employing Darcy's Equation, which relates the gradient in pressure potential to fluid flow velocity by a linear transformation using the intrinsic

permeability of the medium, the viscosity of the fluid, and the relative permeability of the fluid in multiphase systems. In a structured grid oriented orthogonal to the principal axes of anisotropy, the component of flow across a grid cell face can be calculated directly because the pressure gradient and permeability orthogonal to the grid face are known. With an unstructured grid, however, a grid cell face is not necessarily orthogonal to the principal axes of anisotropy (Figure 3-2), so the component of flow across the grid cell face must be calculated using a directional permeability in the direction of the unit outward normal to the grid cell face.
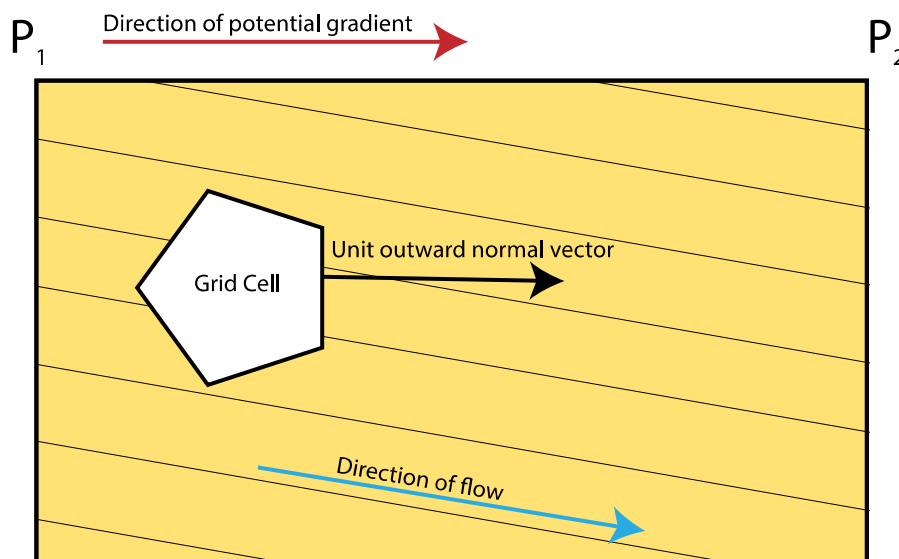
Figure 3-2. A layered medium where the direction of the pressure gradient is not aligned with the direction of flow and grid cell faces are not orthogonal to the principal axes of anisotropy.

When grid block faces are not aligned with the principal axes of anisotropy, rotation of the diagonal principal permeability tensor by the angle of inclination with the principal axes results in a full permeability tensor (off diagonal elements are non-zero). However, to preserve computational efficiency, PFLOTRAN calculates a scalar permeability from the principal components of permeability instead. Two new options for this calculation were added in FY 19: scalar calculations of both the permeability in the direction of flow and permeability in the direction of the potential gradient are now offered as options (Freeze and Cherry 1979; Peters 2012):

Permeability in the direction of flow: $k_{eff} = k_x u_x^2 + k_y u_y^2 + k_z u_z^2$ \hfill (3-9)

Permeability in the direction of the potential gradient: $k_{eff} = \dfrac{1}{\frac{u_x^2}{k_x} + \frac{u_y^2}{k_y} + \frac{u_z^2}{k_z}}$ \hfill (3-10)

where u_x, u_y, and u_z are the components of the unit outward normal vector along the grid block face of interest in principal axes of anisotropy; k_x, k_y, and k_z are the permeabilities along each principal axis; and k_{eff} is the effective permeability across a face that is in general not orthogonal to the principal axes (Freeze and Cherry 1979). As one can see, under either of these formulations grid orientation will not affect the ultimate value of k_{eff} in an isotropic medium. Selection of one of these permeability options should take into account the orientation of the grid in an anisotropic medium with respect to both the potential gradient and the flow field. If grid faces are arranged perpendicular to flow (such as when the edge of a grid follows the edge of a bedding plane along

which permeability is discontinuous), then the permeability in the direction of flow is likely the most accurate option. If grid block faces are oriented perpendicular to the potential gradient (such as if grid block faces are mostly lined up with the boundaries and flow is driven by differences in boundary conditions), then the permeability in the direction of the potential gradient is likely a more accurate option.

The effective directional permeability of the medium in the direction of the unit outward normal will therefore always lie on the ellipse defined by the permeabilities along each principal component axis. Figure 3-3 illustrates an example permeability ellipse in the direction of flow for a 2D medium. A permeability ellipse in the direction of the potential gradient would be constructed similarly.
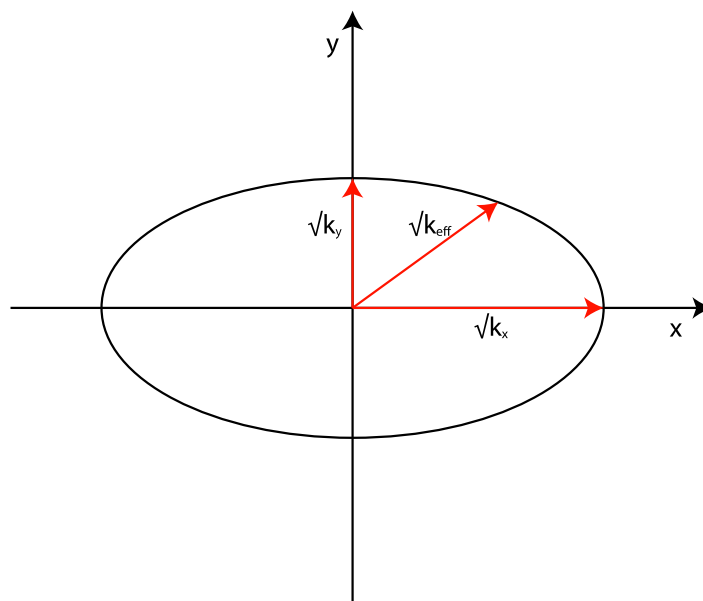
Figure 3-3. 2-D permeability ellipse for calculation of directional permeability in the direction of flow.

3.1.4 Updated General Mode Options

A suite of new options has been implemented in general mode to allow for more user-defined customizability for computational speedup and accuracy on a problem-by-problem basis. These new options encompass the following:

RESTRICT_STATE_CHANGE: This option restricts changes of state to only occur once per grid block per time step. This option reduces unnecessary instances of primary variable switching within a Newton-Raphson solution search that would otherwise result in time step cuts at the expense of greater computation time.

DAMPING_FACTOR applies a universal scaling to the solution update between each iteration of the Newton-Raphson solution search, effectively slowing the progression of the method and preventing significant overshooting.

PHASE_CHANGE_EPSILON applies a fixed initial phase saturation upon a state change from single-phase to two-phase. This requires the system to be slightly past a thermodynamic boundary

before being allowed to change state, which can help limit oscillatory state change behavior that increases computation time.

LOGGING_VERBOSITY enables more verbose logging of Newton-Raphson convergence metrics for simulation diagnostic purposes.

USE_INFINITY_NORM_CONVERGENCE employs the infinity norm convergence metrics as described above.

Additionally, users can now specify their own convergence criteria on any combination of absolute and relative updates on all primary variables when using infinity norm convergence. The same is true for absolute and scaled residual convergence criteria for all governing equations.

3.2 VoroCrust Meshing

A new project has been initiated to test the viability of using the internal Sandia VoroCrust meshing software to generate meshes for use in PFLOTRAN simulations. If this project is successful, the longer-term goal is to develop a meshing software tool that is open-source, more flexible, and better-suited to geological problems than the meshing software currently used by GDSA.

VoroCrust is a software tool that generates Voronoi meshes of arbitrary volumes (Abdelkader et al. 2018). In this project, the focus will be on generating meshes with appropriate refinement for relatively simple models that include waste packages, drifts and large-scale geological features. PFLOTRAN simulations on Voronoi meshes will be more accurate than typical unstructured meshes because on a Voronoi mesh flux between cell centers is always perpendicular to cell faces, which means there is no mass balance error in the flux approximation.

This project will develop the tools within VoroCrust for meshing to highly anisotropic geological features and to export the resulting meshes in a format suitable for PFLOTRAN. Simulations on the resultant meshes will be benchmarked against simulations on structured and unstructured PFLOTRAN meshes with identical geometry.

4   UNSATURATED ZONE REFERENCE CASE

This section presents an update of the UZ alluvium reference case introduced in Mariner et al. (2018), primarily related to the inclusion of DPC waste packages and their representative higher heat output per package, which results in more severe coupled process effects at early times after repository closure. Also, the conceptualization of the natural barrier system has been simplified from Mariner et al. (2018). The current conceptual model places the repository in coarser-grained upper basin alluvial fill rather than finer-grained playa deposits. This modification has been made, because the higher permeability material has the advantage of allowing thermal overpressures associated with the high heat output of 37-PWR waste packages to dissipate more quickly (Section 4.4.1.2).

4.1   Engineered Barriers

Specific post-closure basis information related to the engineered barriers includes

- Characteristics of the repository (Section 5.1.1)

- Inventory characterization (Section 5.1.2)

- Waste form characterization (Section 5.1.3)

- Waste package characterization (Section 5.1.4)

- Characteristics of the backfill (Section 5.1.5)

- Thermal loading basis for the repository layout (Section 6)

4.1.1   Engineered Barrier Characteristics

The unsaturated alluvium reference case assumes a mined repository located approximately 250 m below land surface and 300 m above the water table. The reference case repository contains 70,000 metric tons heavy metal (MTHM) of commercial SNF, which is the maximum allowed by the Nuclear Waste Policy Act of 1982 and about half of the total commercial SNF inventory predicted by 2055 in the "no replacement scenario" (Carter et al. 2013). It is assumed that half of the inventory (35,000 MTHM) is packaged in 3103 24-PWRs and half in 2013 37-PWRs. Waste packages are emplaced axially on the floor of a disposal drift, which would be immediately backfilled with crushed alluvium (Figure 4-1).

Preliminary drift and waste package spacings (chosen on the basis of thermal analyses described in Section 4.1.6 and the sector analysis described in Section 4.4.1) are 40 m center-to-center drift spacing, 20 m center-to-center 24-PWR spacing, and 40 m center-to-center 37-PWR spacing. Assuming a drift length of 1000 m, 62 drifts would hold 3100 24-PWR waste packages and an additional 80 drifts would hold 2000 37-PWR waste packages. The resulting repository footprint would be approximately 5.68 km^2. However, drift and waste package spacings may be modified in the future on the basis of preliminary sector and field-scale model results (Section 4.4.1.6).

Because the model domain for PA simulations has not yet been finalized, the as-gridded dimensions of repository features in the complete half-symmetry model domain are not included in Table 4-1.

Figure 4-1. Schematic cross-section view of drift for disposal of waste packages in an unsaturated alluvial repository.

Table 4-1. Dimensions and counts for the unsaturated alluvium repository layout.

Parameters	Reference Case Value
Waste Package (WP)	
WP length (m) [24-PWRs and 37-PWRs]	5.6 [a]
WP outer diameter (m) [24-PWRs and 37-PWR']	2.0 [a]
WP center-to-center (m) [24-PWRs]	20.0
WP center-to-center (m) [37-PWRs]	40.0
Number of 24-PWR WPs	3100
Number of 37-PWR WPs	2000
Emplacement Drift	
Drift diameter (m)	4.5 [a]
Drift center-to-center spacing (m)	40
Number of WPs per drift [24-PWRs]	50
Number of WPs per drift [37-PWRs]	25
Drift length (m)	1000
Repository	
Repository Depth (m)	250
Number of drifts [24-PWRs]	62
Number of drifts [37-PWRs]	80
Emplacement footprint (km^2)	5.68

[a] Hardin and Kalinina (2016, Section 3)
[b] half-symmetry domain / with reflection
[c] Hardin et al. (2013, Table 4-2)

4.1.2 Radionuclide Inventory

For simplicity, PA simulations assume that the inventory consists entirely of PWR SNF assemblies, each containing 0.435 MTHM (Sevougian et al. 2013). The reference case PWR inventory considers two fuel burn-ups: 40 GWd/MTHM at 100 years out of the reactor (OoR) and 60 GWd/MTHM at 150 years OoR. Initial radionuclide inventories and heat of decay curves were

calculated by performing decay and ingrowth calculations starting from the 5-year OoR inventories in Carter et al. (2013, Table C-1), which assume initial enrichments of 3.72 wt% ^{235}U and 4.73 wt% ^{235}U for 40 GWd/MTHM burn-up and 60 GWd/MTHM burn-up fuels, respectively. Because the average burn-up of SNF under the "no replacement scenario" is predicted to be only 54 GWd/MTHM (Carter et al. 2013), the assumption of 60 GWd/MTHM results in a conservatively high heat load.

The entire PWR SNF inventory includes approximately 450 isotopes with a total mass of 1.44×10^6 g/MTHM. The total mass of the PWR inventory includes actinides (dominated by ^{238}U), oxygen from the UO$_2$, zirconium from cladding, and other fission and activation products. The mass inventory of the radionuclides selected for simulation in the unsaturated alluvium reference case is listed in Tables 4-2 and 4-3. These are the same radionuclides that have been simulated in previous crystalline and shale reference cases, which assume a saturated repository and reducing conditions (Mariner et al. 2016; Mariner et al. 2017; Sevougian et al. 2016). In future, the list will be updated to ensure that radionuclides of importance to the unsaturated zone safety case, in which non-reducing conditions and gas transport may influence radionuclide mobility, are included.

PA simulations assume 0.435 MTHM per PWR assembly and a UO$_2$ density of 10970 kg/m^3, resulting in 10.4 MTHM or 1370 m^3 of fuel in a 24-PWR waste package and 16.1 MTHM or 2113 m^3 of fuel in a 37-PWR waste package. Given the differences in enrichment and burn-up, corresponding heat outputs for the 24-PWR waste package at 100 years OoR and the 37-PWR waste package at 150 years OoR are 3881 W per waste package and 5817 W per waste package, respectively.

Table 4-2. 24-PWR SNF inventory (40 GWd/MTHM burnup, 100-year OoR) of selected radionuclides for the unsaturated alluvium reference case.

Isotope	Inventory (g/MTIHM)[1]	Inventory (g/g waste)[2]	Atomic weight (g/mol)[3]	Approximate Decay Constant (1/s)[4]
^{241}Am	1.35E+03	9.36E-04	241.06	5.08E-11
^{243}Am	1.38E+02	9.61E-05	243.06	2.98E-12
^{238}Pu	1.79E+02	1.24E-04	238.05	2.56E-10
^{239}Pu	6.38E+03	4.43E-03	239.05	9.01E-13
^{240}Pu	2.57E+03	1.79E-03	240.05	3.34E-12
^{242}Pu	5.65E+02	3.92E-04	242.06	5.80E-14
^{237}Np	7.60E+02	5.28E-04	237.05	1.03E-14
^{233}U	1.32E-02	9.18E-09	233.04	1.38E-13
^{234}U	2.66E+02	1.85E-04	234.04	8.90E-14
^{236}U	4.72E+03	3.28E-03	236.05	9.20E-16
^{238}U	9.33E+05	6.48E-01	238.05	4.87E-18
^{229}Th	2.90E-06	2.01E-12	229.03	2.78E-12
^{230}Th	3.34E-02	2.32E-08	230.03	2.75E-13
^{226}Ra	7.34E-06	5.1E-12	226.03	1.37E-11
^{36}Cl	3.52E-01	2.44E-07	35.97	7.30E-14
^{99}Tc	9.16E+02	6.36E-04	98.91	1.04E-13
^{129}I	2.16E+02	1.5E-04	128.9	1.29E-15
^{135}Cs	4.86E+02	3.37E-04	134.91	9.55E-15

[1]Carter et al. (2013, Table C-2)

[2](g isotope/g waste) = (g isotope/MTIHM)/(g waste/MTIHM), where g waste = g all isotopes

[3]Weast and Astle (1981)

[4]Decay constants from ORIGEN (Croff 1983)

Table 4-3. 37-PWR SNF inventory (60 GWd/MTHM burn-up, 150-year OoR) for the unsaturated alluvium reference case.

Isotope	Inventory (g/MTIHM)[1]	Inventory (g/g waste)[2]	Atomic weight (g/mol)[3]	Approximate Decay Constant (1/s)[4]
^{241}Am	1.36E+03	9.42E-04	241.06	5.08E-11
^{243}Am	2.67E+02	1.86E-04	243.06	2.98E-12
^{238}Pu	1.91E+02	1.33E-04	238.05	2.56E-10
^{239}Pu	7.39E+03	5.14E-03	239.05	9.01E-13
^{240}Pu	4.09E+03	2.84E-03	240.05	3.34E-12
^{242}Pu	8.17E+02	5.67E-04	242.06	5.80E-14
^{237}Np	1.51E+03	1.05E-03	237.05	1.03E-14
^{233}U	6.64E-02	4.61E-08	233.04	1.38E-13
^{234}U	6.02E+02	4.18E-04	234.04	8.90E-14
^{236}U	6.29E+03	4.37E-03	236.05	9.20E-16
^{238}U	9.10E+05	6.32E-01	238.05	4.87E-18
^{229}Th	2.65E-05	1.84E-11	229.03	2.78E-12
^{230}Th	1.82E-01	1.26E-07	230.03	2.75E-13
^{226}Ra	1.01E-04	7.04E-11	226.03	1.37E-11
^{36}Cl	5.01E-01	3.48E-07	35.97	7.30E-14
^{99}Tc	1.28E+03	8.89E-04	98.91	1.04E-13
^{129}I	3.13E+02	2.17E-04	128.9	1.29E-15
^{135}Cs	7.72E+02	5.36E-04	134.91	9.55E-15

[1] Carter et al. (2013, Table C-2)
[2] (g isotope/g waste) = (g isotope/MTIHM)/(g waste/MTIHM), where g waste = g all isotopes
[3] Weast and Astle (1981)
[4] Decay constants from ORIGEN (Croff 1983)

4.1.3 Waste Form

Freeze et al. (2013b, Section 3.4.1.1) provides a description of commercial SNF, including the following characteristics. Spent uranium oxide (UO_2) fuel is a polycrystalline ceramic material with stable to high temperatures and the potential for slow degradation in the disposal environment. Cladding protects the fuel from degradation in the reactor and can continue to protect the fuel from degradation in the repository. Cladding from commercial light-water reactors (i.e., boiling water reactors and pressurized water reactors) is generally made from Zircaloy, a zirconium alloy that is chemically stable and resistant to corrosion. In the reactor, fuel undergoes physical changes due to heating, radiation damage, and the build-up of fission products. Lighter elements (fission products) become concentrated in voids and the outer margins of the UO_2 matrix.

Concentration of fission products in voids of the waste form results in the waste form releasing radionuclides in two fractions (Sassani et al. 2012): instant-release (upon waste package breach) and slow-release (according to the UO_2 matrix dissolution rate). Models describing the mobilization of the gap and grain-boundary inventories (instant release fraction) and UO_2 dissolution models appropriate for oxidizing, partially saturated conditions are under development for use in the unsaturated zone reference case. (The two-phase flow simulations presented below do not yet consider radionuclide transport.)

4.1.4 Waste Package

The unsaturated alluvium reference case considers two waste package configurations: a 24-PWR waste package and a 37-PWR waste package. Both are assumed to consist of a stainless-steel dual purpose canister (DPC) similar to the Magnastor TSC (Price et al. 2019; Greene et al. 2013) and a

stainless-steel overpack with a 5-cm thick wall, an outer diameter of 2 m and a length of 5.6 m (Hardin et al. 2013).

Due to the method of gridding typically used to represent commercial SNF waste packages in reference case simulations (e.g. Mariner et al. 2016; 2017), simulated waste packages have dimensions of $1.67 \times 1.67 \times 5.0$ m and a volume of 13.94 m^3, as compared to the actual volume of 17.59 m^3.

Waste package porosity is assumed to be 50%, consistent with the waste package description in Sevougian et al. (2016). Permeability is set several orders of magnitude higher than that of the surrounding materials, so that flow through waste packages is uninhibited. The waste package is given the thermal properties of stainless steel (Shelton 1934). These properties may be modified in the future for consistency with the DPC criticality consequence analysis modeling proposed by Price et al. 2019.

Waste package degradation models appropriate for oxidizing, partially saturated conditions are under development for use in the unsaturated zone reference case.

4.1.5 Backfill

The unsaturated alluvium reference case assumes disposal drifts are backfilled with crushed alluvium amended to increase thermal conductivity. The primary purpose of the backfill is to prevent collapse of the drift walls, the strength of which may be adversely affected by coupled thermal, hydrological, mechanical, and chemical processes driven by the heat generated from the waste. The thermal conductivity of alluvium, whether measured in situ or in recompacted samples (1 to 1.2 W/m/K and 0.3 to 0.5 W/m/K, respectively, Hardin et al. 2012, Appendix B) is low. Semi-analytical thermal analyses to be reported by Matteo et al. (2019) show that given the assumed characteristics of the 37-PWR waste packages, amending the backfill to increase the thermal conductivity is likely to be necessary to maintain waste package temperatures below about 300 C, and preliminary numerical simulations agree (Section 4.4.1.4). Thermal conductivity of the crushed alluvium backfill could be increased by adding a high thermal conductivity admixture such as quartz sand, silica flour, and/or graphite (e.g., Jobmann and Buntebarth 2009).

Thermal, hydrological and mechanical properties for alluvium and for sand-gravel aggregate material are listed in Tables 4-4 and 4-5, respectively, to indicate proxy values for backfill in reference case simulations. The mineralogy and radionuclide sorption behavior of an amended alluvium backfill would be similar to that of the surrounding host rock. These characteristics are described in Mariner et al. (2018, Section 4).

4.1.6 Thermal Loading Basis for Repository Layout

Hadgu et al. (2015) report a parametric study for drift and waste package spacings for sedimentary open repository concepts with 37-PWR size waste packages with a burnup of 60 GW-d/MT and 150 years of ventilation in addition to 50 years decay storage. The analysis compares 70 m and 90 m drift spacings and waste package spacings from 16 m to 40 m. Hadgu et al. (2015) found that the peak host rock target of 100°C was exceeded in all cases. To further evaluate the interplay between drift spacing, waste package spacing, and potential backfill materials for thermal management of a 37-PWR 60 GW-d/MT 150-year OoR sedimentary closed repository concept, a thermal parametric analysis was completed following the workflow described in Hardin et al. (2013) and will be reported in detail in an upcoming report by Matteo et al. (2019).

Table 4-4. Thermal, hydrological and mechanical parameters for alluvium that could be used to simulate backfill in the unsaturated alluvial repository concept.

Parameter	Value	Reference
Porosity (unitless)	0.3 - 0.5	Smyth et al. (1979, Table 1); Kwicklis et al. (2006, Table 1)
Thermal conductivity (W/m-K)	0.5 – 1.5	Hardin et al. (2012, Table D-1 and Appendix B)
Saturated hydraulic conductivity (m/d)	0.54 - 3.5	Cochran et al. (2001, Table 6-15)
Residual moisture content (unitless)	0.057 - 0.084	Cochran et al. (2001, Table 6-15)
Saturated moisture content (unitless)	0.33 - 0.41	Cochran et al. (2001, Table 6-15)
van Genuchten,1982 α (cm^{-1})	0.033 - 0.124	Cochran et al. (2001, Table 6-15)
van Genuchten, 1982 m (unitless)	1.4 - 2.36	Cochran et al. (2001, Table 6-15)
Compressibility (1/Pa)	5.3E-11	Kilroy (1992, Table 7)

Table 4-5. Thermal, hydrological and mechanical parameters for sand-gravel aggregate that could be used to simulate backfill in the unsaturated alluvial repository concept.

Parameter	Value	Earth material	Information Source
Porosity (unitless)	0.155 - 0.323	sand-gravel aggregate mixture	Gupta et al. (2009), Table A2
Thermal conductivity (W/m-K)	2.1 - 2.6	poorly graded sand - gravel mixture	Drefke et al. (2015), Figure 4
Saturated hydraulic conductivity (m/d)	0.0226 - 3.03, 0.76 mean	sand-gravel aggregate mixture	Gupta et al. (2009), Table 3.2
Residual moisture content (unitless)	0.06 - 0.17	sand-gravel aggregate mixture	Gupta et al. (2009), Table 3.2
Saturated moisture content (unitless)	0.16 - 0.32	sand-gravel aggregate mixture	Gupta et al. (2009), Table 3.2
van Genuchten, 1982 α (cm^{-1})	0.03. - 0.13	sand-gravel aggregate mixture	Gupta et al. (2009), Table 3.2
van Genuchten, 1982 m (unitless)	0.10 - 0.79	sand-gravel aggregate mixture	Gupta et al. (2009), Table 3.2

This analysis is an extension of previous work (Hardin et al. 2011, 2012, 2013; Hardin and Vogele 2013). The calculations assumed no ventilation, waste package dimensions of 5.6 m long and 2.0 m diameter, a drift diameter of 4.5 m, and a host rock thermal conductivity of 1.2 W/m-C°. Waste package spacings of 20 and 30 m, drift spacings of 30, 40, 50, 60, and 75 m, and backfill thermal conductivities of 0.6, 1.0, 1.5, and 2.0 W/m-C° were evaluated in the analysis (Figures 4-2 and 4-3). Backfill thermal conductivities of 1.0 W/m-C° and higher are taken as proxies for backfill that is engineered to have high thermal conductivity, and that of 0.6 W/m-C° is taken as a proxy for unsaturated or crushed alluvium backfill.

Outcomes where the peak waste package outer surface is ≤ 300°C and the temperature history there is not over 200°C after the first 500 years, and drift wall and backfill temperatures are between 100 and 200°C, considered to be candidates for the reference-case repository layout (Figures 4-2 and 4-3). The analysis indicates that backfill thermal conductivity has a great effect on the waste package surface temperature compared to drift and waste package spacing. Drift spacing can be reduced from 60 to 50 or 40 m, to limit repository footprint, by changing the properties of the backfill.
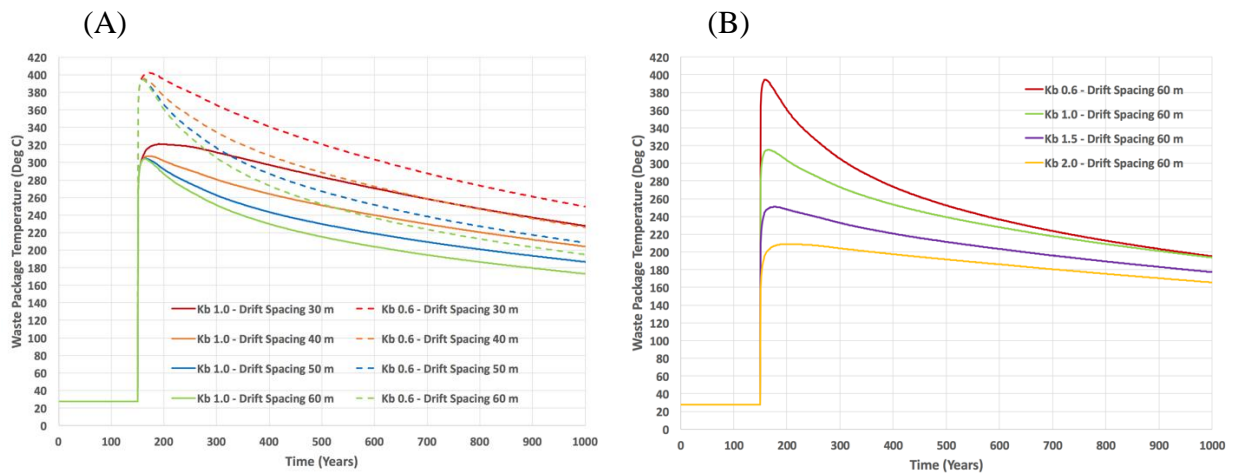
Figure 4-2. Results of thermal parametric calculations that will be reported by Matteo et al. (2019) which shows (A) the effect of drift spacing and backfill thermal conductivity [Kb] on waste package temperature through time and (B) the effect of backfill thermal conductivity on waste package temperature through time.
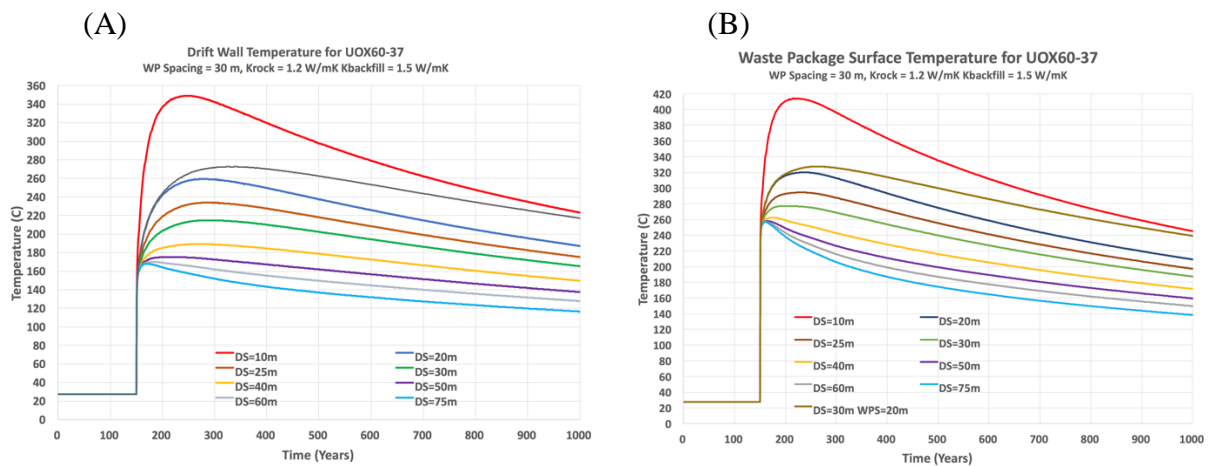
Figure 4-3. Results of thermal parametric calculations that will be reported by Matteo et al. (2019) which shows the effect of drift spacing on (A) drift wall temperature and (B) waste package surface temperature through time. [The calculations are for engineered high thermal conductivity backfill.]

4.2 Geosphere/Natural Barriers

The technical bases and a general description of the natural barrier system for the unsaturated alluvium reference case are given in Mariner et al. (2018), and specific parameter values used in the preliminary simulations in this report are given in Section 4.3.

4.3 Post-Closure Performance Assessment for UZ Reference Case

This section summarizes the progress to date on models and simulation results for post-closure assessment of the UZ reference case. This summary focuses on simulation results for the unsaturated thermal flow field. Transport of radionuclides will be presented in a future report. For the present report two models are considered:

- Simulation of the 37-PWR waste package (WP) array at the drift scale. The purpose of this study is to establish drift spacing and near-field properties in a smaller model that can be simulated in 1 to 1.5 hours on a Linux workstation.

- Using drift spacing and near-field properties from the smaller model model, simulate a field-scale half-symmetry model.

4.3.1 Conceptual Model

The conceptual framework for this preliminary generic post-closure PA includes components of the engineered barrier (Section 4.1) and the natural barrier (Section 4.2; Mariner et al. 2018). Key characteristics and processes to be represented in these components are summarized in Table 4-6.

Table 4-6. Conceptual representation of the engineered and natural barriers in PA. [For future work, not in current report.]

Region	Component	Key characteristics	Key processes included in PA
Engineered Barrier	Waste Form*	SNF (UO_2)	Radionuclide decay, instant release fraction, waste form dissolution
	Waste Package*	Stainless steel	Degradation and breach
	Engineered high thermal conductivity alluvium backfill	High thermal conductivity	Distribute heat flux to a larger area toward drift wall
Natural Barrier	Alluvium Host Rock	Unsaturated, little water flux in undisturbed sediment	Multiphase flow, thermal processes, radionuclide advection*, diffusion*, sorption*, decay*
	Alluvium Aquifer	Saturated, potable water	Fluid flow, radionuclide advection*, diffusion*, sorption*, decay*

Simulations assume: (1) a mined repository at 255 m depth; (2) a head gradient of –0.005 m/m from west to east (Mariner et al. 2018); (3) a regional heat flux of 105 mW/m^2 and a mean annual surface temperature of 25°C (Mariner et al. 2018); and (4) a variably unsaturated/saturated model domain. Processes accounted for in the initial conceptual models documented herein are coupled heat and multiphase fluid flow.

4.3.2 Numerical Implementation

Two types of simulations have been conducted using *GDSA Framework* (Section 4.5) and are described next. These simulations include: (1) a limited parameter uncertainty analysis for 37-PWR WP arrays in a "sector" model representing 4 disposal drifts each with 4 WPs, and (2) a single deterministic PA simulation for 24-PWR WPs in a larger field-scale model with 27 drifts and 24 WPs per drift The field-scale PA unstructured mesh was gridded with Cubit (Blacker et al. 2016). Simulations of two-phase flow and temperature were run with PFLOTRAN (Hammond et al. 2014).

4.3.2.1   37-PWR WP Sector Model Domain and Discretization

The first simulation domain is a sector model of a full field-scale domain. The small subproblem was put to a variety of uses for situations where running the full-scale PA simulation was both time-prohibitive and unnecessary:

- As a test problem in updating the general mode options and default convergence-criteria (see Section 3.1.4)

- Study spacing of the 37-PWR WPs along the drift and spacing between drifts to prevent undesirably high temperatures and pressures near the waste packages.

- It was also used to study the impact of drift backfill properties to prevent undesirable high temperatures and pressures near the waste packages.

The mesh for the sector model is shown in Figures 4-4 and 4-5. It is a structured mesh with variable grid spacing with $30 \times 35 \times 39 = 40{,}950$ grid cells. A one-million-year simulation of flow takes 1 to 1.5 hours on 8 nodes of a Linux workstation.
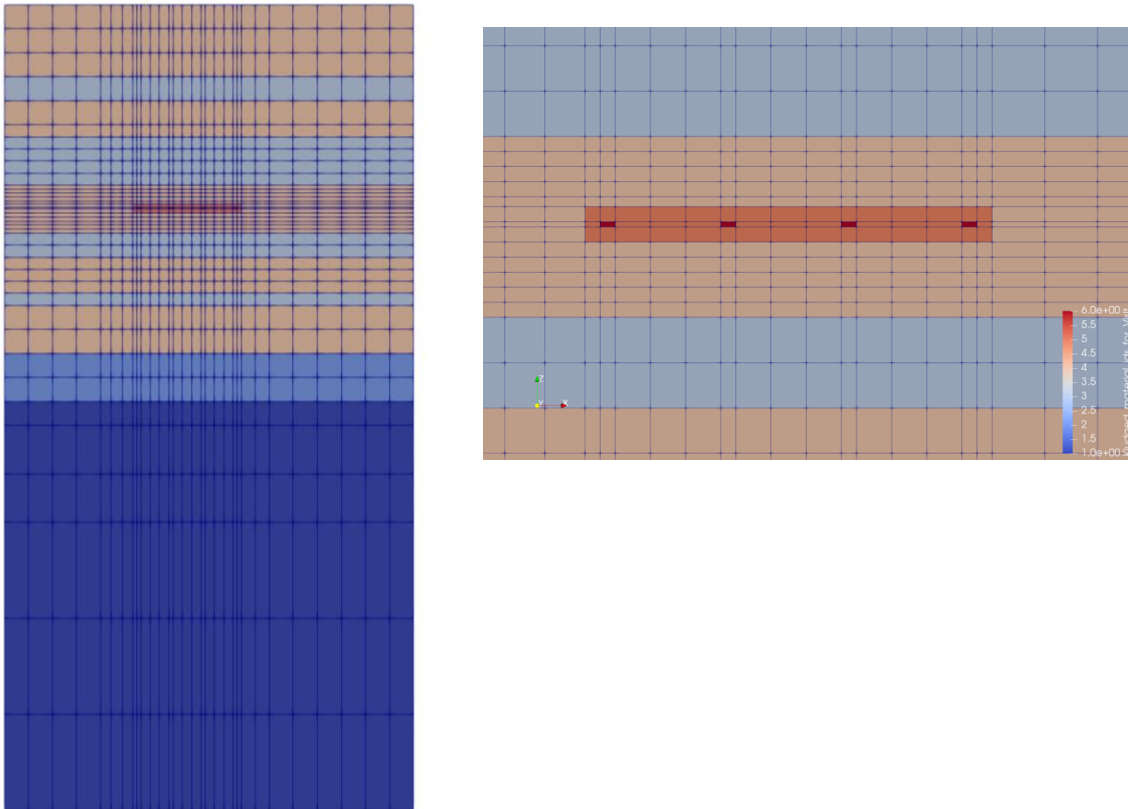
Figure 4-4. Side view of the base case simulation domain in a slice through the second drift at $y = 205.5$ m colored by material and showing the refinement of the simulation mesh around the repository. Left: full domain. Right: detail of the repository region showing waste packages in the drift. Red indicates waste packages, orange indicates drift areas, salmon indicates high permeability channel-fill rock type, light blue indicates confining layers above the water table, medium blue indicates high permeability layers at/below the water table and dark blue is confining layers below the water table. [Drifts are 40 m apart and the center-to-center distance between waste packages along the drift is also 40 m. Dimensions of the domain are $(x, z) = (511$ m, 1005 m$)$. The repository is in a high-permeability channel-facies of the formation that has thickness 60 m.]
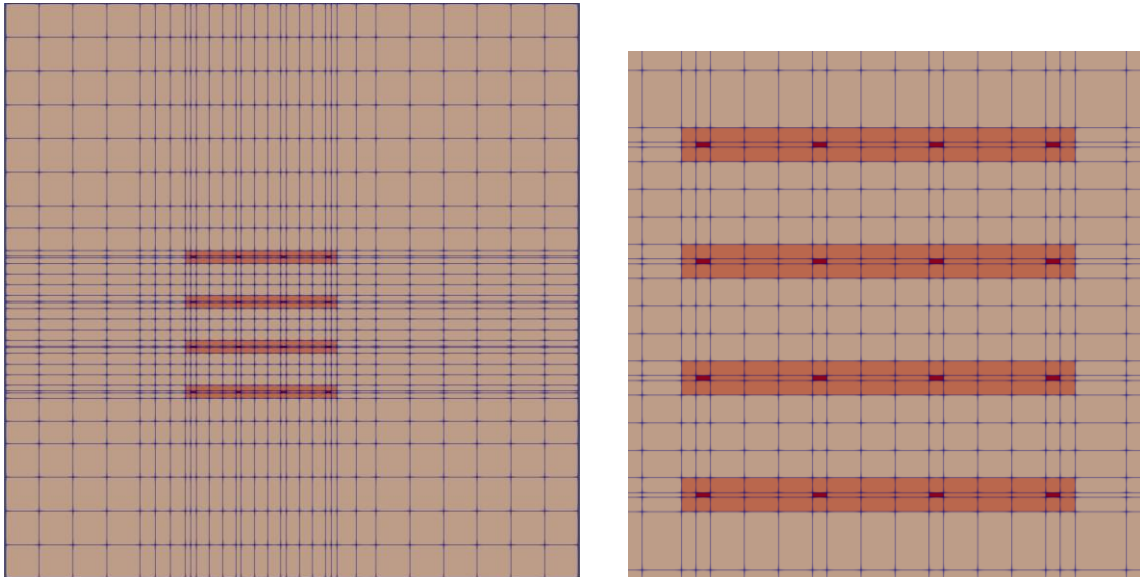
Figure 4-5. Top view of the drifts and waste packages colored by material and showing the refinement of the simulation mesh around the repository. Left: full domain at a depth of 750 m. Right: detail of the area surrounding the repository. Red indicates waste packages, orange indicates drift areas and salmon indicates high permeability channel-fill rock type. [Drifts are 40m apart and the center-to-center distance between waste packages along the drift is also 40 m. Dimensions of the domain are (x, y) = (511 m, 515 m).]

The dimensions of the sector model are (515m×511m×1005m). The domain is a small section taken from the proposed full UZ PA simulation scenario. The boundary conditions, infiltration and static rock properties are all identical to the field-scale model described below in sections 4.4.2.2 – 4.4.2.6.

The grid is refined so that each waste package is in a single 5×1.67×1.67 m grid cell. This mesh should adequately resolve the temperature near each waste package. The drift cells are scaled so that the drift extends 5 m, one grid cell, in every direction from the waste packages. The center-to-center distance between the waste packages is 40 m, both along and between the drifts for the base case. In the rest of the simulation domain, cells are gradually coarsened outward from the array. This refinement near the drifts allows for adequate resolution of saturation, temperature and pressure near the drifts without an excessively large number of grid cells. The vertical grid spacing in this model becomes extremely coarse at the bottom of the simulation domain and would not be suitable for modelling transport in the saturated zone.

Only one set of relative permeabilities, representative of the coarser alluvial sediment is used in this simulation. Furthermore, in the interest of simplicity there is no disturbed rock zone (DRZ) in this model. The 37-PWR 150-year out-of-reactor SNF are used as heat source to study the maximum heat output scenario.

4.3.2.2   24-PWR WP Field-Scale Model Domain and Discretization

The coupled thermal and multiphase flow problem was also simulated on a field-scale model domain with 24 waste packages per drift and 27 drifts. The drift properties and spacing were strongly informed by the results of the small-scale simulation models.

The model domain proposed by Mariner et al. (2018) for field-scale simulations of the UZ reference case is shown on the left of Figure 4-6 and the top of Figure 4-7. This mesh would fully resolve the heat and fluid flow as well as transport of radionuclides on a domain with dimensions (3915m, 1065m, 1005m). The resulting mesh had 2.4 million grid cells. A test simulation on the mesh on 256 nodes of a parallel HPC cluster was only able to simulate the first 292 years in a pre-allocated 2-hour simulation time. This simulation mesh was abandoned, and a coarser-scale simulation mesh was developed.
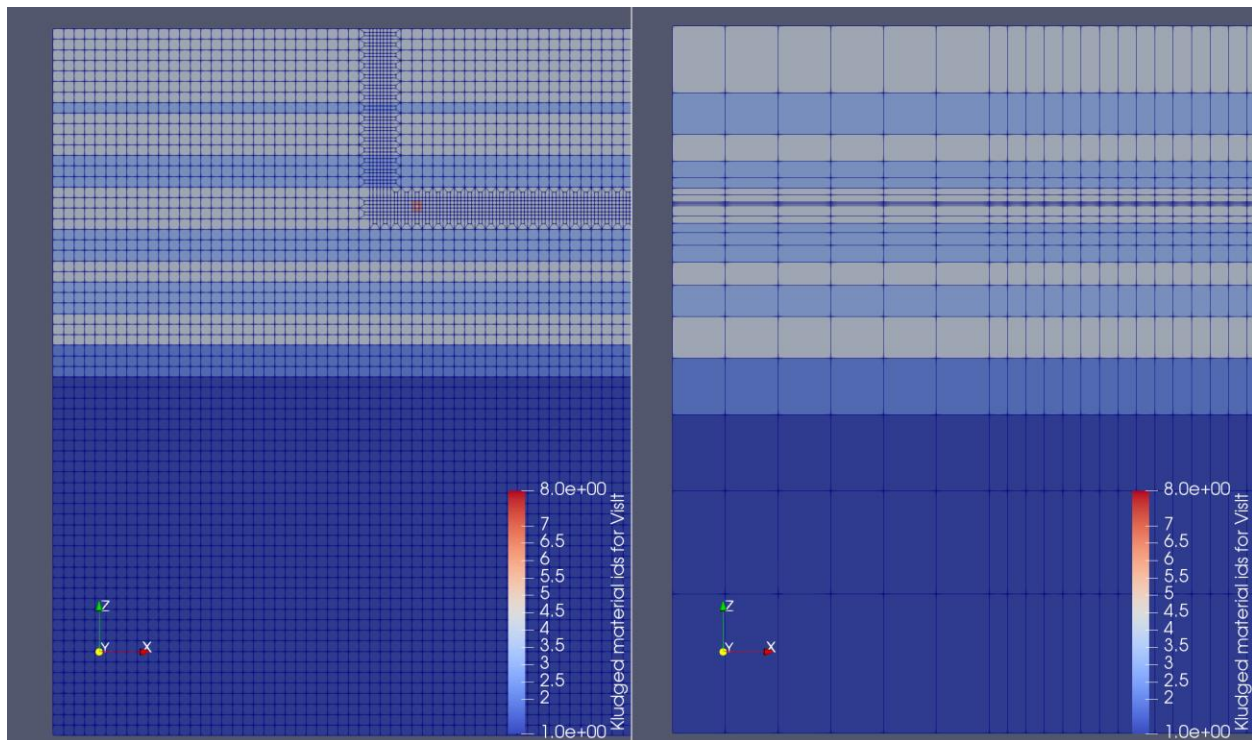
Figure 4-6. Side view of the south west corner of the mesh for the field-scale PA model. Left: Mariner et al. (2018) 2.4-million-grid-cell mesh.   Right: 214,000-grid-cell model developed for initial flow simulations. Grey represents the channel fill deposits above the water table, light blue are the confining regions above the water table, medium blue is high-permeability rock at the water table and dark blue is low permeability rock below the water table. [Both meshes are highly refined around the repository and coarser away from the repository.]

The new PA mesh has 214,000 grid cells, an order of magnitude fewer than the fine mesh. The waste packages and drifts have the same dimensions as the fine scale PA simulation, as can be seen in Figure 4-11. Each drift is 5 m wide in the x-direction and 5 m tall, with the waste packages in the center of the drift. The mesh has a single $5\times1.67\times1.67$m cell for each waste package with three grid cells between each package along the drift. The depth of geological layers of the formation are adjusted to account for the extremely coarse vertical meshing away from the repository, as shown on the right of Figure 4-10.

Outside of the drifts, the mesh coarsens rapidly in all directions. There are only three grid cells between drifts and so the damage zone is omitted, like the sector model (bottom of Figure 4-11). Due to the coarsening of the model away from the drifts, the long hall is 10 m longer on each side than the original model. The short halls are a single grid cell wide and have larger volume than the original model. They are truncated at the intersection with the long hall to avoid extremely wide halls at the south end. The vertical shafts are also omitted from the model, as the coarseness of the model made it impossible to mesh shafts with realistic dimensions.

These simplifications are unlikely to have much impact on the flow field near the repository in the simulation. Like the sector model, this mesh would not be suitable for transport of radionuclides due to the coarseness of the mesh away from the repository and the omission of the vertical shafts.
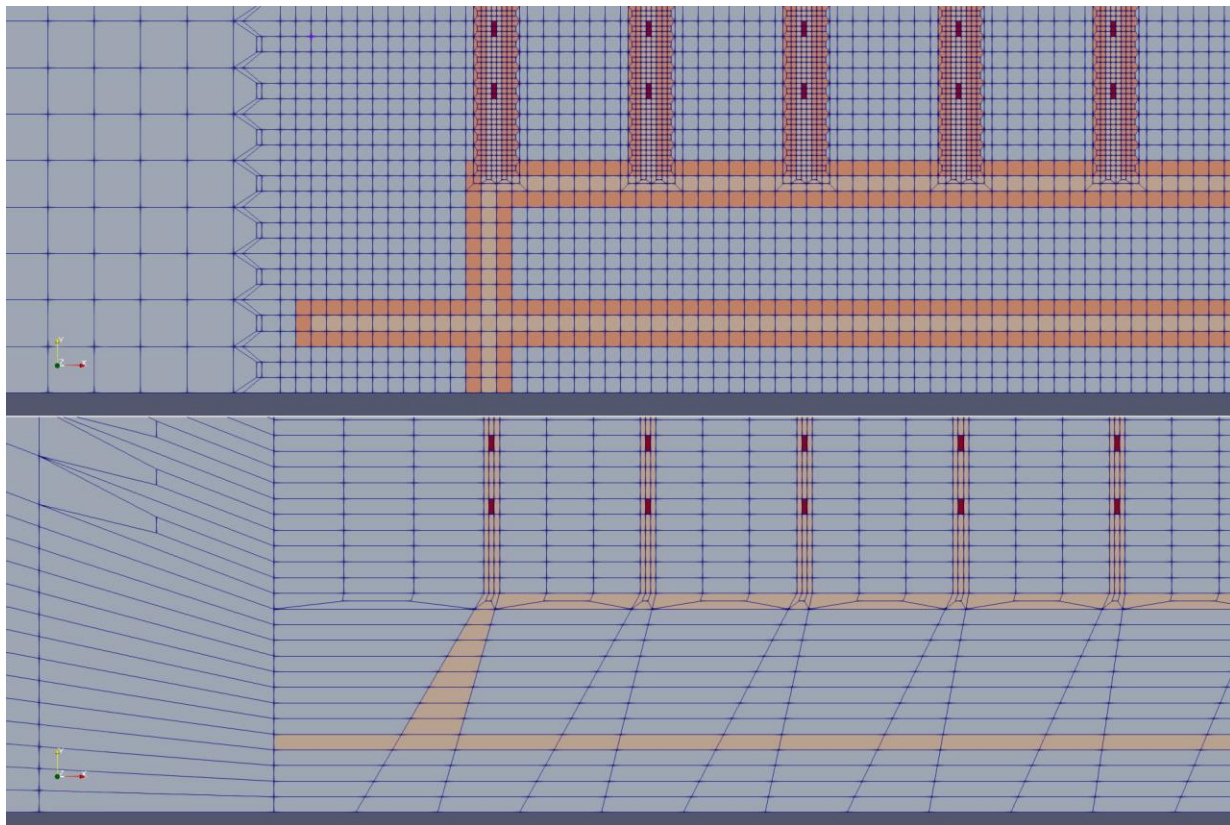
Figure 4-7. Horizontal cross-section of the southwest corner of the mesh through the repository at depth z=255 m for the field-scale PA model. Top: Original 2.4-million-grid-cell mesh. Bottom: 214,000-grid-cell model developed for initial flow simulations. Grey represents the channel fill rock surrounding the repository, orange is DRZ (not in coarse model), salmon is drifts and red is individual waste packages.

4.3.2.3   Initial Conditions

For both simulation models the initial fluid and water infiltration conditions are water infiltration of 1.0 mm/yr and a water table depth of 550 m in the east to 565 m in the west. The initial pressure is atmospheric at the top of the domain. The initial temperature conditions are a surface temperature of 25°C and a natural geothermal temperature gradient of 0.025°C/m. The east and west boundary conditions are based on equilibrated one-dimensional simulations corresponding to these constraints. The full model domain temperature, pressure and saturation are simulated

without drifts, waste packages or damage zone until a convergence tolerance is reached. This guarantees quasi-steady-state initial condition for the simulations with infiltration and a horizontal pressure gradient that drives flow from west to east.

4.3.2.4   Boundary Conditions

Boundary conditions must also be set for the north and south faces of the model domain. Fluxes of heat, fluid, and solute are set to zero at the north and south face of the model domain, creating a reflection boundary and virtually doubling the volume of the model domain. In the sector model the boundaries are far from the drifts, so it is assumed that the zero boundary conditions have negligible impact on the temperature, pressure and saturation near the array. For the field-scale model the boundary on the north of the domain is far from the array of waste packages, so again it is assumed that the zero boundary conditions have negligible impact on the temperature, pressure and saturation near the array.

The zero flux boundary conditions the south side of the field-scale model will act as a reflection boundary, thus effectively doubling the size of the simulation. For the current study this will have a minor impact on the flow field, however the impact on radionuclide transport in future simulations may be much larger.

4.3.2.5   Waste Package Heat Sources

Each waste package is modeled as a transient heat source. The energy (watts per waste package) entering the model domain is updated periodically according to values in a lookup table. The initial value is that for 37-PWR SNF 150 years OoR; the initial value is 5817 W. For 24-PWR waste packages 100 years OoR, the initial value is 3881 W. Between times specified in the lookup table, the energy input is linearly interpolated.

4.3.2.6   Material Properties

Material properties are discussed in Sections 4.1 and 4.2. Values used in the sector model and in the field-scale simulations are summarized in Table 4-7 and the parameters varied in the sector model are in Table 4-8.

Table 4-7. Base case parameter values used in simulations.

Model Region	Permeability (m²)	Porosity ϕ	Tortuosity exponent[1] τ	Saturated Thermal Conductivity (W/m/K)	Unsaturated Thermal Conductivity (W/m/K)	Heat Capacity (J/kg/K)	Grain Density (kg/m³)
Upper basin fill	1×10^{-12}	0.40	1.4	2.0	1.0	830	2700
Upper confining zone	1×10^{-14}	0.40	1.4	2.0	1.0	830	2700
Basin fill below water table	1×10^{-11}	0.40	1.4	2.0	1.0	830	2700
Confining zone below water table	1×10^{-13}	0.40	1.4	2.0	1.0	830	2700
Backfill	1×10^{-13}	0.40	1.4	2.0	2.0	830	2700
Waste Package	1×10^{-13}	0.50	1	16.7	16.7	488	5000

[1] $\tau = \phi^{1.4}$ (Van Loon and Mibus 2015)

Table 4-8. Variable design constraints and their values for sector model.

Parameter	Range	Units
Rock type used for disposal	Upper basin fill, upper confining zone	-
WP spacing within drift	20, 40	m
Spacing between drifts	40, 50	m
Dry thermal conductivity of backfill	1.0, 1.5, 2.0	(W/m/K)
Wet thermal conductivity of backfill	2.0, 2.5, 3.0	(W/m/K)
Drift/backfill permeability	1×10^{-11}, 1×10^{-12}, 1×10^{-13}, 1×10^{-14}	m^2

4.4 Simulation Results for UZ Reference Case

For both models the pressure, temperature and water saturation profiles are presented at key points within and between the waste packages. Distributions are also presented for the sector model base case and field-scale model. The results of the analysis on the sector model are used to define appropriate waste package spacing and drift properties for the field-scale simulation.

4.4.1 Sector Model Results

The sector model will be used to study the impact of several design criteria, as outlined in Table 4-8, on fluid and temperature in and between the waste packages. The mesh is shown in Figures 4-8 and 4-9. The screening criteria are based on three desirable outcomes:

1) The increase in pressure in and around the waste packages is modest. For the purposes of screening, more than a 50% increase in pressure is considered unacceptable.

2) Temperature around the waste packages does not get extremely high. For the purposes of screening the critical temperature of water (374°C) is used as the maximum allowable temperature.

3) The formation should not completely dry out in the space between the drifts.

4.4.1.1 Base Case

The base case model has the repository located in the higher-permeability basin fill zone, with 40 m spacing between drifts and 40 m spacing between waste packages within a drift. It also has a well-compacted engineered backfill with permeability of $1 \times 10^{-13} m^2$, which is two orders of magnitude lower than the surrounding formation. The wet and dry thermal conductivity are both 2.0 W/m/K. This was chosen as the base case because it represents a feasible combination of parameters (see Table 4-8) that results in a scenario that fulfills the three design criteria outlined above.

Figures 4-8 and 4-9 show the temperature and water saturation in the array in a slice through the repository as viewed from above at a series of snapshots in time. As can be seen in Figure 4-8, the temperature increases near the waste packages extremely quickly and as a result the backfill adjacent to the waste packages is dry within less than one year of simulation time (Figure 4-9), and the backfilled-drift surrounding the waste packages has dried out before 10 years.

The low dry thermal conductivity of the basin fill material surrounding the drifts means that the heat is not easily transported away from the repository, and the waste package cells are still over

100°C and completely dry after 1000 years. The rock formation between the drifts does not dry out and temperature outside of the drifts remains well below 100°C at all times.

The two locations within the sector model simulation that need to be monitored are at the hottest waste package and at the midpoint of the array. In the base case simulation the hottest waste package is WP(2,2); the second waste package from the left in the second drift from the bottom (or equivalently WP(3,2) in the third drift from the bottom, due to symmetry). The midpoint in the array, mid(2,2), is located in the center of the array, at the midpoint between drifts 2 and 3 and between the second and third WP in the drift. This location is representative of the conditions that will be observed between central waste packages in central drifts in a much larger disposal array.
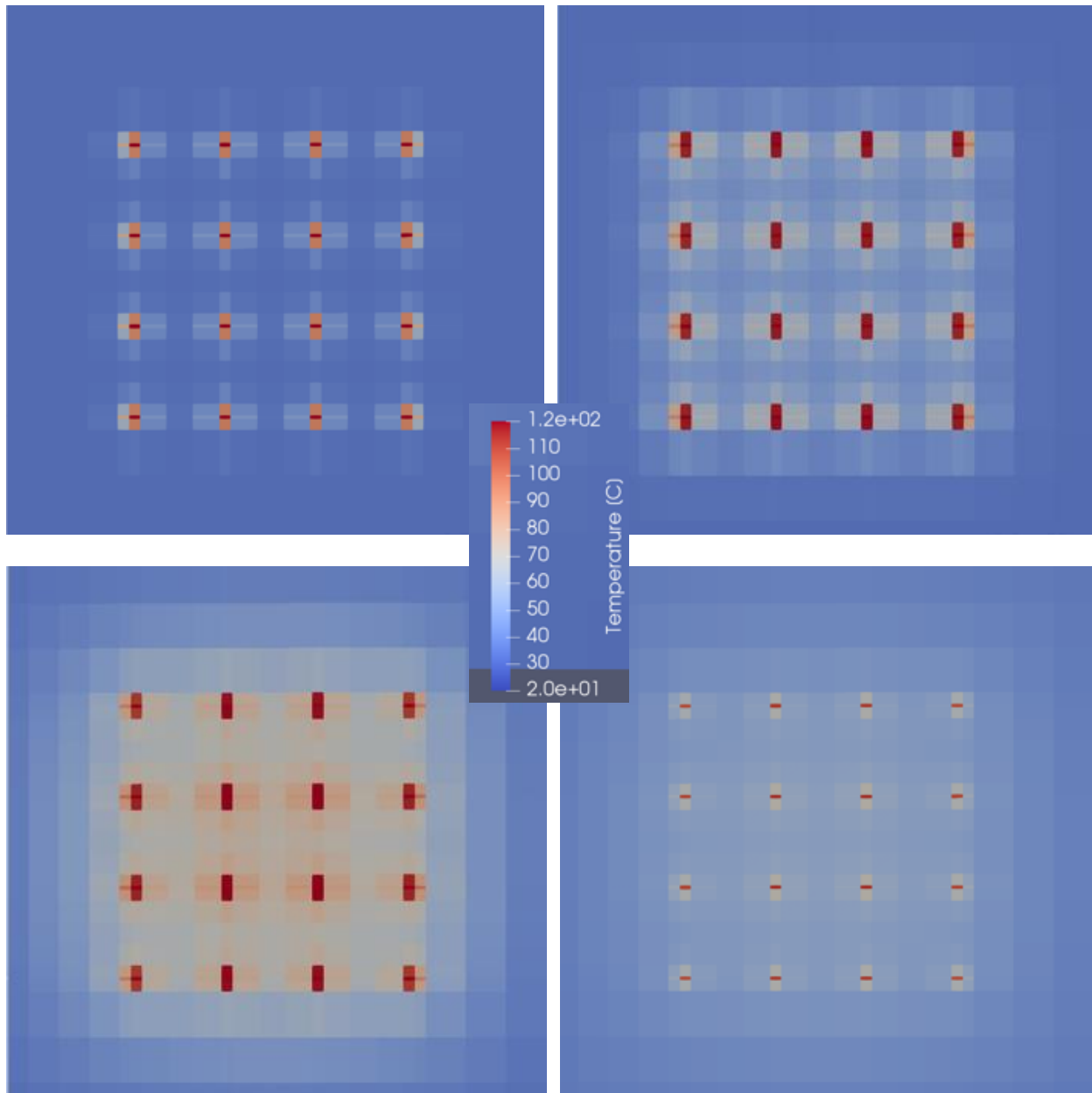
Figure 4-8. Temperature in a z-slice at depth z=255m through the center of the repository for the base case. Times are 1 year (upper left), 10 years (upper right), 100 years (lower left), 1000 years (lower right).
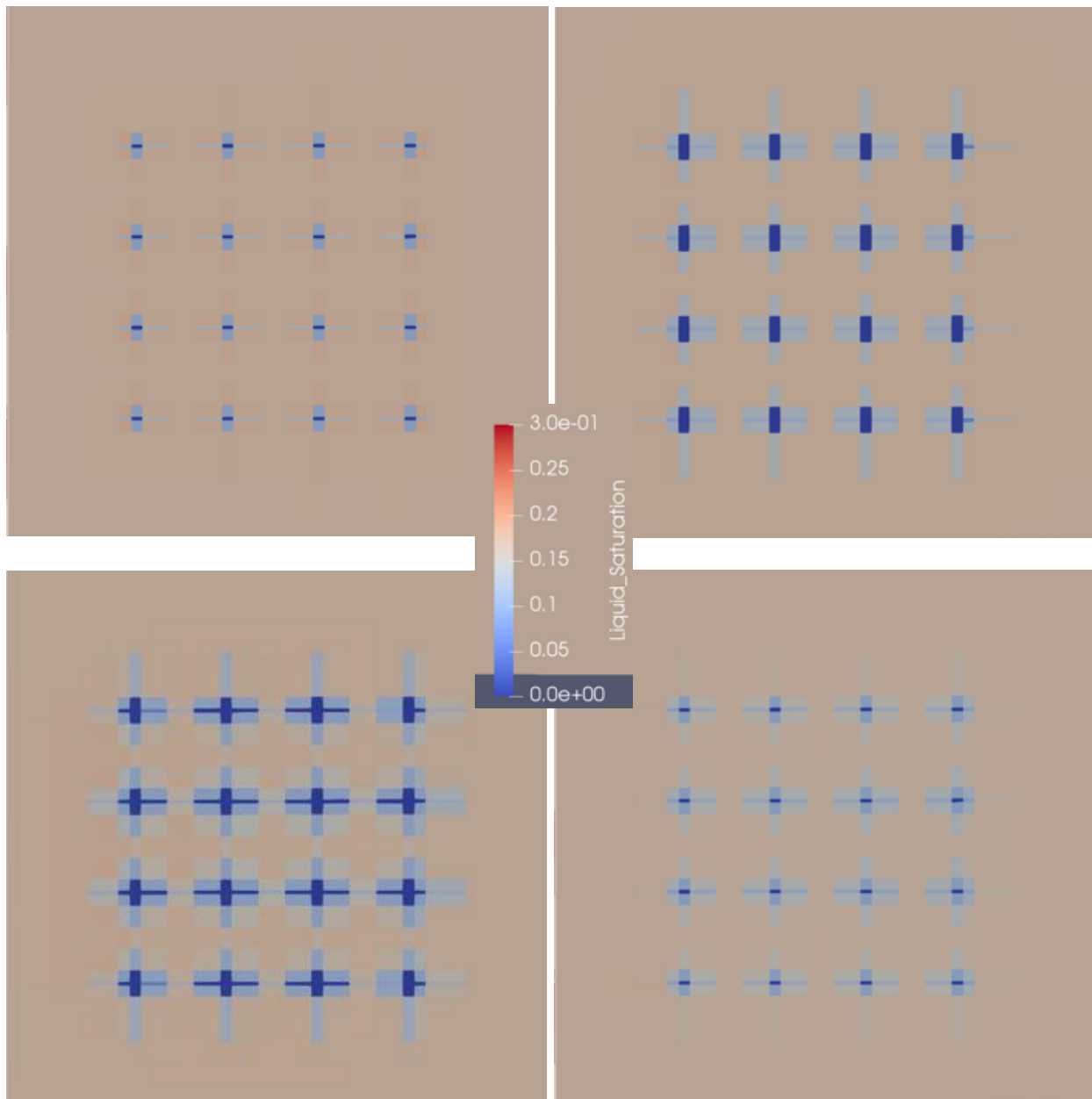
Figure 4-9. Water saturation z-slice at depth z = 255 m through the center of the repository for the base case. Times are 1 year (upper left), 10 years (upper right), 100 years (lower left), 1000 years (lower right).

Figures 4-10 and 4-11 show the gas pressure, temperature and water saturation as a function of log time at WP(2,2) and mid(2,2) for the base case simulation, along with another simulation to be discussed in the next section. The behavior of the system at the waste packages as a function of time can be split up into four distinct time stages.

A) For the first three days the waste package warms up to the boiling temperature of water. This will be termed the initiation stage.

B) For approximately 6 months the water at the waste package surface boils off. This will be termed the boil off stage.

C) Over the course of the next 2500 years the formation is dry near the waste packages as the temperature increases to over 300°C and then gradually drops back down to 100°C. This is the heat up stage.

D) Finally, after 2500 years the temperature drops below 100°C and the area quickly resaturates with water, gradually returning to near the initial water pressure by the end of the million-year simulation. This is the resaturation to initial condition time stage.

All simulations in the sector model show this behavior at all the waste packages, but the time interval between the stages changes with the input parameters.

As can be seen in Figure 4-10, the gas pressure at WP(2,2) increases rapidly at the start of the boil-off stage. This is because the water turning to steam creates a substantial increase in volume of the fluid phase. The steam must be allowed to escape into the drifts and formation during this stage or pressure will increase very quickly to unacceptable levels at the waste packages. In the base case the pressure only increases by a few kPa because the parameters chosen are relatively high permeability of the drift and very high permeability of the surrounding basin fill formation (See Table 4-7). The high permeability of the surrounding basin fill also results in a near-residual initial water saturation of around 16%, which also contributes to lower pressure during the boil off stage because there is little water to evaporate into steam.
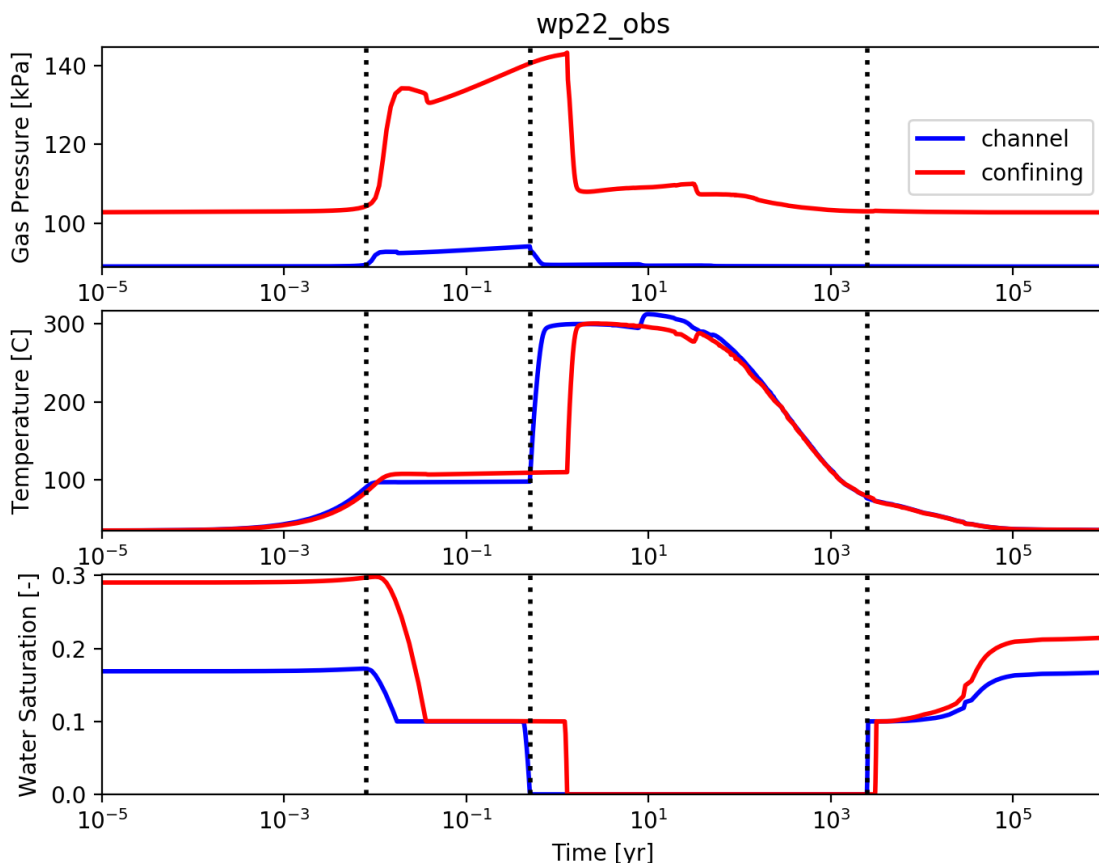
Figure 4-10. Pressure (top), Temperature (middle) and Water Saturation (bottom) at the center most waste package as a function of log time for the base case simulation with the repository located in the channel facies (channel in blue) and the original design with the formation in the confining zone (confining in red). [Black dashed lines denote the four time stages of the base case simulation: (a) initiation, (b) boil-off of water, (c) heat up, and (d) resaturation to initial condition.]

Figure 4-11 shows the gas pressure, temperature and water saturation in the center most point of the disposal array. As can be seen, the pressure and saturation hardly change in the formation between the drifts. This is because of the high permeability of the formation and the low mobility of the near-residual water that is initially present. The temperature has a modest increase to around 70 degrees due to the low dry thermal conductivity of the UZ formation rocks. The region of temperatures above 100°C is confined to the drifts.
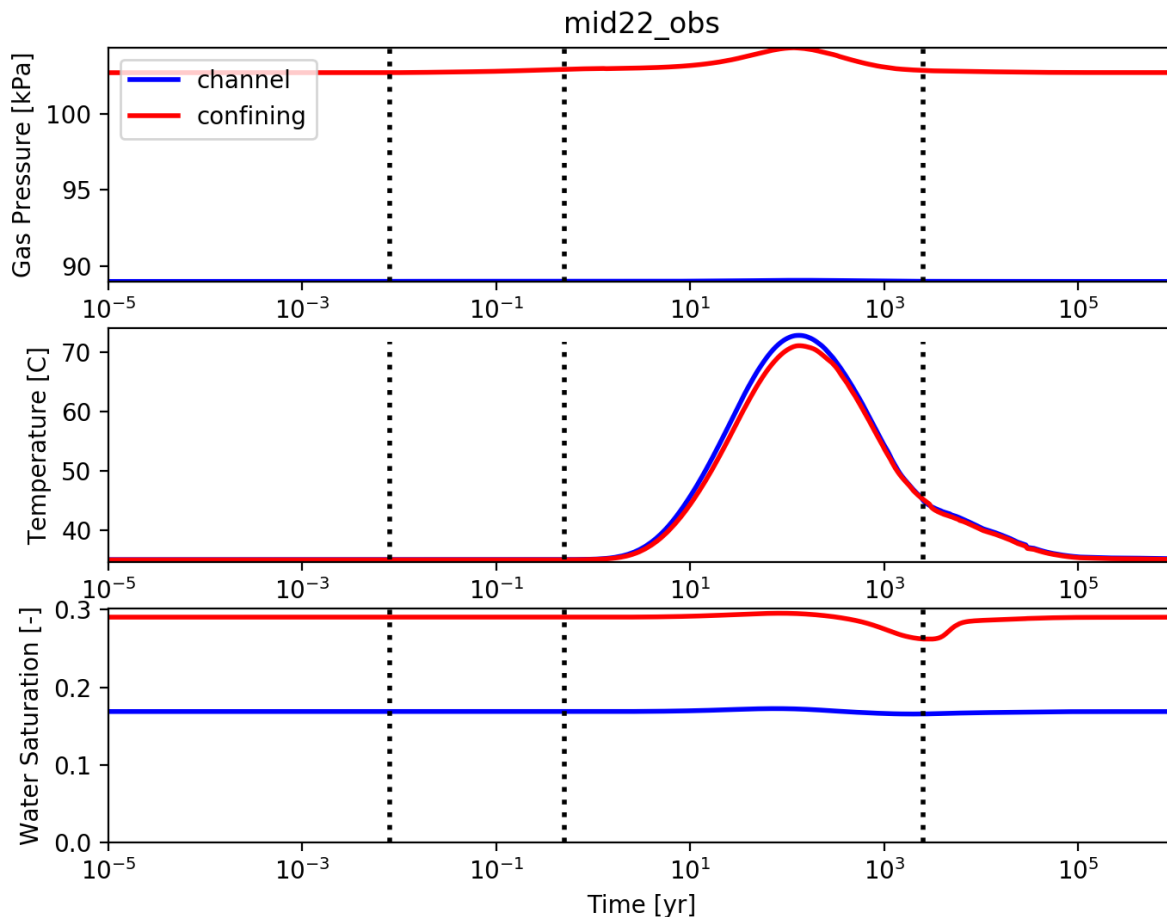
Figure 4-11. Pressure (top), Temperature (middle) and Water Saturation (bottom) at the center most point of the disposal array as a function of log time for the base case simulation with the repository located in the channel facies (channel in blue) and the original design with the formation in the confining zone (confining in red). [Black dashed lines denote the four time stages of the base case simulation: (a) initiation, (b) boil-off of water, (c) heat up, and (d) resaturation to initial condition.]

4.4.1.2 Repository in the Confining Layer

The original design for the UZ simulation had the drifts located in the lower-permeability confining layer of the formation. These simulations resulted in large increases in pressure in the confining host rock. The base case simulation with the area surrounding the drift changed from channel fill to confining layers with permeability of $1 \times 10^{-14} \text{m}^2$ is shown in Figure 4-10 and 4-11 alongside the base case.

When the model is equilibrated with the repository in the confining layers, the initial water saturation increases from 16% to around 30%, even though the relative permeability model implemented for both rock types is the same. This is because the initial model has a continual

vertical and lateral flux of water due to infiltration and the east/west pressure gradient. Water flux is governed by the relation: $q_w \propto kS_w\nabla P$. Thus, if q_w and ∇P stay the same across the equilibrated model, a decrease in permeability, k, must result in an increase in water saturation, S_w.

The lower surrounding permeability and higher water saturation in the drifts at the initial condition have a compounding effect on the pressure near the waste repository when steam is generated during the boil off stage. At 30% initial water saturation, there is a significant increase in steam that needs to escape from the drift as compared to the base case, but the surrounding rock has only 1% of the permeability thus preventing the the steam from easily escaping. Figure 4-10 shows that the pressure at the waste package increases nearly 50% above the initial pressure during the boil-off stage. In the base case the drift permeability is 1×10^{-13}m^2. If the permeability in the drift is lowered from this value, as might be necessary with high thermal-conductivity engineered backfill, the pressure at the waste packages may be unreasonably high (not shown).

Figure 4-11 shows that the pressure and saturation in the center of the array is not significantly impacted by large changes in pressure and saturation at the waste packages, though there is a small increase in pressure during the boil off stage and a small decrease in saturation at the start of the resaturation stage. The change in temperature in the midpoint of the array is similar to the base case and stays well within the acceptable range.

Due to concerns about high pressure near the waste packages in many of the scenarios considered when the waste is stored in the confining layer, and the limited advantage of disposal in the confining layer, it is recommended that the full-scale simulation have the repository located in a channel fill region.

4.4.1.3 *Waste Package Spacing in the Repository*

In this section the impact of waste package spacing is considered. As discussed in Section 4.1.1, an important design criterion is that the rock area between the drifts should not dry out. In the base case the drifts are 40 m apart and the center-to-center distance between waste packages along the drift is 40 m (40/40 case), as shown in Table 4-13. Two additional scenarios for waste package spacing are considered:

1) Drifts 40 m apart with the center-to-center distance between waste packages 20 m along the drift. (40/20m case)

2) Drifts 50 m apart with the center-to-center distance between waste packages 20 m along the drift. (50/20m case)

The simulation results at the hottest waste package are similar to the base case described above and are not shown. Figure 4-12 shows the pressure, temperature and water saturation at the midpoint of the drift array. As can be seen, the change in pressure is extremely small. The temperature for both cases with 20 m spacing along the drift is much higher than the base case, though 100ºC is never reached in either case. This is because of the smaller footprint of the waste packages in both alternate cases, sixteen waste packages in 160m^2, vs 80m^2 or 100m^2.
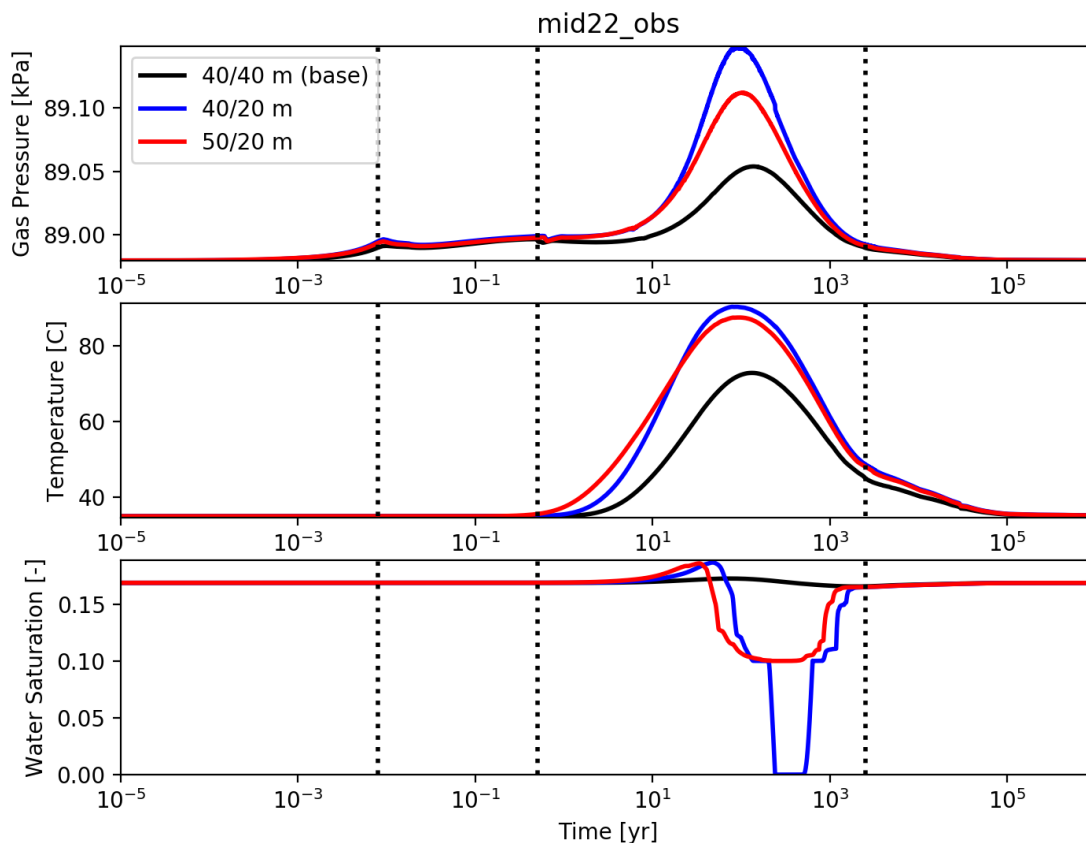
Figure 4-12. Pressure (top), Temperature (middle) and Water Saturation (bottom) at the centermost point of the disposal array as a function of log time for the base case (black), 20 m waste package spacing along the drift (blue) and 50m spacing between the drift (red). [The time domain has been divided up by vertical dashed lines into four segments: (a) initiation, (b) boil-off of water, (c) heat up, and (d) resaturation to initial condition.]
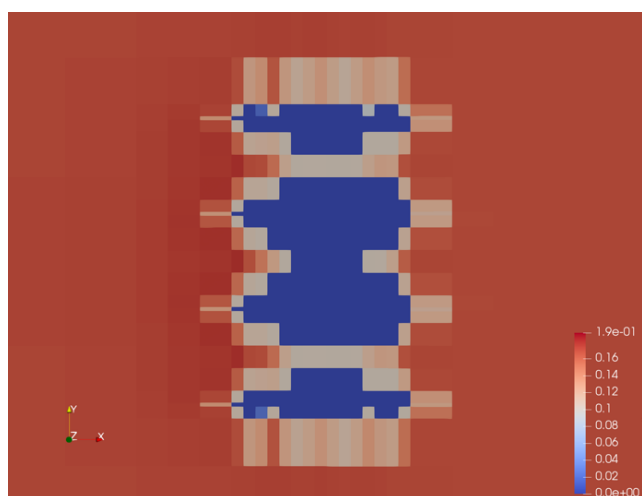
Figure 4-13. Top view of water saturation in the 40/20 m simulation at the time of maximum dry-out at 300 years. Slice is at z=255 m, through the center of the repository.

In the 40/20 m case the formation completely dries out between the drifts and so this case does not meet the desired disposal criteria (Figure 4-12). It is interesting to note that the temperature of the midpoint is around 80°C, well below the boiling point of water, when it is dry from 250 to 500

years. The mechanism behind this result is under investigation. Figure 4-13 shows a top view of the dry-out region in the 50/20 m simulation. The drifts are almost completely dry at this time.

The 50/20 m case does not dry out or experience high temperatures or pressures at any point in the simulation. As the 50/20 m case allows for more disposal per m^2 than the 40/40 m case, it is recommended that this drift and waste package spacing be used for the full-scale repository simulation.

4.4.1.4 Engineered Backfill

The base case scenario has an engineered backfill with both wet and dry thermal conductivity set equal to 2.0 W/m/K. The temperature at the drift wall is very sensitive to the dry thermal conductivity.

Figure 4-14 shows the temperature at the hottest waste package for a variety of dry (top) and wet (bottom) thermal conductivities as outlined in Table 4-8. The saturation and pressure are not very sensitive to thermal conductivity and are not shown. All simulations stop when they reach the critical temperature of water (as shown in the top figure of Figure 4–14). This is an artificial cutoff coded into the water equation of state in PFLOTRAN and has been remedied in a newly implemented water equation of state. However, any simulation that stops because the temperature reaches 374°C is too hot and does not meet design criteria.
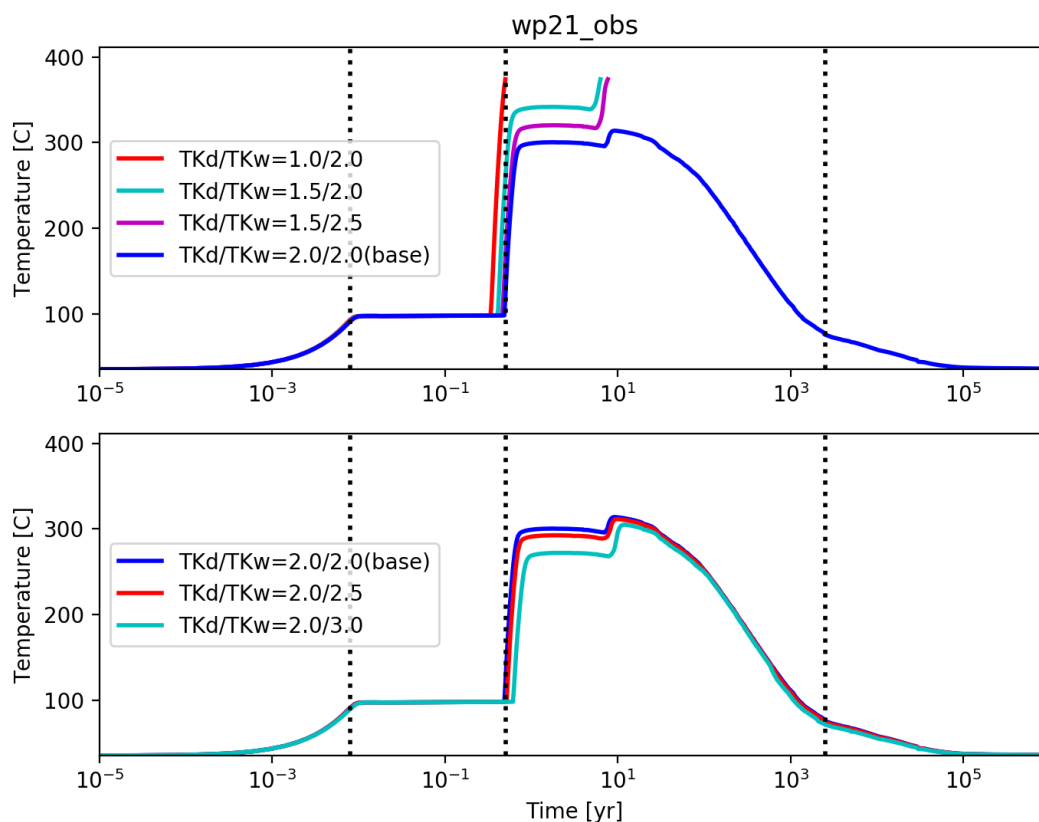
Figure 4-14. Temperature at WP(2,1), the hottest waste package for a series of dry (top) and wet (bottom) thermal conductivities as a function of log time. Simulations stop if the critical temperature of water (374ºC) is reached. [The time domain has been divided up by vertical dashed lines into four segments: (a) initiation, (b) boil-off of water, (c) heat up, and (d) resaturation to initial condition.]

In many of the simulations the hottest waste package was not in the center of the array, as in the base case. The packages at the ends of the central two drifts get hottest. This is because they are 5 m from the surrounding rock material with dry thermal conductivity 1.0 W/m/K on either the east or west side, while the waste packages in the middle of the drifts have higher-conductivity engineered backfill on both the east and west sides. On Figure 4-8 it can be seen that the 5 m of drift immediately to the east and west of the array is hotter than the drift between the waste packages from 1 to 100 years. In the cases with low dry thermal conductivity in the backfill, this thermal barrier makes the edge waste packages get hotter than the central waste packages, even though they are surrounded by other heat sources.

All the simulations with dry thermal conductivity less than 2.0 W/m/K reach the critical temperature and stop during the heat up stage of the simulations, as shown on Figure 4-14. Even the scenario with very high wet thermal conductivity of 2.5 W/m/K is unable to run to completion. Figure 4-14 also shows that the simulations are not very sensitive to the wet thermal conductivity. This is because of the low initial water saturation of 16%. For increased wet or dry thermal conductivity, it takes longer for the water to boil off near the waste packages, but once the immediate surrounding is dry, only the dry thermal conductivity matters during the heat-up stage.

Based on these simulation results it will be necessary to engineer a backfill with thermal conductivity of at least 2.0 W/m/K. It is recommended that the full-scale PA simulation have both wet and dry thermal conductivity of at least 2.0 W/m/K.

4.4.1.5 Drift Permeability

A variety of simulations exploring the impact of drift permeability were also conducted (see Table 4-8). It was determined that if the repository is in the higher-permeability basin fill part of the formation, with the corresponding low initial water saturation, drift permeability as low as 1×10^{-14} m^2 was no longer a limiting factor causing pressure build-up near the waste packages during the boil off stage. If the repository is located in the lower-permeability confining region with the resultant higher initial water saturation, then it is necessary to have relatively high permeability in the drift to prevent pressure build up, as shown in Figure 4-10.

4.4.1.6 Recommendations for Field-Scale Simulation

Based on the above simulation analyses the recommended parameters for the field-scale simulation are to have the repository in the channel-fill part of the UZ formation with the base case parameters outlined in Table 4-7. These parameters should ensure a PA simulation that fulfills the three design criteria of modest temperature and pressure increases at the waste packages, and no dry out off the formation between the drifts.

The only exception is that the waste package and drift spacing in the field-scale simulation should be 50 m between drifts and 20 m between waste packages within a drift. This drift spacing is more space-efficient than the base case 40/40 m spacing and should give a PA simulation that satisfies the design criteria considered for the flow field.

4.4.2 Field-Scale PA Simulation Results

The design parameters recommended in Section 4.5.1.6 above and shown in the base-case Table 4-7 are used here. In this scenario the 24-PWR assemblies that are 100y OoR are used as heat sources. They are considerably cooler than the 37-PWR assemblies used in the previous section.

The simulation (wall-clock) time for the coarse-scale model is very long at present (and is being investigated), so only the first 250 years of the simulation are presented in this deliverable.

4.4.2.1 Field Scale Results

Figures 4-15 and 4-16 show the temperature and saturation in the repository after 1, 10, and 100 years of disposal. As can be seen, the temperature reaches a maximum of nearly 200°C in the waste packages after around 10 years of disposal. The regions of high temperature are in the immediate vicinity of the drifts, with little or no change in temperature outside the array.

The backfill adjacent to the waste packages dries out very quickly, as can be seen in Figure 4-16. The region around the waste packages continues to dry out for the first 100 years, though the area between the drifts remains above residual for this time period. Water saturation around the array increases slightly after 100 years. This is because the water that has turned to steam in and around the waste packages flows outward and condenses in the cooler temperatures away from the array. The water saturation increases the most in the long and short halls because these are filled with high-permeability backfill (see Figure 4-16), creating preferential flow paths.

Figure 4-17 shows the pressure, temperature and water saturation as a function of log time at 5 points near the center of the array. WP1 is a waste package in the middle of the central drift. The other points are in the drift next to WP1, just outside of the drift, in what would be the damage zone, and midway between the drift containing WP1 and the next drift. This final point should represent the coolest and wettest spot in the interior of the array. The initiation time for the full-scale array lasts 23 days before the water in WP1 begins to boil off.   It takes 102 days for all the water to boil off, and the maximum temperature at the waste package is reached after 20 years and then begins to cool while the area around the drift continues to heat up. Water will begin to resaturate the waste package after centuries.

The thermal front and resultant dried out region propagate relatively quickly in the drift, with the temperature reaching the monitoring point in the drift after about 70 days, and then moves very slowly into the formation rock. The temperature in the nearby monitoring point reaches boiling after nearly 60 years, the temperature never reaches the boiling the midpoint between the two drifts during the 250 years of simulation.

A large number of other monitoring points in and around the array were also considered for completeness but are not shown. A summary of those results is as follows:

(1) The centermost waste package location has remarkably similar pressure, temperature and water saturation profiles to the waste package locations in the center of the edge drifts, and the four waste package locations at the corners of the array. The main difference is that the corner waste packages do not reach as high a peak temperature and start to cool faster than the others;

(2) At monitoring points 60 m away from the array in each cardinal direction, very little happens during the simulation. There is a small increase in pressure from 1-10 years, while temperature increases and saturation decreases starting after around 50 years and continuing until the end of the simulation; and
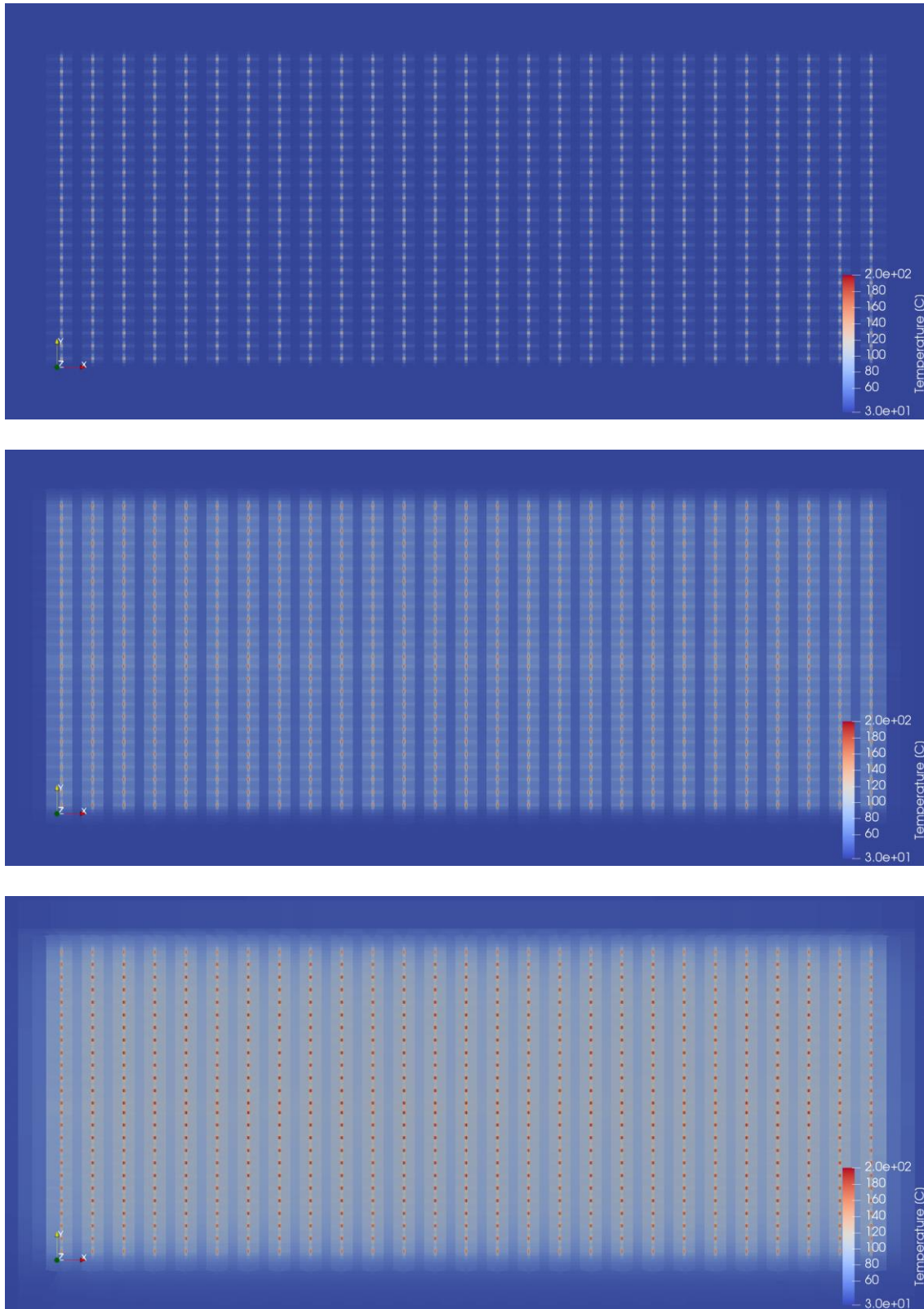
Figure 4-15. Top view of temperature in the PA-scale array in a slice through the center of the repository at z=255m at several snapshots in time. <u>Top</u>: 1 year. <u>Middle</u>: 10 years. <u>Bottom</u>: 100 years.
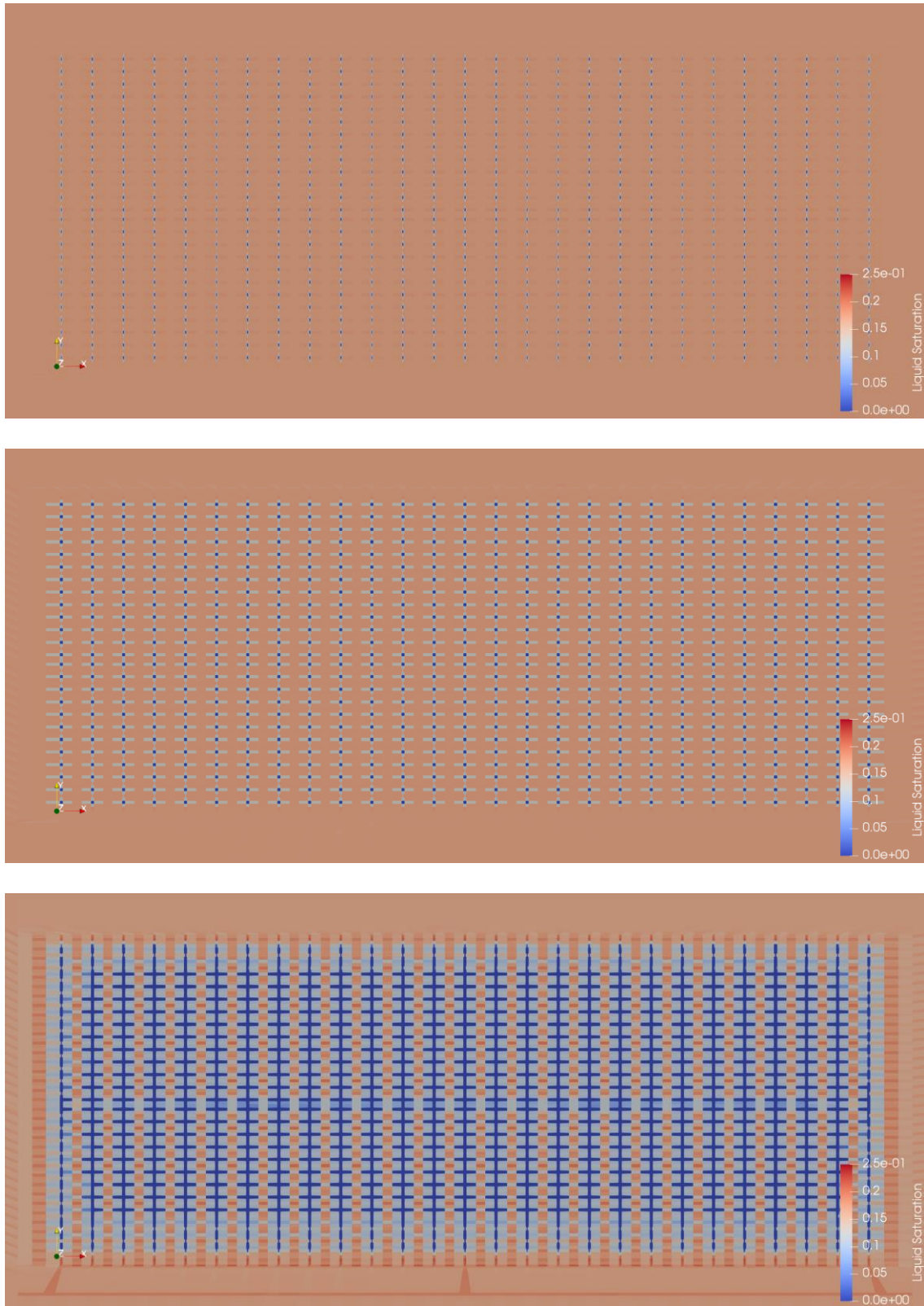
Figure 4-16. Top view of water saturation in the PA-scale array in a slice through the center of the repository at z=255m at several snapshots in time. Top: 1 year. Middle: 10 years. Bottom: 100 years.
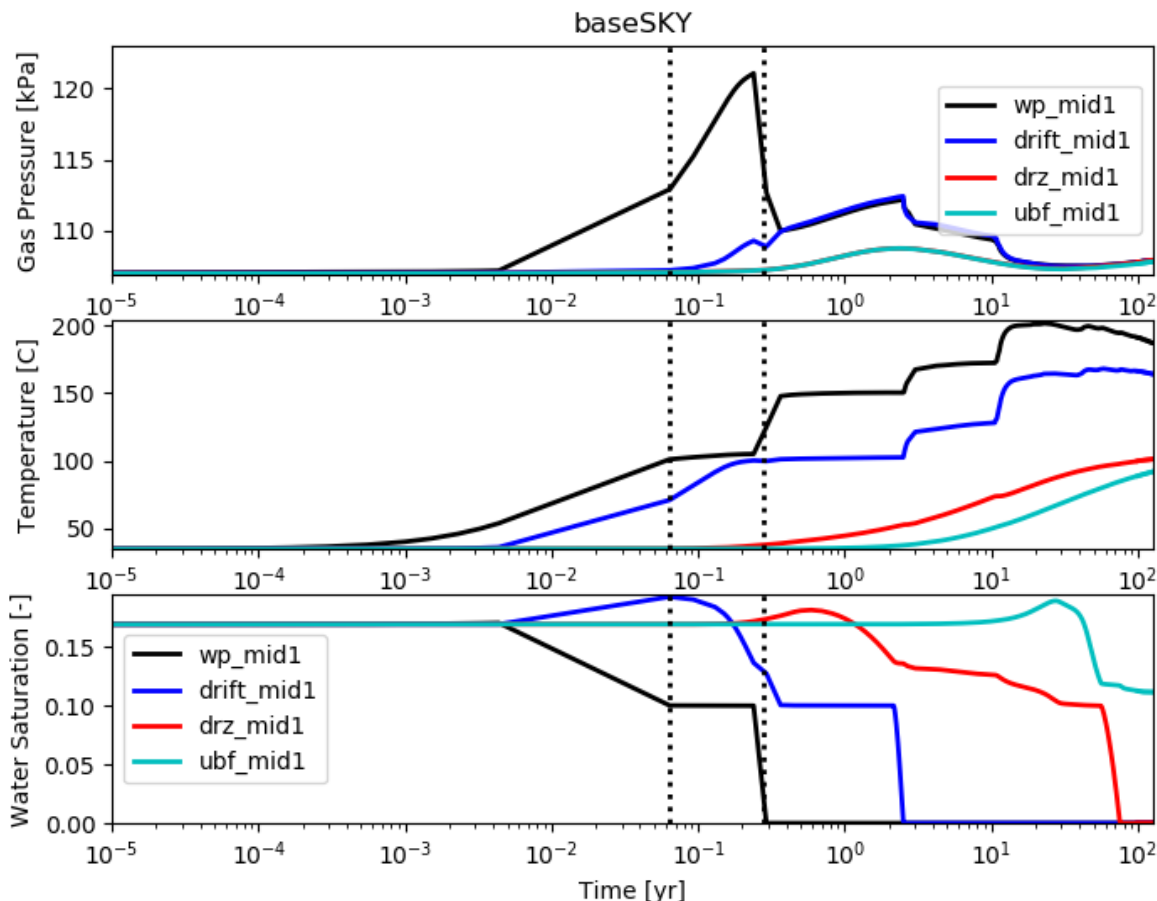
Figure 4-17. Pressure (top), Temperature (middle) and Water Saturation (bottom) near the centermost waste package in the full-scale disposal array as a function of log time. Values in the waste package are shown in black, in the drift next to the waste package is blue, just outside the drift is red, and the midpoint between the drift and the next drift east is cyan. [The time domain has been divided up by vertical dashed lines into three segments: (a) initiation, (b) boil-off of water, and (c) heat up. Resaturation to initial condition is never achieved in this 250-year simulation.]

(3) At monitoring points between the two drifts on the east and west side of the array the results are very similar to the monitoring point between the two most central drifts. The temperature is slightly lower for the corner monitoring points, and the water saturation remains near the initial water saturation for longer.

4.4.2.2   Comparison of Field-Scale Results with the Sector Model

In the field-scale model the initiation time it takes to reach 100°C is nearly an order of magnitude longer than the sector model (23 days instead of 3 days), likely due to the lower energy source in 24-PWR 100 years OoR as compared with 37-PWR 150 years OoR. On the other hand, the time to dry-out is 0.28 years for the field scale model instead of 0.5 years. The shorter time to dry-out is likely because in the sector model the drifts extended for a larger region around the waste packages due to mesh coarseness. In the sector model the drift surrounded each waste package for 5 m on each side, while in the field-scale model the entire drift is 5m wide. Thus only 1.67 m of high thermal conductivity drift material is between the waste package and the formation in the *x* and *z* directions. This doesn't seem to have much impact on the initiation time because the time

scale is too short for the temperature to have moved far into the drift before the water starts to boil at the waste package.

4.5 Observations and Recommendations for Future Work

Even using the coarser model with simplified two-phase flow parameters, computation time for flow and temperature in the field-scale simulation remains prohibitively long. There is the distinct possibility that the computations in GENERAL mode are not slow because of any issues in the simulator *per se*, but rather due to the numerical difficulty of the coupled thermal and fluid flow problem.

As can be seen in Figures 4-10 and 4-17 temperature increases extremely quickly at and near the waste packages at early times in the simulation. There are also two abrupt changes in the water saturation that propagate outward into the formation from each waste package. The first is the dry-out front as water boils off and the second is the resaturation front as water infiltrates back into the drifts when they cool off. All three of these features require very small timesteps to resolve numerically.

The following steps should be explored:

- Have the development team assess whether any changes can be made to GENERAL mode to speed up simulations

- Divide the simulation workflow up into two separate <u>areal-cale</u> simulation models. In this concept:
    - o The first model will be a finely gridded domain focusing on the smaller scale ("sector"), and will accurately capture heat, flow, and radionuclide transport near the waste packages. This model would not address issues of far field flow and transport of radionuclides.
    - o The second model will have a relatively coarse and uniform mesh covering the full domain of interest for radionuclide transport. It will be used to assess transport in the subsurface but cannot accurately capture heat and fluid flow in and around the waste packages. Heat and fluid behavior near the repository would have to be checked to be sure that the coarse model captures the same essential features as the fine scale model.
    - o UQ/SA analysis could potentially be run on only the coarse model for many of the scenarios.

- Divide the simulation workflow up into two separate <u>time-scale</u> simulation models. In this concept the two modeling stages would be on the same mesh, the extent and discretiztion of which would be suitable for modeling both near repository heat and fluid flow and far field transport of radionuclides. In this concept:
    - o The first model would run GENERAL flow mode to the compute flow and temperature for the first several hundred years or until the waste packages are relatively cool. This model would likely be very slow and should not be run many times.
    - o The second model will restart at the end of the first and be used for radionuclide transport. After the waste packages are relatively cool it should be possible to simulate in RICHARDS mode without incurring much error, though this assumption

must be verified. This will speed up the longer-term simulations enormously. Some PFLOTRAN development may be required to allow the simulation to restart in a different flow mode.

5   BEDDED SALT REFERENCE CASE UPDATE

The past bedded salt reference case (Sevougian et al. 2016) for deep geologic disposal of defense-related HLW and SNF was developed from (1) the reference case for a commercial SNF/HLW repository in bedded salt, described in Sevougian et al. (2012) and Vaughn et al. (2013), (2) the repository design proposed in Carter et al. (2012) for a defense-only repository, and (3) elements of the engineered and natural barriers described in previous performance assessments of CSNF disposal in bedded salt (Mariner et al. 2015; Sevougian et al. 2014; Sevougian et al. 2013; Freeze et al. 2013a, Clayton et al. 2011)—the characterization of which drew heavily upon parameter values developed for the Waste Isolation Pilot Plant (WIPP) performance assessments. This update relies on the same history but changes the repository design to accept 24- and 37-PWR DPCs, in a 50/50 split by weight of heavy metal for each canister size. This report details the simulations of a near-field repository model simulation that was conducted in anticipation of a full-scale PA simulation that will be documented in a September 27, 2019 M3 deliverable (M3SF-19SN010304052). Descriptions of the full-scale PA conceptual and numerical model are also included, but with no results.

The conceptual model includes a mined repository 600 m below the surface in a thick bedded salt host rock in a geologically stable sedimentary basin. Characteristics of the bedded salt host rock that contribute to or impact post-closure safety include (Freeze et al. 2013b):

- The ability of salt to creep, which is expected to heal fractures, reconsolidate crushed salt backfill, and encapsulate waste, contributing to waste containment.

- The geologic stability of deep salt beds, which have been isolated from surface processes for hundreds of millions of years and can be expected to isolate the repository for the duration of the regulatory period.

- The low permeability and porosity of the host rock, which limits exposure of waste to water, thereby limiting and delaying radionuclide releases.

- The reducing chemical environment, which limits radionuclide solubility, limiting and delaying radionuclide releases.

- The potential presence of anhydrite interbeds, which are more brittle and of higher permeability than halite, providing potential pathways for radionuclide release.

The remainder of this section includes a description of the engineered (Section 5.1) and natural (Section 5.2) barriers followed by a repository scale, deterministic post-closure assessment (PA) (Sections 5.3 and 5.4).

5.1 Engineered Barriers

Specific post-closure basis information related to the engineered barriers includes

- Characteristics of the repository (Section 5.1.1)

- Inventory characterization (Section 5.1.2)

- Waste form characterization (Section 5.1.3)

- Waste package characterization (Section 5.1.4)

- Characteristics of the buffer, drifts, and access halls (Sections 5.1.5 and 5.1.6)

5.1.1 Engineered Barrier Characteristics

For the full-scale PA, the salt reference case assumes a mined repository located 600 m below land surface, accessed by vertical shafts, and containing 35,000 MTHM of commercial SNF in 24-PWRs and another 35,000 MTHM in 37-PWRs. This inventory is accommodated with 3103 24-PWR waste packages and 2013 37-PWR waste packages in 102, 1525-m long emplacement drifts (62 drifts contain 24-PWRs and 40 contain 37-PWRs). Each drift, regardless of package type, contains 50 waste packages emplaced lengthwise and spaced 30 m center-to-center. A 25-m long seal is placed at either end of each emplacement drift. Drifts are 5.0 m per side spaced 30 m center-to-center. These dimensions are similar to those described by Hardin and Kalinina (2016, Section 3) for a 12-PWR repository in shale, and results in a total emplacement footprint of approximately 4.88 km^2 (5.24 km^2 including area for shafts, longhalls, etc.). The spacing results in ~11 W/m^2 peak heat production, after aging (see below). After rounding the number of canisters down to 3100 24-PWRs and 2000 37-PWRs to provide an even distribution across the repository, the actual inventory is 34,968 MTHM in 24-PWRs, 34,780 MTHM in 37-PWRs, for a repository total of 69,748 MTHM.

The PA simulations use a half-symmetry model domain consisting of thirty-one 24-PWR drifts and twenty 37-PWR drifts. With the reflection boundary condition, 50% (21,924 MTHM) of the 69,748 MTHM inventory is included in PA simulations. The configuration for both the full-scale and the near-field repository scale model is listed in Table 5-1.

Table 5-1. Dimensions and counts for the salt repository layout.

Parameters	Reference Case Value	Full-Scale Simulated Value	Repository Scale Simulated Value
Waste Package (WP)			
WP length (m) [24-PWRs and 37-PWRs]	5.20 [a]	5.00	5.00
WP outer diameter (m) [24-PWRs and 37-PWR']	1.37 [a]	1.67 / side	1.50 / side
WP center-to-center (m) [24-PWRs and 37-PWRs]	30.0	30.0	30.0
Inventory per 24-PWR WP (MTHM)	11.28 [c]	11.28 [c]	11.28 [c]
Inventory per 37-PWR WP (MTHM)	17.39 [c]	17.39 [c]	17.39 [c]
Number of 24-PWR WPs	3100	1550 / 3100 [b]	15
Number of 37-PWR WPs	2000	1000 / 2000 [b]	10
Emplacement Drift			
Drift diameter (m)	4.5 [a]	5.0 (on a side)	10.0 (x) / 5.75 (z)
Drift center-to-center spacing (m)	30 [a]	30	30
Number of WPs per drift	50 [a]	50	5
Drift seal length (m)	25	25	25
Drift length, including seals (m)	1525	1525	175
Repository			
Repository Depth (m)	600	600	600
Number of drifts	102	51 / 102 [b]	5
Number of shafts	Not specified	3 / 6 [b]	1
Shaft access size (m^2)	Not specified	5 x 10	5 x 5
Emplacement footprint (km^2)	4.88	2.44 / 4.88 [b]	0.023

[a] Hardin and Kalinina (2016, Section 3)
[b] half-symmetry domain / with reflection
[c] Hardin et al. (2013, Table 4-2)

5.1.2 Inventory

For simplicity, PA simulations assume that the inventory consists entirely of PWR SNF assemblies, each containing 0.47 MTHM (Hardin et al. 2013). Radionuclide inventories and decay heat versus time curves are taken from Carter et al. (2013) and assume an initial enrichment of

4.73 wt% ^{235}U for 60 GWd/MTHM burn-up fuel and 3.72 wt% ^{235}U for 40 GWd/MTHM burn-up fuel. The 24-PWRs assume a 40 GWd/MTHM burn-up rate and 50 years OoR storage prior to emplacement and the 37-PWRs assume 60 GWd/MTHM burn-up rate and 100 years OoR. Because the average burn-up of SNF under the "no replacement scenario" is predicted to be only 54 GWd/MTHM (Carter et al. 2013), the assumption of 60 GWd/MTHM results in a conservatively high heat load. Radionuclide inventory in each type of package is shown in Tables 5-2 and 5-3.

Table 5-2. 24-PWR 40-GWd/MTHM, 50-year OoR SNF inventory of selected radionuclides for the salt reference case.

Isotope	Inventory (g/MTIHM)[1]	Inventory (g/g waste)[2]	Atomic weight (g/mol)[3]	Approximate Decay Constant (1/s)[4]
^{241}Am	1.35E+03	9.36E-04	241.06	5.08E-11
^{243}Am	1.38E+02	9.61E-05	243.06	2.98E-12
^{238}Pu	1.79E+02	1.24E-04	238.05	2.56E-10
^{239}Pu	6.38E+03	4.43E-03	239.05	9.01E-13
^{240}Pu	2.57E+03	1.79E-03	240.05	3.34E-12
^{242}Pu	5.65E+02	3.92E-04	242.06	5.80E-14
^{237}Np	7.60E+02	5.28E-04	237.05	1.03E-14
^{233}U	1.32E-02	9.18E-09	233.04	1.38E-13
^{234}U	2.66E+02	1.85E-04	234.04	8.90E-14
^{236}U	4.72E+03	3.28E-03	236.05	9.20E-16
^{238}U	9.33E+05	6.48E-01	238.05	4.87E-18
^{229}Th	2.90E-06	2.01E-12	229.03	2.78E-12
^{230}Th	3.34E-02	2.32E-08	230.03	2.75E-13
^{226}Ra	7.34E-06	5.1E-12	226.03	1.37E-11
^{36}Cl	3.52E-01	2.44E-07	35.97	7.30E-14
^{99}Tc	9.16E+02	6.36E-04	98.91	1.04E-13
^{129}I	2.16E+02	1.5E-04	128.9	1.29E-15
^{135}Cs	4.86E+02	3.37E-04	134.91	9.55E-15

[1] from Carter et al. (2013, Table C-2)
[2] (g isotope/g waste) = (g isotope/MTIHM)/(g waste/MTIHM), where g waste = g all isotopes
[3] Weast and Astle (1981)
[4] Decay constants from ORIGEN (Croff 1983)

5.1.3 Waste Form

Freeze et al. (2013b, Section 3.4.1.1) provides a description of commercial SNF, including the following characteristics. Spent uranium oxide (UO_2) fuel is a polycrystalline ceramic material with stable to high temperatures and the potential for slow degradation in the disposal environment. Cladding protects the fuel from degradation in the reactor and can continue to protect the fuel from degradation in the repository. Cladding from commercial light-water reactors (i.e., boiling water reactors and pressurized water reactors) is generally made from Zircaloy, a zirconium alloy that is chemically stable and resistant to corrosion. In the reactor, fuel undergoes physical changes due to heating, radiation damage, and the build-up of fission products. Lighter elements (fission products) become concentrated in voids and the outer margins of the UO_2 matrix.

Concentration of fission products in voids of the waste form results in the waste form releasing radionuclides in two fractions: instant-release (upon waste package breach) and slow-release

(according to the UO$_2$ matrix dissolution rate). See Mariner et al. (2016, Section 3.2.2) for a description of the UO$_2$ waste form degradation model implemented in PFLOTRAN.

Table 5-3. 37-PWR 60-GWd/MTU, 100-year OoR SNF inventory of selected radionuclides for the salt reference case

Isotope	Inventory (g/MTIHM)[1]	Inventory (g/g waste)[2]	Atomic weight (g/mol)[3]	Approximate Decay Constant (1/s)[4]
^{241}Am	1.46E+03	1.01E-03	241.06	5.08E-11
^{243}Am	2.69E+02	1.87E-04	243.06	2.98E-12
^{238}Pu	2.84E+02	1.97E-04	238.05	2.56E-10
^{239}Pu	7.40E+03	5.14E-03	239.05	9.01E-13
^{240}Pu	4.11E+03	2.85E-03	240.05	3.34E-12
^{242}Pu	8.17E+02	5.67E-04	242.06	5.80E-14
^{237}Np	1.40E+03	9.72E-04	237.05	1.03E-14
^{233}U	4.33E-02	3.01E-08	233.04	1.38E-13
^{234}U	5.11E+02	3.55E-04	234.04	8.90E-14
^{236}U	6.27E+03	4.35E-03	236.05	9.20E-16
^{238}U	9.10E+05	6.32E-01	238.05	4.87E-18
^{229}Th	1.48E-05	1.03E-11	229.03	2.78E-12
^{230}Th	1.04E-01	7.22E-08	230.03	2.75E-13
^{226}Ra	3.99E-05	2.77E-11	226.03	1.37E-11
^{36}Cl	5.01E-01	3.48E-07	35.97	7.30E-14
^{99}Tc	1.28E+03	8.89E-04	98.91	1.04E-13
^{129}I	3.13E+02	2.17E-04	128.9	1.29E-15
^{135}Cs	7.72E+02	5.36E-04	134.91	9.55E-15

[1] from Carter et al. (2013, Table C-2)
[2] (g isotope/g waste) = (g isotope/MTIHM)/(g waste/MTIHM), where g waste = g all isotopes
[3] Weast and Astle (1981)
[4] Decay constants from ORIGEN (Croff 1983)

5.1.4 Waste Package

The salt reference case considers two waste package configurations: a 24-PWR waste package and a 37-PWR waste package. Both are assumed to consist of a stainless-steel canister and a stainless-steel overpack and are each assumed to be 4.7 m in length and 1.8 m in diameter (Greene et al. 2013). The 24-PWR waste package 24 PWR SNF assemblies (11.28 MTHM), scaled from the 12-PWR waste package described by Hardin et al. (2013) while the 37-PWR contains 37 PWR SNF assemblies (17.39 MTHM).

Due to gridding limitations, the size of simulated waste packages in the full-scale PA model is $1.67 \times 1.67 \times 5.0$ m, giving it a simulated volume of 13.94 m^3, as compared to the actual volume of 11.96 m^3. The waste package size in the near-field repository model is $1.5 \times 1.5 \times 5.0$ m, giving it a volume of 11.25 m^3.

Waste package porosity is set equal to 50% consistent with Sevougian et al. (2016). Permeability is set several orders of magnitude higher than that of the surrounding materials, so that flow through waste packages is uninhibited. The waste package is given the thermal properties of stainless steel (Shelton 1934). These properties may be modified in the future for consistency with the DPC criticality consequence analysis modeling proposed by Price et al. 2019.

The salt reference uses a temperature-dependent waste-package degradation rate with a truncated log normal distribution on the base degradation rate such that 50% of waste packages breach within a few tens of thousands of years. See Mariner et al. (2016, Section 4.3.2.5) for a description of the implementation in PFLOTRAN.

5.1.5 Crushed Salt Backfill

The salt reference case assumes that disposal rooms and access halls are filled with run-of-mine-crushed salt backfill. As summarized in Sevougian et al. (2012; 2013), crushed salt backfill is expected to have an initial porosity of approximately 0.35 (Rothfuchs et al. 2003), and correspondingly, permeability higher than and thermal conductivity lower than that of intact salt. Over time, it will consolidate to a state approaching that of intact salt (Hansen and Leigh 2011, Section 2.4.1.7), a process expected to be mostly complete within approximately 200 years (Clayton et al. 2012).

Following the example of Sevougian et al. (2013), to assign properties to the consolidated backfill, the full-scale PA model assumes that the backfill will evolve similarly to a crushed-salt shaft seal. Porosity and permeability values can be drawn from the WIPP parameter database (Fox 2008), which lists two distributions for the porosity and permeability of the shaft seal component in the host rock ("the lower portion of the simplified shaft seal"), one distribution for the first 200 years after emplacement and one for 200-10,000 years after emplacement. The permeability is higher during the initial period, prior to consolidation. The reference case uses the values for the initial 200-year period, because shaft seal consolidation is enhanced at WIPP with the addition of 1 wt. % water (Hansen et al. 2012, Section 4.1.1), which might not be used in run-of-mine backfill. Backfill is assigned a porosity of 0.113 (Fox 2008, Table 19) and a permeability of 10^{-18} m^2 (Fox 2008, Table 4).

5.1.6 Shaft Seals

Shafts will be sealed to prevent migration of water and radionuclides. Seals may be similar to those proposed for WIPP, consisting of clay, asphalt, concrete, and crushed salt components (James and Stein 2002). Concrete, clay, and asphalt components are expected to provide an immediate barrier to fluid flow, while the crushed salt component is expected to provide a permanent barrier to flow after consolidation (DOE 2009, Section PA-2.1.3).

The near-field repository model assumes shaft seal properties identical to those assumed for the crushed salt backfill (previous section).

5.2 Geosphere/Natural Barriers

Specific post-closure basis information related to the geosphere and natural barriers include:

- Characteristics of the natural barriers (e.g., location, geologic setting) (Section 5.2.1)

- Host rock characterization (Section 5.2.2)

- Disturbed rock zone (DRZ) characterization (Section 5.2.3)

- Characterization of additional geologic units (Sections 5.2.4 and 5.2.5)

5.2.1 Natural Barrier Characteristics

Bedded salt formations, often hundreds of meters thick, form in near-shore and shallow-marine environments during cycles of marine transgression and regression. In addition to beds of very low permeability and low porosity halite (the target for waste isolation), they may contain beds rich in other evaporite minerals (anhydrite, polyhalite), and carbonate and clastic (shale, sandstone) interbeds (Perry et al. 2014, Section 4.2.1). The present concept for a mined repository in a bedded salt formation places the repository in a stratum of relatively pure halite (> 50%) at least 76 m thick. Depth to top of the formation is between 305 m and 1067 m below land surface (Sevougian et al. 2012, Section 3.2.3), sufficiently deep to isolate the salt formation from surface processes, and shallow enough to make mining a repository technically feasible. Regionally, the topographic slope is ≤ 1°, providing little driving force for deep fluid flow.

The reference repository site occurs in a geologically stable sedimentary basin with low probabilities of seismicity and igneous activity. The bedded salt formation is expected to have a lateral extent of tens of thousands of square kilometers (Perry et al. 2014; Sevougian et al. 2012), more than sufficient for the establishment of a controlled area "no more than 5 kilometers in any direction from the outer boundary" of the repository as specified in 40 CFR 191.12 and 10 CFR 60.2 (Sevougian et al. 2012). The probability of human intrusion is reduced by siting the repository a sufficient distance from known geologic resources (other than the salt itself) such as extensive fresh water aquifers, ore deposits, fossil fuels, or high geothermal heat flux (which offers the potential for geothermal development).

Large areas fitting the depth criteria occur in the Michigan and Appalachian Basins, the Permian Basin, and the Paradox Basin, as shown in Figure 5-1. Small areas of other basins fit the criteria as well. Salt formations in the Michigan, Appalachian, Permian, and Paradox Basins range in age from Silurian (444 to 419 Ma) to Permian (299 to 252 Ma) (Sevougian et al. 2012, Section 3.2.3.1). Measured heat flow in these locations is generally between 35 and 65 mW/m^2 (Blackwell et al. 2011), though it may be locally higher or lower. At repository depth, the host rock is saturated with brine (see Section 4.2.2.1). The driving force for regional flow at depth is assumed to be on the order of 0.001 m/m, as observed in deep sedimentary basins (e.g., Downey and Dinwiddie 1988).

The full-scale stratigraphic section consists of beds of halite and anhydrite, a fractured dolomite aquifer, which is assumed to provide a potential pathway for radionuclide release, mudstone, and siltstone (Figure 5-2). The repository-scale model looks only at the halite section and does not include the mudstone or siltstone layers. Properties of each material, including the undisturbed host rock (halite) and the disturbed rock zone (DRZ) created by mining, are described in the following sections.
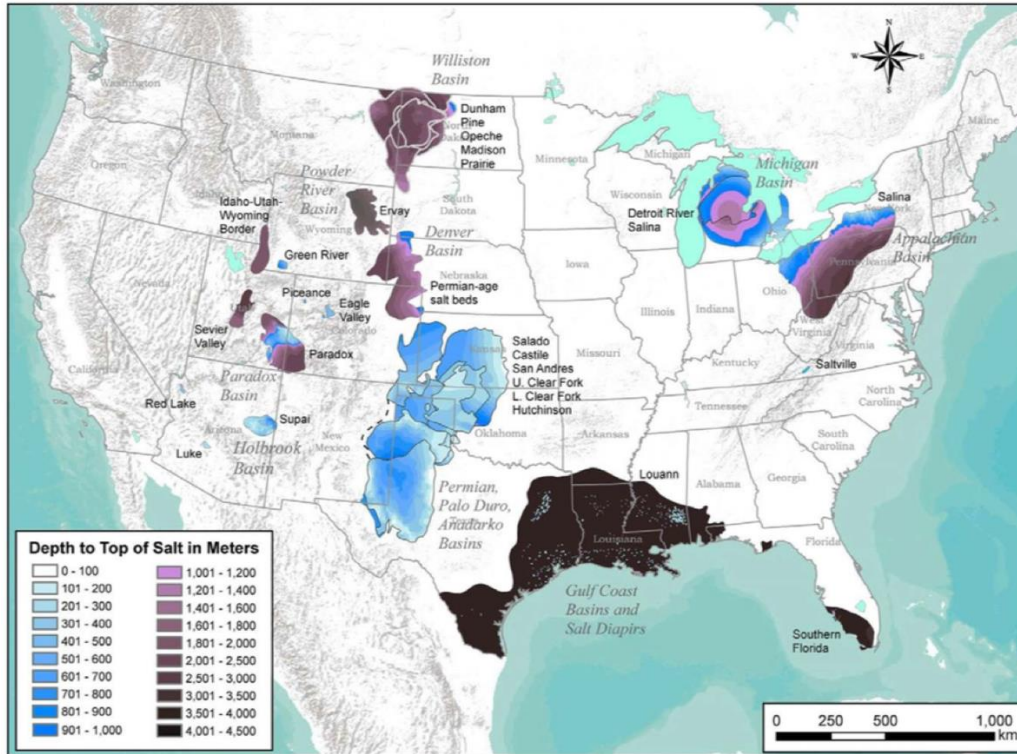
Figure 5-1. Distribution and depth to top of salt formations in major sedimentary basins of the U.S. Salt formations are labeled by name or by common reference and listed in stratigraphic order where more than one salt formation is present in a basin. [Figure from Perry et al. (2014).]
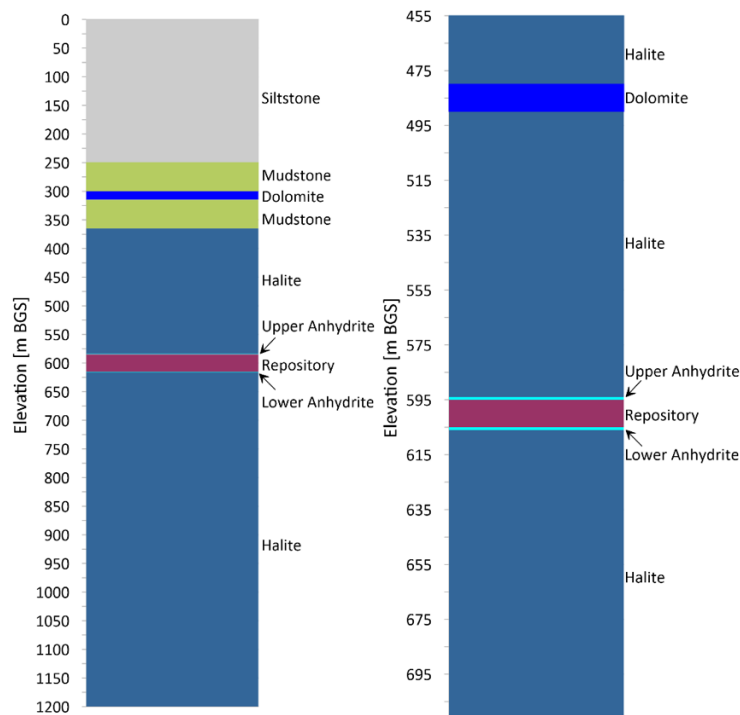
Figure 5-2. Generic stratigraphic column for salt reference case: full-scale PA domain on the left, near-field repository model domain on the right. The repository horizon, including the DRZ, is centered between the two thin beds of anhydrite at $z = 600$ m.

5.2.2 Halite Host Rock

For the full-scale PA model, the depth to the top of the halite is 355 m, and the thickness of relatively pure halite is 845 m (255 m for the repository-scale model), defining the base of the relatively pure halite at the bottom of the model domain. Within this thickness, two 1-m thick interbeds of anhydrite sandwich a 30-m thick repository horizon, which includes the DRZ. The repository in the near-field repository model is 10 m thick and does not include a DRZ. Halite is represented using permeability and porosity drawn from the WIPP parameter database. The WIPP database gives a cumulative distribution for halite porosity with a minimum of 0.001, median of 0.01, and maximum of 0.0519 (Fox 2008; Freeze et al. 2013a; Sevougian et al. 2013; 2014; Mariner et al. 2015). The near-field repository model uses the median value of 0.01.

5.2.2.1 Chemical Environment

Pore fluid chemistry will influence waste package degradation rate, waste form dissolution rate, and solubility and transport (diffusion and sorption) of dissolved radionuclides. Pore fluid chemistry is site-dependent and may vary locally depending on composition and proximity of interbeds and impurities within the halite. Representative brine compositions from several salt formations are given in Table 5-4 (Sevougian et al. 2012, Table 3-2). Solubility is discussed in the following section. The salt reference case assumes no sorption in the halite as per Clayton et al. (2011) and does not account for the effects of pore water composition on radionuclide diffusion rates. Waste package degradation and waste form dissolution are discussed in Section 5.4.2.5.

Table 5-4. Representative brine compositions for the salt reference case (Sevougian et al. 2012)

Description	Concentration (mg/l)							pH	SG
	Na+	K+	Mg2+	Ca2+	SO4 2−	Cl−	C		
1. ONWI Composite Permian Brine (Molecke, 1983)	123000	39	134	1560	3197	191380	30	7.05	NR
2. WIPP Generic Brine A (Molecke, 1983)	42000	30000	35000	600	35000	190000	700	6.5	NR
3. WIPP Generic Brine B (Molecke, 1983)	115000	15	10	900	3500	175000	700	6.5	NR
4a. WIPP GWB Salado (DOE 2009, App. SOTERM)	81150	18260	24790	560	17000	207750	NR	NR	1.2
5a. WIPP ERDA-6 Castile (DOE 2009, App. SOTERM)	111960	3790	460	480	16330	170170	980	6.17	1.22
6. MCC Brine (Molecke, 1983)	35400	25300	29600	NR	NR	164000	NR	6.5	NR
7. German Quinare Brine Q (Molecke, 1983)	6500	29000	85000	NR	13000	270000	NR	NR	NR
8. Michigan Basin Devonian Brine (Wilson and Long 1993)	12400-103000	440-19300	3540-14600	7390-107000	0-1130	120000-251000	NR	3.5-6.2	1.136-1.295
9. Paradox Formation Brine-Moab Region (DOE 2007)	9800-25966	23400-41957	21000-47789	34000-65800	80-1800	29800-259106	NR	4.8-6.0	NR
10b. Paradox Basin Mississippian Formation (Garrett 2004; Mayhew and Heylmun 1966)	132000-168000	NR	324-9000	288-14400	2160-8800	183600-264000	NR	4.6-6.7	NR
11b. Paradox Basin Paradox Formation (Garrett 2004; Mayhew and Heylmun 1966)	26640-119880	25680-63000	5160-39480	6036-51240	306-5268	145080-260640	NR	4.9-6.2	NR

a. Brines 4 and 5 are now considered more representative of WIPP conditions in recent performance assessment calculations than Brines 2 and 3 (DOE 2009, App. SOTERM, Table SOTERM-2, http://www.wipp.energy.gov/library/CRA/2009_CRA/CRA/Appendix_SOTERM/Appendix_SOTERM.htm .

b. Converted from ppm assuming an average brine density of 1.2 g/cc.

5.2.2.2 *Solubility*

Both models apply element solubility limits calculated for a concentrated, reducing brine (Clayton et al. 2011; Wang and Lee 2010) to the entire model domain. The original authors (Wang and Lee 2010) described solubility limits in terms of triangular distributions (Table 5-5). The current iteration of the reference case uses the mode of each of these distributions.

Assuming that no fractionation of isotopes occurs between the liquid and solid phases, the solubility limit of a given isotope (e.g., ^{238}Pu, ^{239}Pu, ^{240}Pu, or ^{242}Pu) in the transport domain of a cell can be calculated by multiplying the element solubility limit by the isotope's element mole fraction in the transport domain (e.g., $^{238}Pu/Pu_{Total}$) (Mariner et al. 2016, Section 3.2.4).

Table 5-5. Element solubility calculated at $T = 25°C$ in concentrated brine (Wang and Lee 2010 as cited in Clayton et al. 2011).

Element	Distribution Type	Dissolved Concentration (mol kg^1)		
		Min	**Mode**	**Max**
Am	Triangular	1.85×10^{-7}	5.85×10^{-7}	1.85×10^{-6}
Np	Triangular	4.79×10^{-10}	1.51×10^{-9}	4.79×10^{-9}
Pu	Triangular	1.40×10^{-6}	4.62×10^{-6}	1.53×10^{-5}
Sn	Triangular	9.87×10^{-9}	2.66×10^{-8}	7.15×10^{-8}
Tc	Log-triangular	4.56×10^{-10}	1.33×10^{-8}	3.91×10^{-7}
Th	Triangular	2.00×10^{-3}	4.00×10^{-3}	7.97×10^{-3}
U	Triangular	4.89×10^{-8}	1.12×10^{-7}	2.57×10^{-7}
Cs, Cl, I	N/A	Unlimited[a]		

[a] Assumed by Clayton et al. (2011).

5.2.3 Disturbed Rock Zone (DRZ)

The DRZ is defined as the portion of the host rock adjacent to the engineered barrier system that experiences durable (but not necessarily permanent) changes due to the presence of the repository (Freeze et al. 2013b). The DRZ is expected to have elevated permeability and porosity with respect to the properties of the host rock matrix due to the changes in stress induced by mining. For the full-scale PA model, the lateral extent of the DRZ within the repository is assumed to be equal to half the width of a room (or hall). Vertically, the DRZ extends to the thin (1-m-thick) anhydrite interbeds above and below the repository (a total thickness of 30 m). The simulations will include a 5-m-thick DRZ surrounding each 5-m-wide shaft. Within the halite, DRZ permeability and porosity are based on values in the WIPP parameter database: 0.0129 for porosity and 1.12×10^{-16} m^2 for permeability, which is the mean of a log uniform distribution with a range of $10^{-19.4}$ to $10^{-12.5}$ m^2 (Fox 2008; Freeze et al. 2013a; Sevougian et al. 2013; 2014; Mariner et al. 2015). The shaft DRZ is continuous from the repository to the top of the model. Where it crosses overlying units, its permeability is set one order of magnitude higher than that of the adjacent unit.

As mentioned above, the near-field repository model does not include DRZs.

5.2.4 Anhydrite

Anhydrite beds and interbeds are more permeable than the surrounding halite. Near the repository, they may become fractured as a result of the excavation, and therefore serve as potential pathways for radionuclide transport. Both models assume 1-m-thick anhydrite interbeds located immediately above and below the repository (above and below the repository DRZ for the full-scale PA model). On the basis of parameters used to characterize WIPP, anhydrite porosity is assumed to be 0.011. Log permeability (m^2) in the deterministic simulation is assumed to be −18.9 (permeability = 1.26×10^{-19} m^2), which is the mean of a Student-t distribution with a range of −21.0 to −17.1 (Fox 2008; Freeze et al. 2013a; Sevougian et al. 2013; 2014; Mariner et al. 2015).

The near-field repository model simulates radionuclide sorption in anhydrite using linear distribution coefficients (K_ds) compiled in Clayton et al. (2011), as shown in Table 5-6. K_d values for the halite, backfill, and waste package will be updated for the September 27, 2019 milestone, entitled *GDSA Repository Systems Analysis FY19 Update* (M3SF-19SN010304052).

Table 5-6. K_ds (compiled in Clayton et al. 2011) for the materials included in the near-field repository model.

Element	K_d [kg H_2O/ m^3 bulk]				
	Halite	**Dolomite**	**Anhydrite**	**Backfill**	**Waste Package**
Am	0.0	5.10e5	1.53e5	0.0	0.0
Cm	0.0	0.0	0.0	0.0	0.0
Cs	0.0	3.69e6	2.58e4	0.0	0.0
I	0.0	1.22e5	9.62e0	0.0	0.0
Np	0.0	2.44e5	1.35e4	0.0	0.0
Pu	0.0	1.22e7	2.09e5	0.0	0.0
Ra	0.0	0.0	0.0	0.0	0.0
Tc	0.0	1.22e5	2.45e3	0.0	0.0
Th	0.0	1.30e7	1.35e6	0.0	0.0
U	0.0	2.43e4	1.47e3	0.0	0.0

5.2.5 Fractured Dolomite Aquifer

The near-field repository model assumes a 15-m-thick aquifer, embedded directly in the halite. The full-scale PA model separates the dolomite from the halite by 15-m thick layers of mudstone, below a top siltstone formation (Figure 5-2). Aquifer properties are based on those of the Culebra dolomite, which occupies a similar stratigraphic position above the Salado halite at the WIPP site (DOE 2014). In deterministic simulations, aquifer porosity and permeability are derived from those of the Culebra (0.15 and 10^{-13} m^2, respectively; Fox 2008; Freeze et al., 2013a; Sevougian et al., 2013; 2014; Mariner et al., 2015).

The near-field repository model simulates sorption in the aquifer using radionuclide K_ds compiled in Clayton et al. (2011) (Table 5-6).

5.3 Biosphere

Dose to the biosphere is not addressed in the near-field repository model and thus is not discussed here. It will be part of the full-scale PA model and will be addressed in the September report.

5.4 Post-Closure Performance Assessment Model

5.4.1 Conceptual Model

The conceptual framework for the salt reference case is similar for both the full-scale and the near-field repository models and focuses on the components of the engineered barrier, the natural barrier, and the biosphere (for the full-scale model only) in the undisturbed scenario. Key characteristics of, and processes occurring in the components of each system, are summarized in Table 5-7, taken from Mariner et al. 2016 and Sevougian et al. 2016. The primary performance metric for the near-field repository model is maximum radionuclide concentration rather than dose

Table 5-7. Conceptual representation of key components in PA.

Region	Component	Key characteristics	Key processes included in PA
Engineered Barrier	Waste Form	Commercial SNF (UO_2)	Radionuclide decay, instant release fraction, waste form dissolution
	Waste Package	Stainless steel	Degradation and breach
Natural Barrier	Halite	Low permeability, high heat conductance	Radionuclide advection, diffusion, sorption, decay
	DRZ	Enhanced permeability	Radionuclide advection, diffusion, sorption, decay
	Dolomite Aquifer	High permeability, potable water	Radionuclide advection, diffusion, sorption, decay
Biosphere	Regional Flow	Regional flow in aquifer to model boundary	Radionuclide advection, diffusion, sorption, decay

Processes accounted for in the conceptual model include waste package degradation, waste form (UO_2) dissolution, equilibrium-controlled radionuclide sorption and precipitation/dissolution, radioactive decay and ingrowth in all phases (aqueous, adsorbed, precipitate), coupled heat and fluid flow, and radionuclide transport via advection and diffusion. Mechanical dispersion is conservatively neglected in this iteration of the salt reference case. Including it would result in earlier arrival of radionuclides at observation points, but lower peak concentrations.

5.4.2 Numerical Implementation

For this report, the near-field, repository model establishes model control parameter values to maximize computational performance and accuracy for the full-scale model. For September, the PA simulations will comprise one full-scale deterministic simulation and a suite of 50 probabilistic simulations. The unstructured mesh of the full-scale model was gridded with Cubit (Blacker et al. 2016). Probabilistic inputs for the simulations will be prepared using Dakota's Latin Hypercube Sampling (LHS) capability. Both models simulate flow and transport with PFLOTRAN (Hammond et al. 2014).

5.4.2.1 Model Domain and Discretization

Two model domains were gridded, the near-field repository model and the full-scale PA model. The near-field model assumes a small, mined repository 600 m below the land surface, accessed by a single vertical shaft, and containing 170 MTHM of commercial SNF in 24-PWR waste packages and another 173 MTHM in 37-PWR waste packages. This inventory is accommodated with fifteen 24-PWR waste packages and ten 37-PWR waste packages in five 175-m long emplacement drifts (three drifts contain 24-PWRs and two contain 37-PWRs). Each drift, regardless of package type, contains five waste packages emplaced lengthwise and spaced 30 m

center-to-center. A 25-m long seal is placed at either end of each emplacement drift. Drifts are 10.0 m wide and 10.0 m tall, which is larger than the full-scale PA model but is necessary to accommodate the larger scale structured grid. The drifts are spaced 30 m center-to-center, which results in ~11 W/m^2 peak heat production, after aging. The domain is 240 m × 275 m × 255 m (*X* × *Y* × *Z*) in size, split into 53 × 55 × 54 grid cells (157,410 total grid cells) that vary in width but are limited to a maximum of 5 m. Figure 5-3. is a full block and *X-Y* cross section through the repository that shows the access halls, drifts, waste packages, shaft, and the anhydrite layers. Figure 5-4 shows similar cuts in the *X-Z* and *Y-Z* orientations.
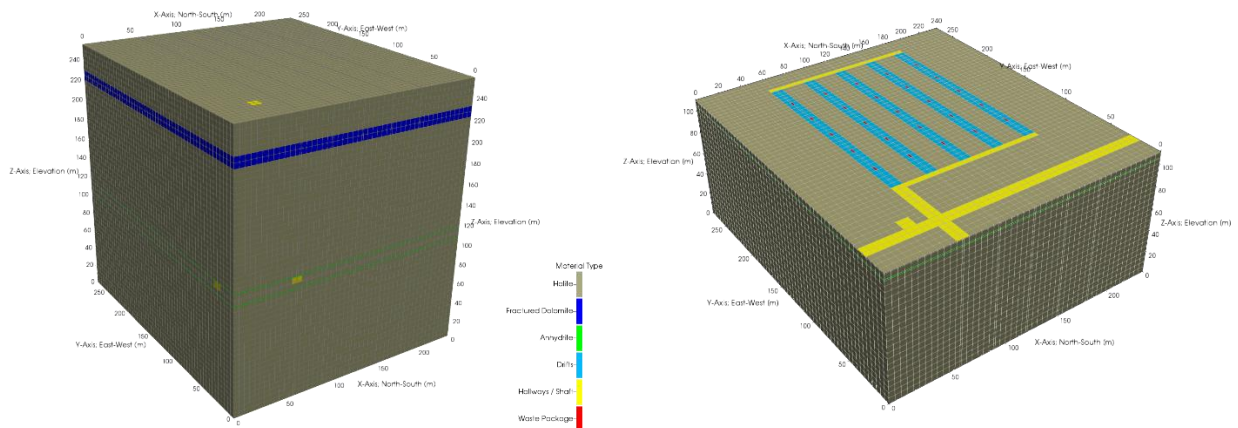
Figure 5-3. Repository-scale full domain (left) and X-Y cross section showing the various material types in the model. Drifts are numbered left to right (north to south) 1 to 5 and waste packages are numbered bottom to top (west to east) 1 to 5 (e.g., waste package 2_3 is the third waste package in the second drift).
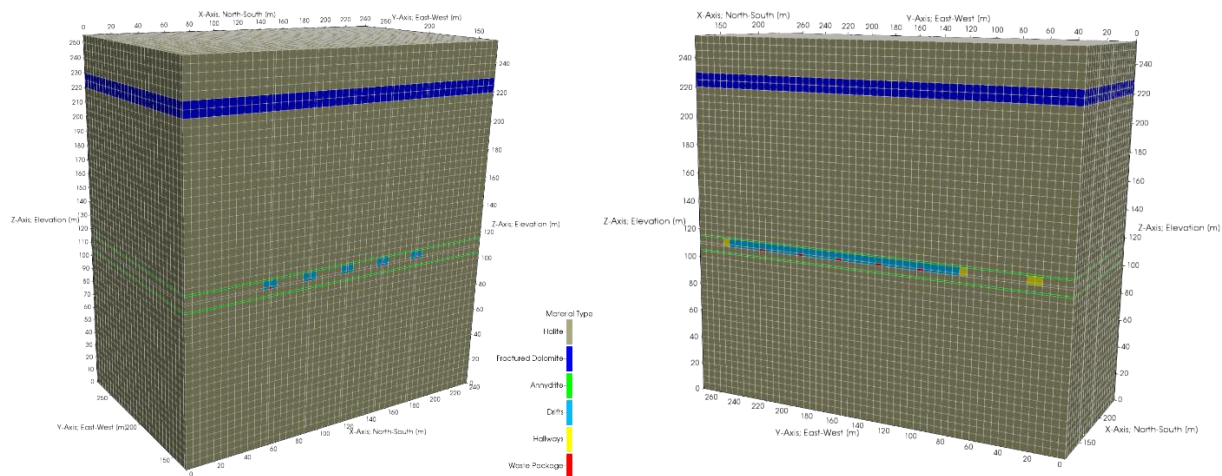
Figure 5-4. Cross-sections in the X-Z (left) and Y-Z (right) planes through the repository-scale model domain.

The full-scale PA grid also assumes mined repository 600 m below the land surface, accessed by six vertical shafts, and containing 34,968 MTHM of commercial SNF in 24-PWRs and another 34,780 MTHM in 37-PWRs. This inventory is accommodated with 3100 24-PWR waste packages and 2000 37-PWR waste packages in 102 emplacement drifts 1525-m in length (62 drifts contain 24-PWR packages and 40 contain 37-PWR packages). Each drift, regardless of package type, contains 50 waste packages emplaced lengthwise and spaced 30 m center-to-center. A 25-m long

seal is placed at either end of each emplacement drift. Drifts are 5.0 m wide on all sides and are spaced 30 m center-to-center, which results in ~11 W/m² peak heat production, after aging.

The half-symmetry model domain is 2250 m in width (*Y*; east-west), 1200 m in height (*Z*; elevation), and 7155 m in length (*X*; north-south). The *X* domain is long enough to place an observation point 5000 m down gradient from the edge of the repository (regional flow is north to south). The default grid size for most of the domain is 15 m in each direction, which is refined to 5 m per side in the repository area, and 5/3 m per side in the drifts. The grid consists of 9,156,747 elements and 9,313,850 nodes.
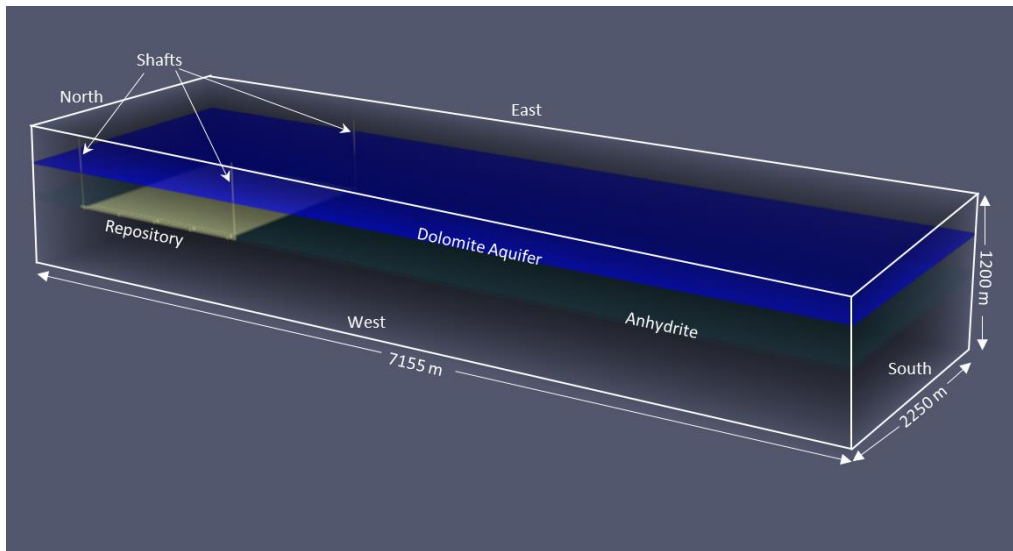
Figure 5-5. Full-scale PA model grid showing the repository and shafts in relation to the dolomite aquifer and anhydrite layers.

5.4.2.2 Initial Conditions

For the full-scale PA, initial conditions specified are pressure, temperature, and radionuclide concentrations. Initial pressures and temperatures throughout the model domain are calculated by applying a liquid flux of 0 m/s and an energy flux of 60 mW/m2 to the base of the domain and holding temperature (10°C) and pressure (approximately atmospheric) constant at the top of the domain and allowing the simulation to run to 106 years. Pressure at the top of the domain decreases from north (left) to south (right) with a head gradient of −0.0013 (m/m). This technique results in initial conditions that represent a geothermal temperature gradient and hydrostatic pressure gradient in the vertical direction, and a horizontal pressure gradient that drives flow from north to south. Simulations include the 18 radionuclides listed in Section 5.1.2. Initial concentrations of all radionuclides in all cells are 10^{-20} mol/L.

The near-field repository model is similar to the full-scale PA except that the bottom boundary is set to no-flux and the temperature is set at a constant 25°C.

5.4.2.3 Boundary Conditions

Boundary conditions must be set for the six faces of the model domain. For both the full-scale PA model and the near-field repository model, fluxes of heat, fluid, and solute are set to zero at the west face of the model domain, creating a reflection boundary. At all other faces, initial pressures

and temperatures are held constant, with a pressure gradient of −0.0013 m/m between the north and south faces. Radionuclide concentrations are held such that any fluid entering the model domain contains 10^{-20} mol/L of each radionuclide, while fluid exiting the model domain carries ambient concentrations. Diffusive flux across outflow boundaries is disallowed by specifying a zero-concentration gradient.

5.4.2.4 Waste Package Heat Sources

Each waste package is modeled as a transient heat source. The energy (watts per waste package) entering the model domain is updated periodically according to values in a lookup table that is generated from the inventory in Carter et al. (2013, Table C-1). To keep the initial heat-load consistent between the 24-PWR packages and the 37-PWR packages, the inventory in the 24-PWR canisters is assumed to be 50 years OoR with a burn-up of 40 GWd/MTHM while that in the 37-PWR canisters is assumed to be 100 years OoR with a burn-up of 60 GWd/MTHM. This results in initial heat generation of 7058 W for the 24-PWR packages and 8810 W for the 37-PWR packages. Between times specified in the lookup table, the energy input is linearly interpolated. A plot of the heat generation decay for each canister type is shown in Figure 5-6.
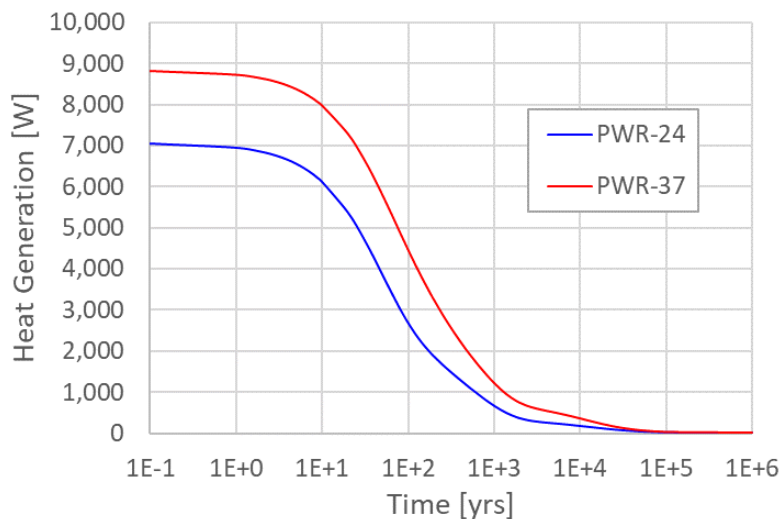
Figure 5-6. Plot of heat generation over time for the PWR-24 and PWR-37 canisters.

5.4.2.5 Waste Package Breach and Radionuclide Source Term

The waste package degradation model implemented in PFLOTRAN (Mariner et al. 2016, Section 4.3.2.5) calculates normalized remaining canister thickness at each time step as a function of a base canister degradation rate, a canister material constant, and temperature. Waste package breach occurs when this thickness reaches zero. Deterministic simulations assign a base canister degradation rate for each waste package by sampling on a truncated log normal distribution with a mean of $10^{-4.5}$/yr, a standard deviation of 0.5 (log units) and an upper truncation of −3.0 (log units). The mean and standard deviation parameter values used in these simulations are placeholders used to approximate the conceptual timeline for waste package failure as presented in Wang et al. (2014, Figure 2-19), where the waste package failure period extends from $10^{-4.3}$ to $10^{-6.5}$ yr, while also including heterogeneity across waste packages. Mechanistic models and appropriate data are needed for robust simulation of waste package degradation under predicted environmental conditions.

PFLOTRAN calculates the decayed radionuclide inventory in each waste package region at each time step. From the time of waste package breach, the waste form releases radionuclides in two fractions: instant-release and slow-release. The instant-release fraction is due to the accumulation of certain fission products in void spaces of the waste form and occurs at the time of waste package breach. The salt reference case assumes a non-zero instant-release fraction for ^{135}Cs, ^{129}I, ^{99}Tc, and ^{36}Cl (Johnson et al. 2005) and zero for all other radionuclides in the simulations. The slow-release fraction is due to fuel matrix (UO$_2$) dissolution, which is modeled using a fractional dissolution rate of 10^{-7}/yr starting from the time of waste package breach. This rate is the mode of a log triangular distribution appropriate for fuel 3,000 – 10,000 years OoR and strongly reducing conditions – for a complete discussion refer to Sassani et al. (2016, Section 3.2.1). Probabilistic simulations sample on the waste form dissolution rate over the range 10^{-8}/yr to 10^{-6}/yr but simplify the distribution to log uniform rather than log triangular. This distribution is identical to that used in the most recent generic crystalline repository PA (Mariner et al. 2016).

Dissolution rates for the near-field repository model set to 1×10^{-6} / day. for both waste forms.

5.4.2.6 Material Properties

Material properties for the full-scale PA model are not yet finalized and thus are not reported here. For the near-field repository model, the material properties are listed in Table 5-8.

Table 5-8. Parameter values used in deterministic simulations. [Compiled from Fox 2008; Freeze et al. 2013a; Sevougian et al. 2013, 2014; Mariner et al. 2015.]

Model Region	Permeability (m^2)	Porosity ϕ	Tortuosity τ	Effective Diffusion Coefficient[1] (m^2/s)	Saturated Thermal Conductivity (W/m/K)	Heat Capacity (J/kg/K)	Grain Density (kg/m^3)
Halite	3.16×10^{-23}	0.01	1.0	1.0×10^{-11}	5.0	880	2180
Dolimite	1.00×10^{-13}	0.15	0.11	1.65×10^{-11}	1.4	920	2820
Anhydrite	1.26×10^{-19}	0.011	0.20	2.2×10^{-11}	1.4	890	2700
Backfill	1.00×10^{-18}	0.113	0.20	2.6×10^{-11}	1.4	880	2180
Waste Package	2.40×10^{-14}	0.50	1.0	5×10^{-10}	16.7	466	5000

[1] Effective diffusion coefficient = $D_w \phi \tau s$, where the free water diffusion coefficient (D_w) = 1 x 10^{-9} m^2/s (Li and Gregory 1974) and saturation (s) = 1

5.5 PA Simulation Results for the Near-Field Repository Model

The near-field repository model results presented here are preliminary and are meant to verify the model set-up and parameter settings. As such, these results will change and will be included with the full-scale PA simulations for the September 27 M3 deliverable. To examine the results, we look at temperature and select radionuclide concentrations at various points in the domain, including the waste packages themselves and the aquifer.

Figure 5-7 shows the observation points monitored for the simulation in relation to the repository layout. The EstObs, SthObs, WstObs, and NthObs exist at both the repository and aquifer elevation and are distinguished below using '_repo' or '_aq' suffixes (e.g., EstObs_repo is in the repository). The star labeled 'Top/Bot' are points at the indicated x-y location on the top and bottom face, respectively. The 'a' and 'd' 'D' points are centered between drifts 1 and 2 and 3 and 4 at the

repository elevation and are averaged to get the centerline value. As a reminder, there is an approximate −0.0013 groundwater pressure gradient from north to south.
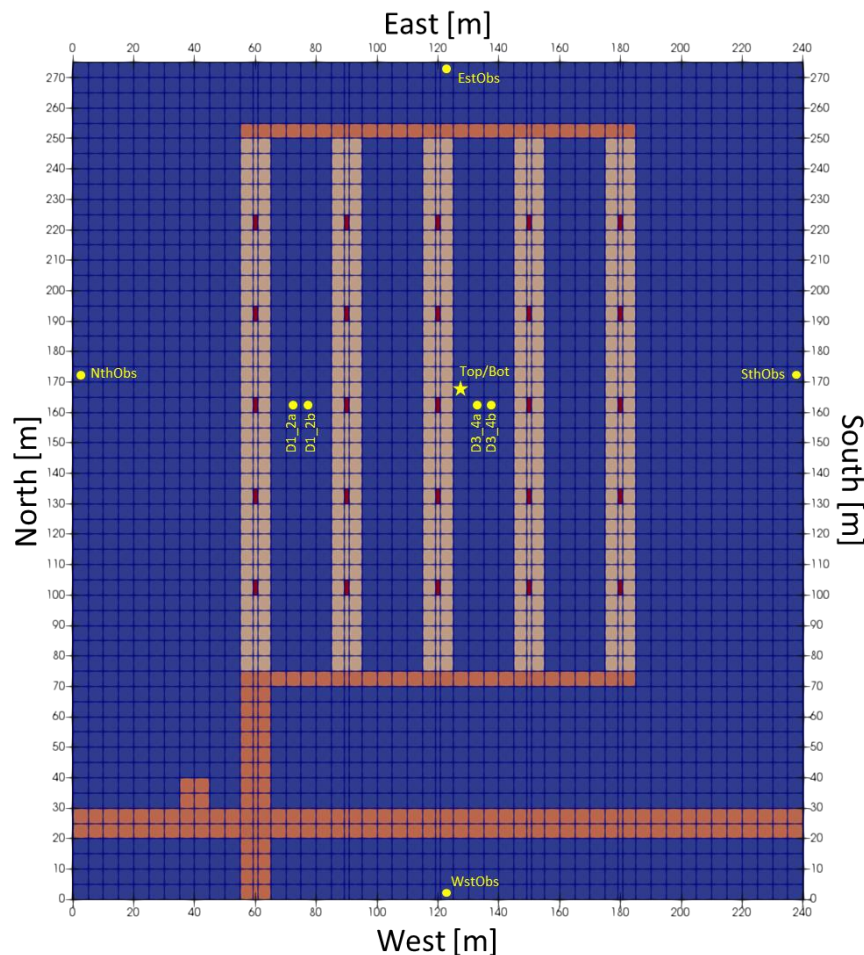
Figure 5-7. Plan view of the observation points referenced in the results sections below. The EstObs, SthObs, WstObs, and NthObs exist at both the repository and aquifer elevation. Top/Bot refers to the x-y position of observation points on the top and bottom faces. The 'a' and 'b' 'D' points between the drifts are at the repository elevation and are averaged to get the centerline value.

5.5.1 Temperature and Flow Fields

The initial temperature across the entire repository is 25°C. The waste packages heat up and dissipate relatively quickly, with peak temperatures reached by the 24-PWR waste packages and 37-PWR packages between the second and third year. For both canister sizes, they are within 10% of the initial temperature after 50,000 years. The 24-PWR packages reach an average peak of about 300°C while the 37-PWR packages peak are about 360°C. Both temperatures are well above the defined limit of 200°C and are likely caused by the mis-match between the canister size and the grid spacing. Figure 5-8 shows the plots of temperature over time for the middle waste package (WP #3) in each drift (left plot) and for the cell immediately downgradient of the waste package (right plot). There is a clear difference between the heat generated by the 37-PWR packages and that of the 24-PWR packages, although both cool down to nearly the same value after 50,000 years. Also note how the relative temperature of the adjacent cells increases in the downgradient direction, except for Drift 5, which is along the repository boundary.
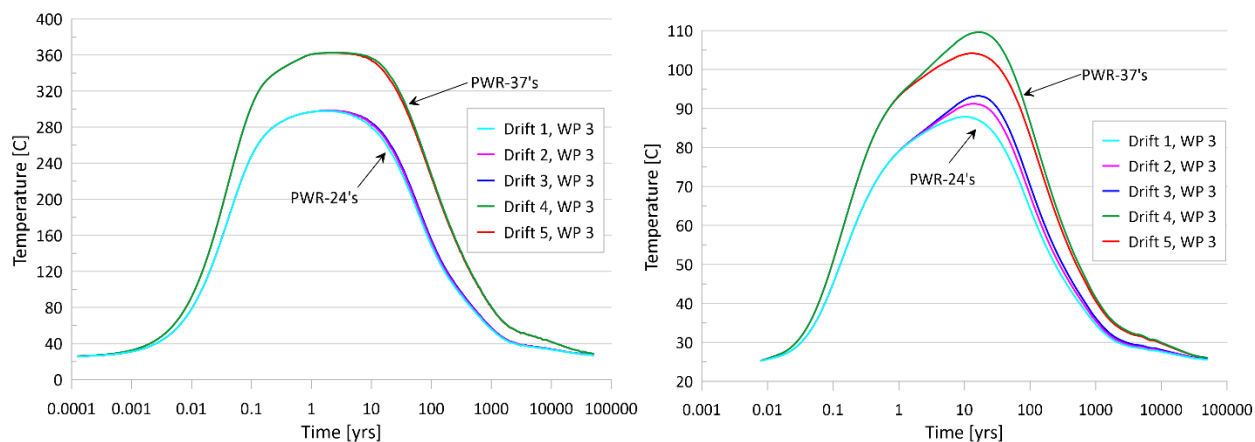
Figure 5-8. Waste package temperature versus time (left plot) and cell temperature for the cell immediately downgradient of the waste package (right plot) for the third (middle) waste package in each drift.

Figure 5-9 shows the temperatures at the various observations points, which appear to be behaving as expected. Temperatures along the southern boundary of both the repository and the aquifer are higher than any of the other boundaries due to the north to south regional flow. The eastern boundary is warmer than the western boundary, mainly because the western boundary is twice the distance from the repository than the eastern boundary. Likewise, the temperature on the bottom face of the domain is higher than the top, due to it being closer to the repository and the fact that the higher permeability aquifer is between the repository and the top of the model domain. Temperatures at the centerline between Drifts 3 and 4 are higher than the centerline between Drifts 1 and 2 since Drift 4 contains the hotter PWR-37 waste packages.

One anomaly that is not yet clear as of this writing is the relatively high temperatures along the northern boundary. Examination of the transport plots below indicate that there may be a density flow effect that is causing warmer water from the repository to be forced up-gradient by cooler water from the boundary. This may be an artifact of the proximity of the boundary condition, which should theoretically not be an issue in the full-scale model.

5.5.2 Waste Package Breach

The near-field repository model simulates just 25 waste packages so a full statistical analysis of waste package breaching is not relevant; however, it is still useful to examine the rate of breaching over time. Over the 50,000-year simulation period, approximately 64% of the waste packages have been breached, 73% of the PWR-24 waste packages and 50% of the PWR-37 waste packages. Figure 5-10 shows a plot of the total percent of waste packages breached along with a fitted exponential model. Extrapolating the model forwards indicates that all the waste packages should be breached after about 90,000 years.
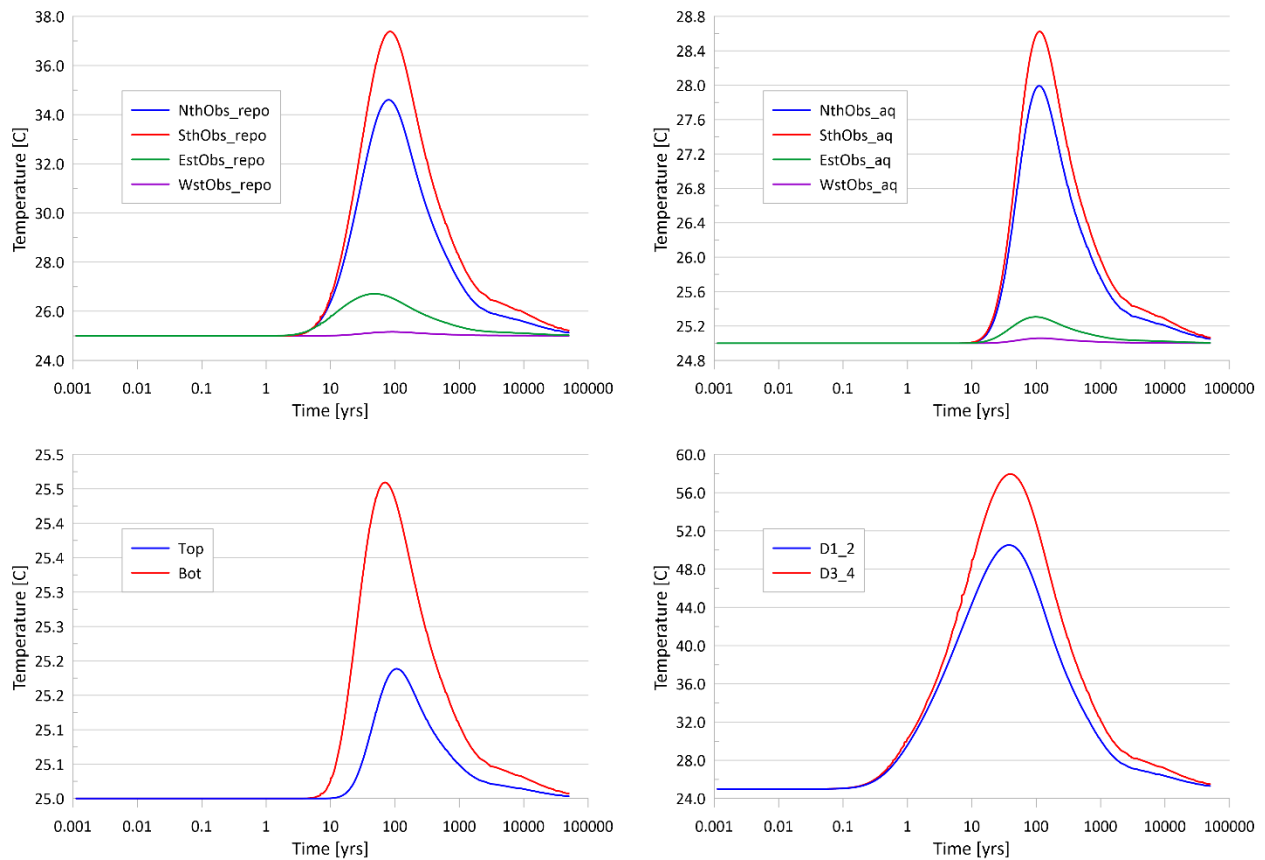
Figure 5-9. Plots of temperature over time at the various observation points. [See Figure 5-7 for the observation point locations.]

5.5.2.1 Radionuclide Transport

To investigate radionuclide transport, ^{237}Np is considered, since it is relatively persistent over the 50,000-year simulation period. Figure 5-11 shows the molar ^{237}Np concentration at three different times; 1000 years (upper left), 10,000 years (upper right), and 50,000 years (bottom left and right). At 1000 years, only one waste package has been breached, which is clearly evident in the figure. At 10,000 years, three waste packages have been breached, which is also evident. At 50,000 years, the spread of ^{237}Np covers nearly all the repository, despite only 64 % of the waste packages being breached. Evidence for the density can be seen in the 50,000-year plan view (bottom right) where a 'tongue' of water from the repository has moved towards the northern border (towards the left in the figure) as cooler water from the boundary pushes itself into the repository. The plan view plot also shows transport through the higher permeability backfilled access halls.
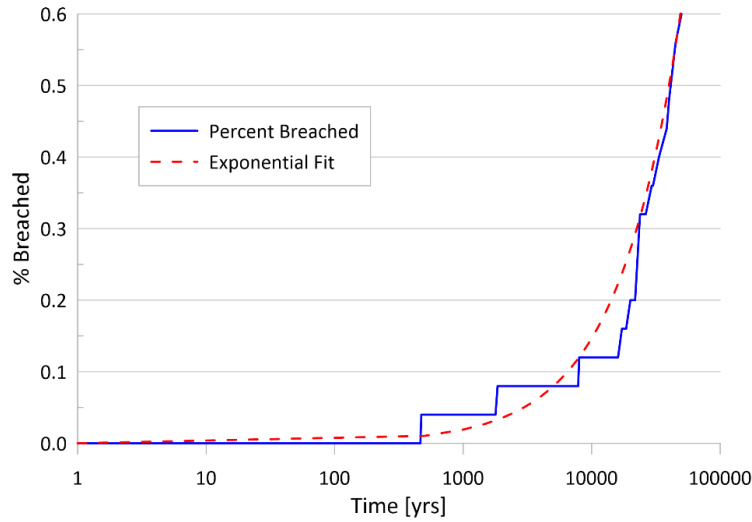
Figure 5-10. Percentage of the waste packages breached over time along with a fitted exponential model of the breach rate.
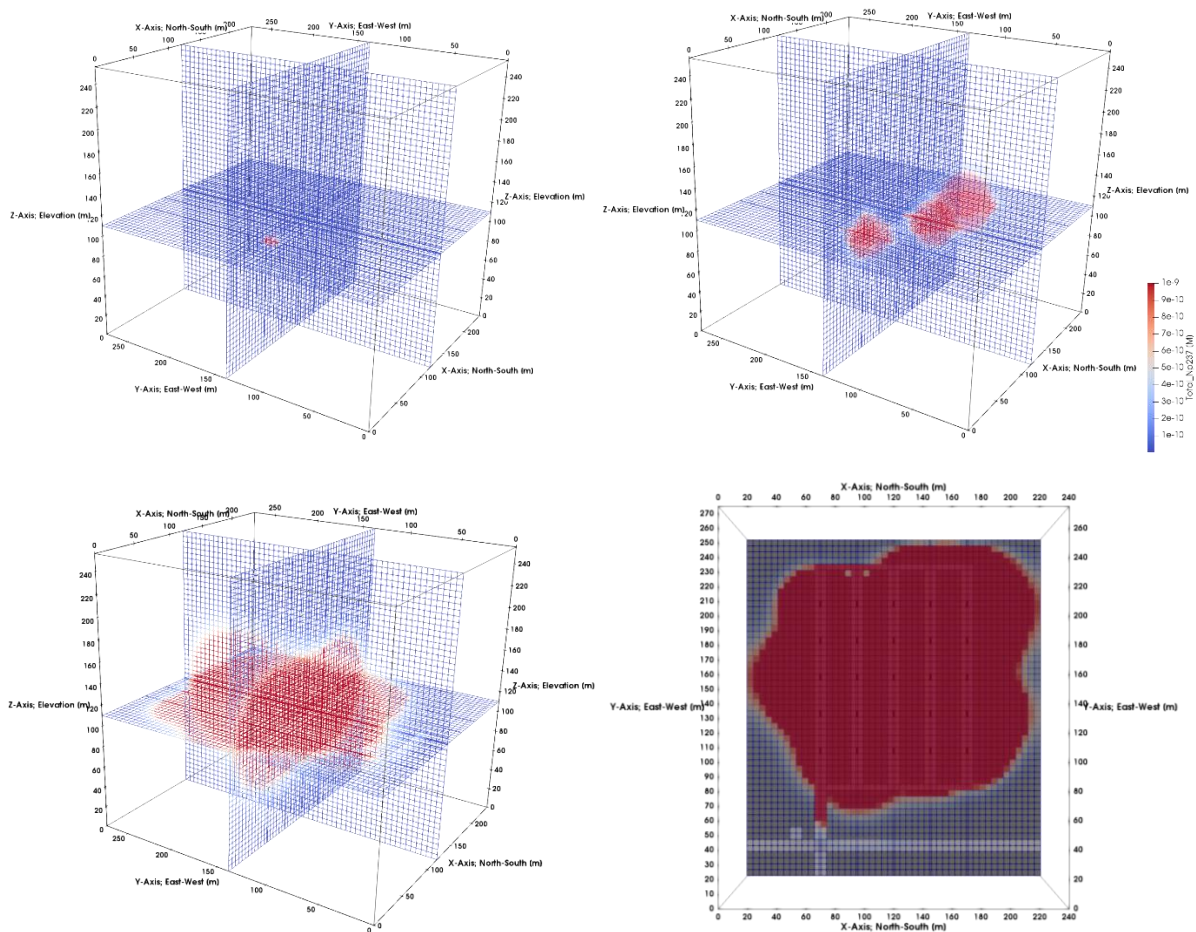
Figure 5-11. The concentration of ^{237}Np [M] at 1,000 (upper left), 10,000 (upper right), and 50,000 (lower left) years. The lower right plot shows a plan view of the ^{237}Np concentrations at 50,000 years at the repository elevation underlaid by a map of the repository. Transport along the drifts and halls is readily apparent at 50,000 years.

Figure 5-12 shows two cross sections looking from the northwest corner towards the southwest for ^{237}Np and ^{135}Cs along a *y*-plane through Drift #3 and along an *x*-plane through the shaft. The presence of both nuclides is evident in the aquifer and shaft. The importance of the access hall to transport is seen in the ^{135}Cs plot as evidenced by its red color on the x-plane cross section. The contamination in the aquifer appears to mainly come from vertical movement above the repository for ^{237}Np whereas the transport mechanism for ^{135}Cs to the aquifer is through the access halls and shaft. This is due to the higher K_d value for ^{135}Cs in the anhydrite, which slows its vertical transport as compared to the ^{237}Np.
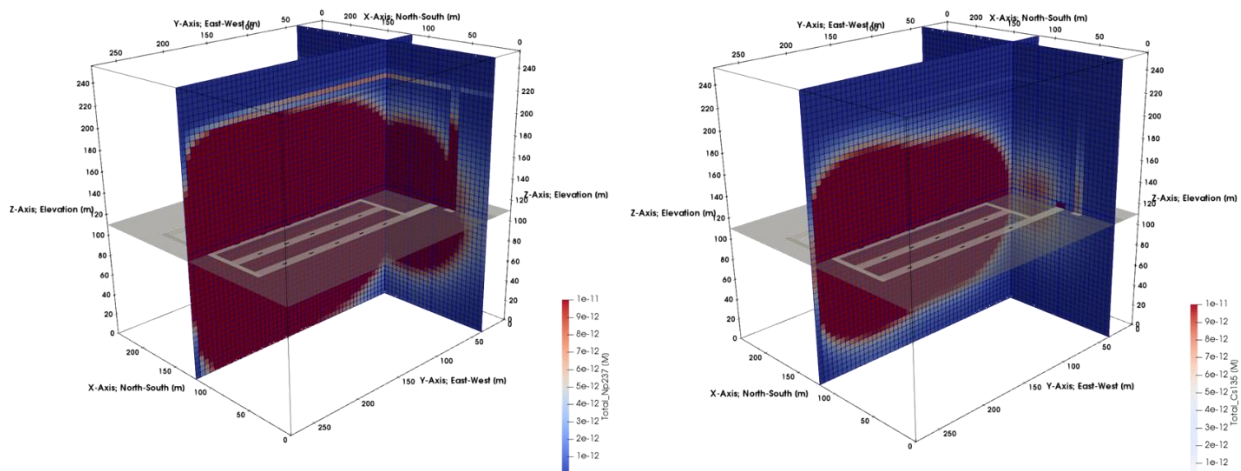
Figure 5-12. Cross-sections through the middle of Drift #3 in the repository along the y-plane, and through the middle of the shaft along the *x*-plane for ^{237}Np (left) and ^{135}Cs (right).

5.6   Bedded Salt Reference Case Conclusions and Future Work

The work presented here is preliminary and meant to be a precursor to the full-scale salt reference case to be reported in the September 2019 M3 deliverable. The near-field repository model provides expected results for its 50,000-year simulation and provides confidence that the repository conceptual model and numerical design will be suitable for the full-scale PA simulations. However, several important steps need to take place before those simulations can occur:

1. Expand the near-field repository model to include coarse-grid far-field boundaries to remove boundary influences on the repository. Right now, the near-field model assumes constant pressure and constant temperature boundary conditions, which is impacting the results. Understanding the influence of the boundary conditions will be important.

2. Reconcile parameter values to represent the current state-of-the-art. Currently, parameterization has built upon the lineage of past studies but did not adequately consider conflicting values and/or conceptualizations. While much of this reconciliation will be addressed through the upcoming probabilistic simulations, we want to ensure that parameter values agree, to the best that we can, with the most current estimations.

3. Determine the cause of the high temperatures in the waste packages. This may or may not be a modeling artifact but as of this writing, the cause is not clear.

4. Examine flow paths and fluid velocities more carefully, which was not done as part of this milestone. This will have an impact on both model set-up and computational efficiency and will help determine the impact of density flows, as theorized above, on the spread of radionuclides and to what extent the boundary conditions are impacting transport.

6   SHALE REFERENCE CASE UPDATE

This section describes updates to the generic shale reference case reported in Mariner et al. (2017). Section 6.1 discusses progress on modeling and software for a generic shale Geologic Framework Model, including the geologic and hydrologic features represented in the initial shale GFM. Section 6.2 shows a fine-scale (i.e., high resolution grid) for the EBS, developed for the eventual goal of showing how processes at this scale can be coupled to a coarser-scale PA grid. Finally, Section 6.3 reports progress on developing a full-scale generic shale host rock repository containing 24-PWR and 37-PWR DPC-canisterized commercial SNF, which will be an update to Mariner et al., 2017 and will be reported on more completely in M3SF-19SN010304052, *GDSA Repository Systems Analysis FY19 Update*.

A conceptual model of the Natural Barrier System (NBS) for the shale reference case was presented by Perry and Kelley (2017) and Mariner et al. (2018) based on the geology and geologic setting of the Pierre Shale in the Northern Great Plains Province of the north-central U.S. Several of the key points of the shale conceptual model are summarized here.

The Pierre Shale was chosen as the basis of the shale conceptual model due to its large areal extent, thickness (>400 meters), accessible depth, stable tectonic history and desirable mechanical and hydrologic properties (Perry and Kelley 2017). The Pierre Shale is near the top of a thick sequence (>1km) of sedimentary rocks dominated by marine shales in the upper part and sandstones and limestones in the lower part. The regional evaluation of the Pierre Shale provided a reference stratigraphy and hydrologic properties of the sedimentary units based on the stratigraphic column of the region (Perry and Kelley 2017).

Based on properties of the Pierre Shale, the generic shale host rock is conceptualized as a sealing shale, i.e., a shale with high clay content, low permeability, and low compressive strength (Bourg 2015). Shales under consideration for nuclear waste repositories and carbon capture and disposal fall in the category of sealing shales, while shales that are hydraulically fractured for oil and gas extraction have distinctly different properties and can be categorized as brittle shales (Bourg 2015).

The relationship between the clay content of shales and their hydrologic/mechanical properties are summarized by Perry and Kelley (2017) and Mariner et al. (2018). The Pierre Shale is typically comprised of 65 to 85% clay minerals (best estimate 70%) and has a porosity between 0.09 and 0.33 (best estimate 0.21) (Nopola 2013). Permeability calculated from laboratory measurements, borehole tests, and regional-scale flow models falls between 10^{-21} and 10^{-19} m^2 (Neuzil 1993; Neuzil 1994; Konikow and Neuzil 2007), although the permeability of individual samples (Neuzil 1986) and estimates of regional permeability based on the assumption of permeable faults can be higher (Bredehoeft et al. 1983). The compressive strength of the shale is =17 MPa (Gonzalez and Johnson 1985), and fractures induced by mining can be expected to self-heal within 20 years (Nopola 2013). Due to the high clay content, thermal conductivity is low – regional heat flow models assume a saturated thermal conductivity of 1.2 W/m/K (Forster and Merriam 1997).

The permeability of shale may be scale-dependent due to regional fracture networks (Bredehoeft et al. 1983; Neuzil, 1986, 1993, 1994). From numerical simulations of the regional flow system in the Northern Great Plains, Bredehoeft et al. (1983) concluded that vertical leakage from the Dakota Sandstone into the overlying Cretaceous shale units constituted the dominant flow in the overall groundwater system. The hydraulic conductivity of the shales (i.e., the Pierre Shale) estimated from the simulations indicate a regional-scale permeability on the order of 10^{-16} m^2, which is several orders of magnitude higher than permeabilities estimated from laboratory and borehole

tests reported in the same report. The higher permeability estimated at the regional scale suggested to Bredehoeft et al. (1983) that flow in the shale was primarily through vertical fractures, while permeabilities measured at smaller scales represented intact shale.

Neuzil (1993, 1994) pursued the question of the scale-dependent permeability in shales, and, for the case of the Pierre Shale, the relationship between low permeability, fractures, and the ability of the shale to preserve anomalously low fluid pressures. Neuzil (1993) measured low fluid pressures within the formation interior that he concluded were created by erosion and rebound of the Pierre Shale. The geologic forcing was rapid relative to the time required for fluid pressures to re-equilibrate (i.e., return to steady state flow) within the low-permeability shale, allowing preservation of low fluid pressures. With this model, Neuzil (1993; 1994) was able to reconcile the apparent discrepancy in permeabilities estimated at the large (regional) and small scale. He concluded that a system of sparse transmissive fractures (spacing of greater than a few kilometers) could account for higher (10^{-16} m^2) regional permeabilities (scale >100 km) while allowing lower permeabilities to be preserved in intervening and unfractured large blocks. If this concept is correct, it would be desirable to site a repository within a large block that has preserved low fluid pressure (i.e., inward flow) over long time periods (Neuzil 1994). On this same topic, Neuzil (2015) observed that formations with pressure anomalies (either low or high) have smaller ratios of permeability to formation thickness compared to formations with no pressure anomalies. In other words, formations with low permeability can maintain pressure anomalies over length scales (formation thickness) that a formation with higher permeability could not. From this relationship, Neuzil (2015) concluded that the presence of pressure anomalies within shale indicate a sizeable volume of low permeability rock where transport is dominated by diffusion rather than fracture flow. This conclusion has implications for siting of a repository within a thick and really extensive shale body.

6.1 Geologic Framework Model for the Shale Reference Case

The purpose of this section is to describe the methods used to develop a Geologic Framework Model for a representative shale environment and to briefly describe the geologic and hydrogeologic features represented in the GFM. A full discussion of the geology and hydrogeology of the region represented by the GFM and the implications for the shale conceptual model is left to a later report.

Shale has been evaluated as a potential geologic media for HLW disposal in the U.S. for more than four decades (e.g., Shurr 1977; Hansen et al. 2010; Perry and Kelley 2017). Several studies have focused on the Pierre Shale in the Northern Great Plains province as a potential host rock because of characteristics considered favorable to repository siting. These characteristics include a stable tectonic environment, large aerial extent, accessible depth, adequate thickness, high clay content, and an overall lack of natural resources that could lead to human intrusion (Perry and Kelley 2017).

Construction of the GFM is the first step in developing a workflow that consists of constructing the GFM, exporting the relevant features of the GFM for meshing, and using the mesh for flow and transport modeling in PFLOTRAN. This discussion focuses on the mechanics of creating the GFM as the first step of the workflow. The shale GFM described here represents a relatively simple geologic environment of a horizontally layered sedimentary rock sequence consisting predominantly of shale formations interbedded with limestone and sandstone formations.

A second goal of the GFM development is to determine the extent to which a GFM can be developed using publicly available data. This would be relevant for a future site screening and site evaluation process where existing geologic and hydrologic information would be integrated for assessing and screening alternative candidate sites. At the site characterization stage, new data would be collected and incorporated into the GFM.

6.1.1 Development of the GFM

Modeling of a shale reference case benefits from representing a realistic geological environment (the NBS). Regional assessments of the Pierre Shale have shown it has many characteristics considered desirable to host a HLW repository (Shurr 1977; Gonzales and Johnson 1985; Perry and Kelley 2017). Once the decision was made to base the GFM on the Pierre Shale and its geologic and hydrologic environment, the following steps were used to develop the GFM:

1. Define the GFM domain based on an understanding of the regional geologic and hydrogeologic setting.

2. Identify available data that will be used to construct the initial GFM.

3. Define the stratigraphic column that will be represented in the GFM based on the known stratigraphy of the region and the availability of information contained in borehole logs.

4. Import a digital elevation model (DEM) that represents the land surface and the upper surface of the GFM.

5. Import borehole data into the GFM software and evaluate alternative interpolation methods to represent the upper and lower surfaces of geologic formations.

6. Calculate the geometry of the GFM based on the preferred interpolation method for representing formation surfaces.

7. Evaluate the results of the 3D stratigraphic model using 3D block diagrams and 2D cross-sections to compare with established information on regional geology.

8. Evaluate how features of the GFM (surfaces or volumes) can be exported for mesh generation.

The shale GFM was developed using RockWorks17® software (Rockware Inc., www.rockware.com), which allows import and management of borehole logs, interpolation of formation surfaces, modeling of stratigraphy and other geologic features and 2D/3D visualization of models.

6.1.2 Defining the GFM domain

The area chosen for the GFM is based on formation thickness and depth data presented in Perry et al. (2014) and Perry and Kelley (2017). We focused on areas where the Pierre Shale has a thickness of at least 400-500 meters and where the top is at or near the surface, allowing construction of a HLW repository in a depth range of approximately 300-500 meters. The region represented by the GFM is in the northern Great Plains Province of the north-central U.S. and to the northeast of the Black Hills uplift (Figure 6-1). The Black Hills uplift, which dominates the hydrologic processes of the region, is one of several uplifts that formed near the easternmost margin of the Laramide Orogeny that formed the Rocky Mountains.

Paleozoic and Mesozoic sedimentary rocks ramp up towards the Black Hills in the southwest area of the GFM and dip generally to the north towards the Williston Basin and away from the Black Hills uplift (Driscoll et al. 2002). The upper part of the stratigraphic column in the region consists of upper Cretaceous sandstones and shales (including the Pierre shale near the top of the section), lower Cretaceous sandstones (a regional aquifer), and Jurassic through Triassic shales and sandstones (Driscoll et al. 2002; Fahrenbach et al. 2010; Table 6-1). The lower part of the section consists of Paleozoic limestones and sandstones (Table 6-1).
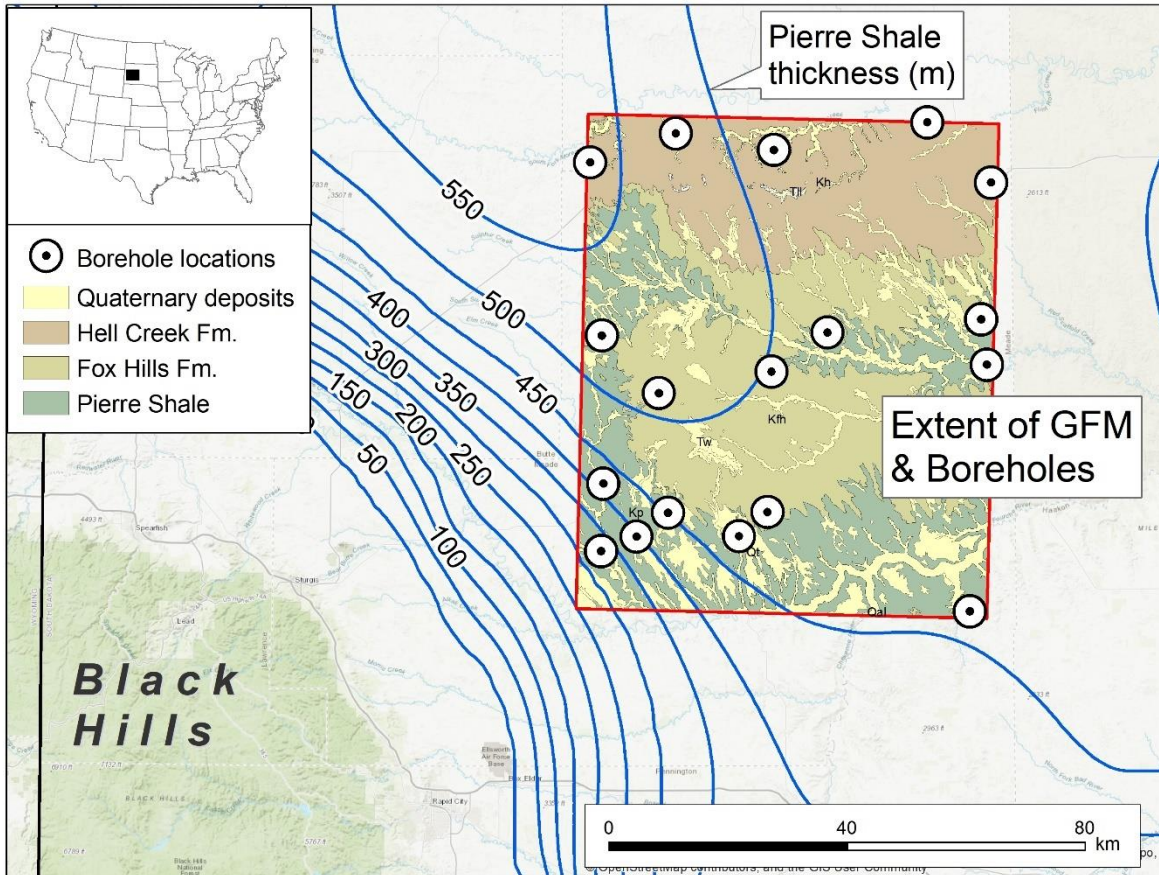
Figure 6-1. Location of the GFM and boreholes used as data inputs. [The surface geology of the GFM region is from Martin et al. (2004). Thickness contours for the Pierre Shale are from Perry et al. (2014).]

The areal extent of the GFM was chosen to provide a relatively large regional representation of the geology (dimensions of several 10s of kilometer). The size of the region allows for potential down-selection to smaller model domains within this area if smaller domains are desired for flow and transport modeling. The region meets the following criteria related to siting considerations:

1. The top of the Pierre Shale lies at a depth of ~100 meters or less so that it is reasonably accessible for site characterization and repository construction.

2. Thickness of the Pierre Shale is in the range of 400-600 meters to accommodate a repository at a depth of ~300-500 meters while still allowing a thickness of shale beneath the repository of at least 100 meters (and effectively more, given that older shale formations with a combined thickness of several hundred meters lie beneath the Pierre Shale).

3. A reasonable number of boreholes are within the region, i.e., enough to provide data on the basic subsurface characteristics of the regional stratigraphy, but not as many as would be found in a major oil and gas producing region.

6.1.3 Data Inputs

Development of a GFM requires data to constrain the subsurface geology and hydrology of a specific region. The most important data are geologic maps that provide a context for understanding the distribution of rock units and structure at depth and borehole data that provide information on the depth and thickness of specific geologic and hydrologic units. Geologic mapping is available in GIS format for import into the GFM (Martin et al. 2004). The geologic map provides information on the distribution of sedimentary formations and how they intersect the land surface (Figure 6-1).

Borehole data was obtained from the South Dakota Geologic Survey Online Databases website (http://www.sdgs.usd.edu/other/db.aspx). The borehole data necessary for constructing GFMs resides in two online databases, the Lithologic Logs Database (primarily water wells) and the Oil and Gas Database. For this version of the GFM, we relied on the Oil and Gas Database because these boreholes have more consistent picks of downhole stratigraphy. The borehole logs supply the formation elevation data that is the basis of defining the geologic surfaces in the GFM. We also used cross sections based on borehole logs in the region of the GFM from Fox et al. (2009) to further define the set of specific boreholes that would be useful as data inputs into the GFM.

Groundwater studies supply information concerning the regional hydrology and the distribution of aquifers in the GFM region. A study of the hydrology of the Black Hills area (Driscoll et al. 2002) provides information on the geologic and hydrologic framework to the immediate southeast of the GFM region and is applicable to the area of the GFM. Hydrologic properties of the formations in the upper 1200 meters of the stratigraphic column represented in the GFM were summarized by Perry and Kelley (2017). These properties will be reviewed and expanded to include all the formations represented in the GFM in a future report.

6.1.4 Representation of Stratigraphy in the GFM

The stratigraphy represented in this initial version of the GFM was derived from information in oil and gas borehole logs and verified against the established understanding of the stratigraphy of the region (Fahrenbach et al. 2010). The Oil and Gas Borehole Database contains data for depth to formations tops for the formations encountered in each borehole. Borehole data was downloaded for a 120 by 160 km region to the immediate north and east of the Black Hills uplift. This region contains records for 75 boreholes. These boreholes were screened for those containing depth data (formation 'picks') for the top of the Niobrara Formation. Establishing the elevation of the top of the Niobrara Formation is key to construction of the GFM because it defines the base and thickness of the Pierre Shale throughout the region. The boreholes with data for the Niobrara Formation were evaluated for their distribution within the region and to identify a sub-region with an adequate number and spacing of boreholes to allow for construction of the GFM (Figure 6-1). The sub-region selected defines the boundary of the GFM and has dimensions of 69 by 83 km (Figure 6-1). These dimensions reflect small adjustments to allow inclusion of a several boreholes that were located near the GFM boundaries. The GFM region can be clipped to smaller areas of any orientation if smaller modeling domains are desired within the larger region of the GFM. Twenty-three boreholes within the GFM region contained elevation data for the Niobrara Formation. A

few of these boreholes added little additional data of value because of locations near other boreholes or because they provided data for only the uppermost formations due to relatively shallow borehole depths. Removal of these boreholes left 18 boreholes that were used to construct the stratigraphy of the GFM (Figures 6-1 and 6-2).

The stratigraphy represented in the GFM is detailed in Table 6-1 and displayed as 3D borehole logs in Figure 6-2. Several decisions were made to simplify the stratigraphy represented in the GFM (Table 6-1). The uppermost formation (not including surficial deposits) in the region is the Hell Creek Formation, which has a similar lithology as the underlying Fox Hills Formation. The Hell Creek Formation was not picked in any of the boreholes and was therefore combined with the Fox Hills formation for purposes of constructing the GFM. The deepest unit represented in the GFM is the Madison Group, a limestone aquifer (Figure 6-2). Geologic units below the Madison Group were not consistently identified in the borehole logs and the data was insufficient to define formations below the Madison Group. The base of the Madison Group was therefore defined as the base of the GFM, with a depth of between 1450 and 1800 meters beneath the surface. The surface of the Precambrian basement (McCormick 2010) lies approximately 500 meters below the Madison Formation and is shown for reference in subsequent figures.
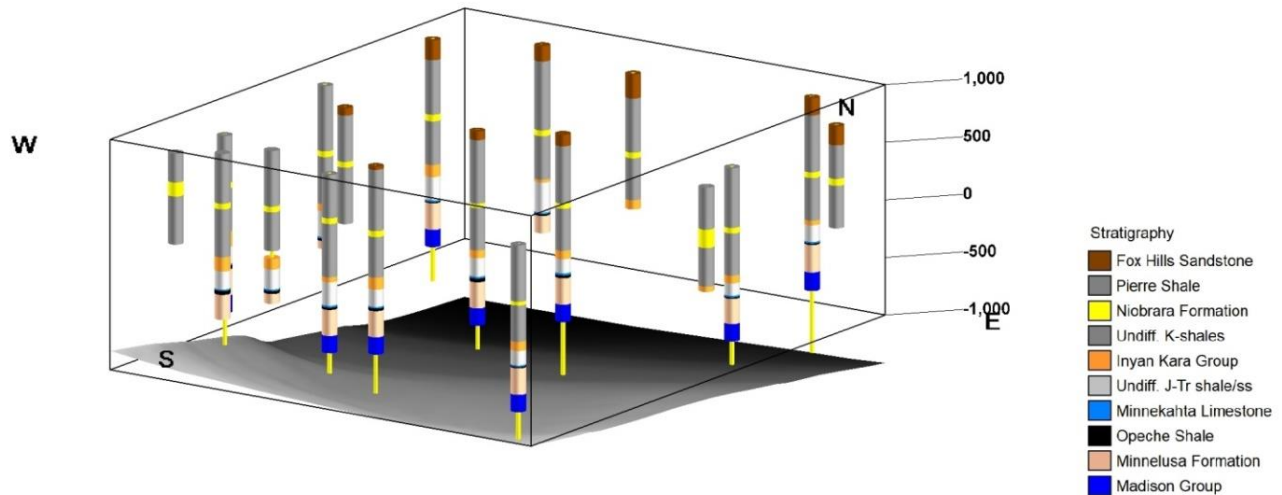
Figure 6-2. Borehole logs and stratigraphy used for construction of the GFM. [Vertical exaggeration is 16X. View is from the southeast. Shown for reference is the Precambrian crystalline rock surface in the GFM region (McCormick 2010).]

Table 6-1. Stratigraphy from boreholes and simplifications used in the GFM.

Age	Borehole Stratigraphy	Lithology	GFM stratigraphy	Thickness (m)[1]
Mesozoic (Cretaceous, Jurassic, Triassic)	Fox Hills Sandstone[2]	Sandstone, shale, siltstone	Fox Hills Sandstone	0-209
	Pierre Shale	Shale with minor sand or silt intervals	Pierre Shale	250-598
	Niobrara Formation	Shale, chalky limestone	Niobrara Formation	33-159
	Carlile Shale	Shale	Undifferentiated Cretaceous Shales	315-509
	Greenhorn Formation	Shale, limestone		
	Graneros Group[3]	Shale, sandstone		
	Inyan Kara Group (regional aquifer)	Sandstone, shale	Inyan Kara Group	26-136
	Morrison Formation	Shale, sandstone	Undifferentiated Jurassic-Triassic Shales/Sandstones	106-259
	Sundance Formation	Sandstone, shale		
	Spearfish Formation	Shale, gypsum		
Paleozoic (Permian, Pennsylvanian, Mississippian)	Minnekahta Limestone (regional aquifer)	Limestone	Minnekahta Limestone	12-18
	Opeche Shale	Shale	Opeche Shale	12-34
	Minnelusa Formation (regional aquifer)	Sandstone	Minnelusa Formation	219-239
	Madison Group (regional aquifer)	Limestone	Madison Group	150-160

1. Based on borehole picks
2. Overlain by the Hell Creek Formation in the northern part of the GFM (Figure 6-1)
3. Includes Belle Fourche Shale, Mowry Shale, Newcastle Sandstone, Skull Creek Shale

The sedimentary formations within two primarily shale intervals were combined to create the undifferentiated Cretaceous (K) shales and the undifferentiated Triassic and Jurassic shales (Tr-J). In both cases, the formations were grouped into undifferentiated intervals because these formations were not consistently identified in the boreholes due to the difficulty of identifying the contacts between different shale units based on borehole cuttings. The undifferentiated Cretaceous shales include the Carlile, Mowry and Belle Fourche shales, and limestone of the Greenhorn Formation, which have a combined thickness of 300-500 meters. The undifferentiated Triassic and Jurassic

shales include the Morrison, Sundance and Spearfish Formations, which have a combined thickness of 100-250 meters.

6.1.5 Interpolation of Borehole Data

The surfaces that define the tops of geologic units in the GFM were generated by interpolation based on the elevations (z values) of the formation tops in the boreholes shown in Figure 6-2. The GFM uses a grid spacing of 250 meters in the x and y directions and 10 meters in the vertical direction. These grid spacings are considered adequate to represent the geologic features of the GFM at a regional scale.

RockWorks17 provides several standard interpolation methods for interpolating 3D surfaces based on a set of x,y,z data points. Most of these methods (e.g., Kriging, inverse distance weighting) attempt to fit the surface to the elevation values in each borehole. For a region of sparse boreholes, these methods can produce "bullseye" effects at the borehole locations that can produce a misleading representation of the shape of the overall regional surface. For the purposes of the GFM, we chose to represent broad regional trends in the formation surfaces to capture regional dip and not attempt to specify the detailed "shape" of the surfaces. This is appropriate given the limited number of boreholes available to define the regional surfaces. For these reasons, the elevation surfaces were fit using a 2nd degree polynomial fit ("trend polynomial") that captures the regional trends of the borehole elevations without attempting a best fit to the elevations.
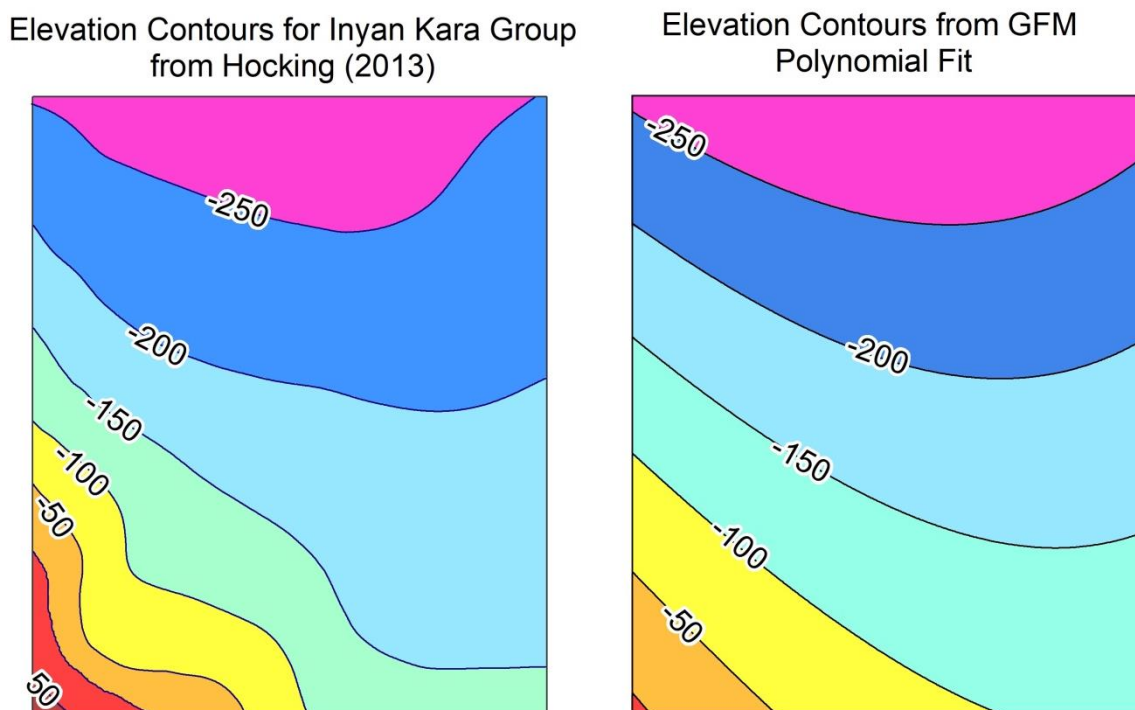
Figure 6-3. Comparison of surface contours of the Inyan Kara Group from Hocking (2013) and the polynomial fit used for the GFM.

Figure 6-3 shows the results of a polynomial fit to the borehole elevation data for the Inyan Kara Group compared to the elevation contours derived from a more detailed regional analysis of the geometry of the Inyan Kara Group (Hocking 2013). The Inyan Kara Group has the most complete and reliable set of elevation data in the region because of its relatively shallow depth (more

boreholes intercept it) and because of the relative ease in identifying the top of the formation due to its distinct sandstone lithology. The polynomial fit compares well with the detailed analysis by Hocking (2013) and adequately captures the regional "shape" of the formation surface. Based on this comparison and, for consistency, the polynomial fit was used to interpolate all the formation surfaces.

6.1.6 Geology and Hydrology Represented in the GFM

The sedimentary formations and aquifers represented in this version of the GFM are shown in Figures 6-4 through 6-7. The GFM represents a stratigraphic column of approximately 1500-1800 meters of sedimentary rock, depending on location. The upper half of the stratigraphy is dominated by Cretaceous shales (the Pierre Shale near the top as well as several hundred meters of underlying shale units) while the lower half of the stratigraphy includes the major regional sandstone and limestone aquifers as well as shale confining units (Figures 6-4 and 6-5). The Pierre Shale and the other sedimentary rocks ramp up to the southwest towards the Black Hills uplift and dip generally to the north and the northeast in the region of the GFM (Figures 6-3 through 6-5).
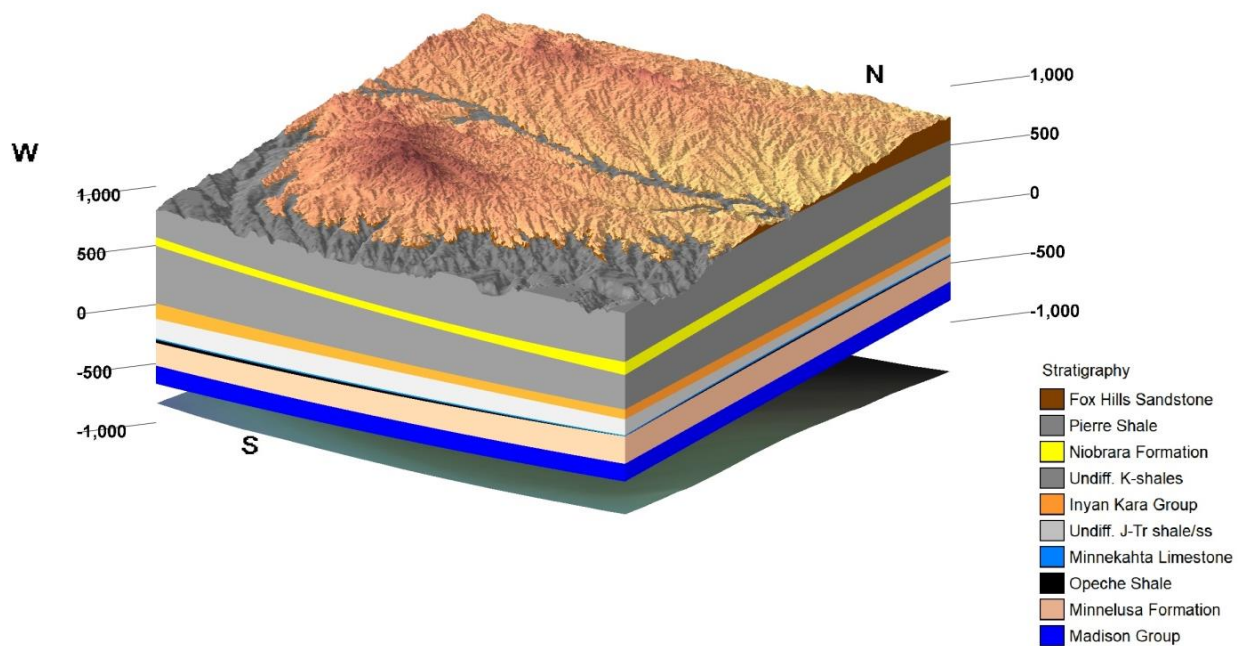
Figure 6-4. Stratigraphy represented in the GFM at 16X vertical exaggeration. View is from the southeast. [Note that the Fox Hills sandstone and part of the Pierre Shale are truncated at the land surface. The base of the GFM is the bottom of the Madison Group limestones. The Precambrian surface (McCormick 2010) at the base of the model is shown for reference. Scale is elevation in meters relative to sea level.]

The stratigraphic column represented in the GFM includes four regional aquifers that lie approximately 1000 meters (Inyan Kara aquifer) to 1500 meters (Madison aquifer) below the surface (Driscoll et al. 2002; Figure 6-6). Groundwater flow in the region of the GFM is controlled largely by recharge in the Black Hills uplift and flows from the southwest to the northeast (Driscoll et al. 2002). The Inyan Kara aquifer is composed of several sandstone units and has a typical thickness of 100 meters. The Minnekahta aquifer is composed of laminated limestone and has a typical thickness of 15 meters. The Minnelusa aquifer is composed of sandstone in the upper half of the Minnelusa Formation and has a typical thickness of 100 meters (Greene 1993). The Madison

aquifer is composed predominantly of massive limestones of the Madison Group. The aquifer is contained within the upper 70 meters of the Madison Group, where fractures and solution features have increased the permeability (Greene 1993). These aquifers, and the regional groundwater system, will be described in more detail in a later report to support the geologic and hydrologic conceptual model of the region.
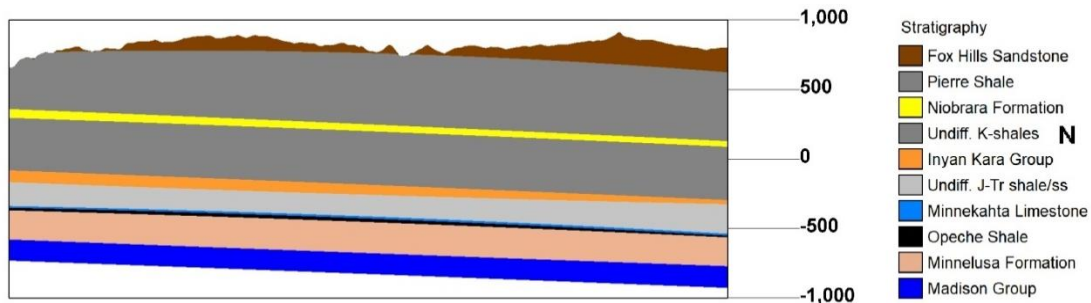
Figure 6-5. N-S cross section through the approximate middle of the GFM at 16x vertical exaggeration. North is to the right. Scale is elevation in meters relative to sea level.
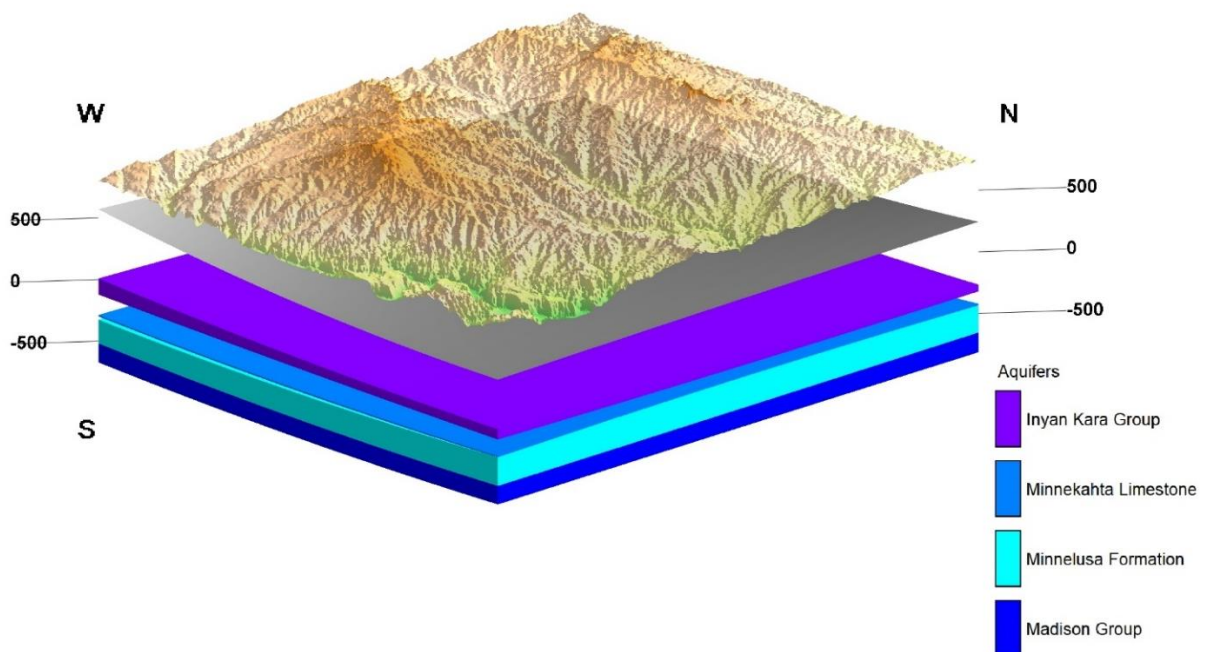
Figure 6-6. Simplified view of the aquifers in the GFM, based on the thickness and geometry of the containing formations. View is from the southeast. Vertical exaggeration is 16X. [The gray-scale surface above the aquifers is the base of the Pierre Shale. Scale is elevation in meters relative to sea level.]

The GFM is a tool to document the geologic and hydrologic features of a region or site. The GFM allows visualization of the geology and hydrology using several visualization tools that are common to most GFM software packages (Figure 6-7). Tools that aid in visualization of the GFM include vertical exaggeration and transparency of selected units. The GFM allows creation of 2D cross-sections of any orientation. The GFM can also be animated and rotated about different axes to aid in 3D visualization. Underground facilities (e.g., a repository) can also be represented in the

GFM by specifying facility coordinates. Figure 6-7 shows an example of a simple rectangular repository facility with horizontal dimensions of 2 x 5 kilometers and a height of 30 meters.
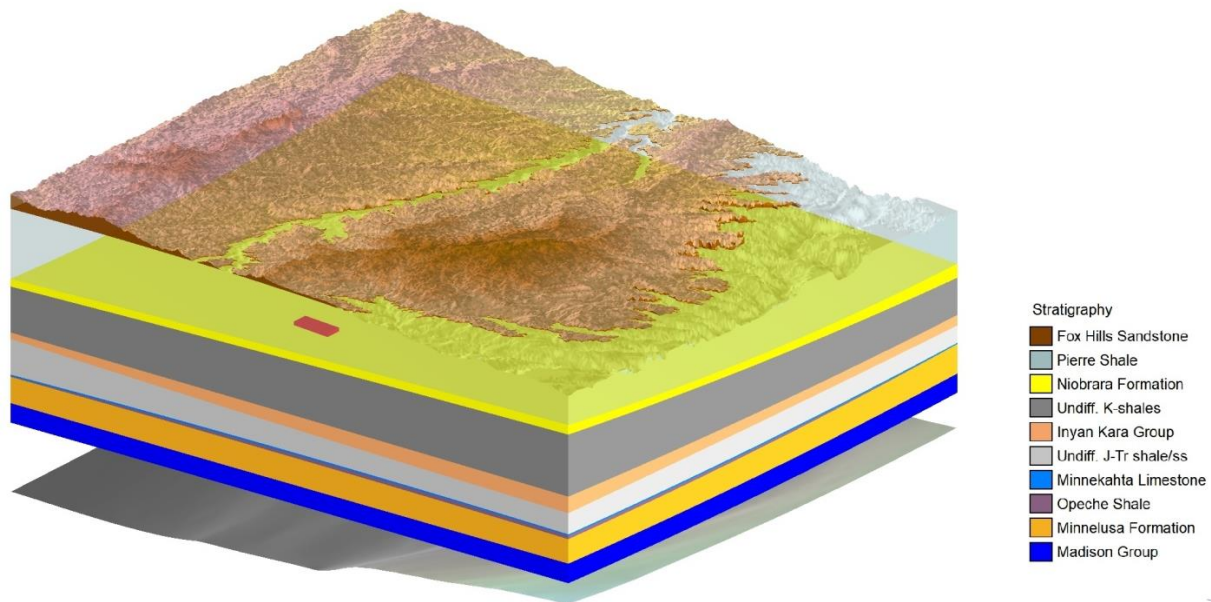
Figure 6-7. GFM stratigraphy showing visualization options and representation of a subsurface facility (e.g., repository) in red. View is from the southwest. Vertical exaggeration is 16X. [The Fox Hills Sandstone and Pierre Shale are rendered semi-transparent to view features "inside" the model.]

6.1.7 Meshing the Features of the Shale GFM

The next step in the workflow is to generate a mesh that represents the geologic features of the GFM. This requires export of 3D surfaces and volumes from the GFM to formats that can be brought into the mesh generation software. The elements in a GFM that require definition as a mesh include non-intersecting surfaces (e.g., formation tops and bottoms), intersecting surfaces (pinch outs, truncated surfaces), lens-like bedding and features offset by faulting. Non-intersecting surfaces are the simplest geometry to mesh and require meshing of the volume between the surfaces.

Rockworks17 can export features of the GFM as either surfaces grids (*x,y,z* values of the grid nodes) or volumes (solid model/voxels) that represent geologic units and interfaces within the overall rock mass. Elements in the GFM represented by volumes are exported as a regularly spaced uniform hexahedral mesh with (*x, y, z, g*) representing the cell center coordinates and a cell property (*g*) such as lithology. Volume elements can represent the space between stratigraphic surfaces, stratigraphic pinch outs or lens, or stratigraphic elements adjoining and offset by a fault.

Import of the GFM surfaces and volumes into a mesh generation tool would be required if further manipulation and refinement of a mesh is needed. Methods are being tested for exporting geologic elements of the GFM to formats that can be imported into meshing software such as Cubit and VoroCrust.

6.2 Grid-Scale Effects and Reduced Order Modeling

The objective of this study is to investigate the near-field thermal-hydrologic (TH) behavior of pore fluids in a geologic repository located in a shale host rock. The focus is on the impact of the hydrogeological properties of the engineered buffer and DRZ on the near-field performance of a typical bentonite back-filled nuclear waste repository.

6.2.1 Model Domain and Discretization

This model domain represents one quarter of the whole repository system using reflection symmetry (Figure 6-8a), which saves on computation time. The waste packages in the repository system are located at the middle of the domain and are surrounded concentrically by buffer material, DRZ, and shale host rock.

The whole domain is 15 m (width) ×12.5 m (length) × 75 m (thickness), focuses on one waste package, and includes three cylindrical sections of waste package, buffer, and disturbed rock zone (DRZ) at 0.42 m, 1.5 m, and 3.17 m in radius, respectively, within the shale host rock. The waste package is discretized in the *zx*-plane with 128 grid cells. Note that the previous basin-scale model contains cubic cells representing individual waste packages sized $1.67 \times 1.67 \times 5$ m^3 as shown in Figure 6-8b. The effect of refined cells on numerical results will be discussed in Section 6.2.4. The simulations presented here were run up to 1000 years.

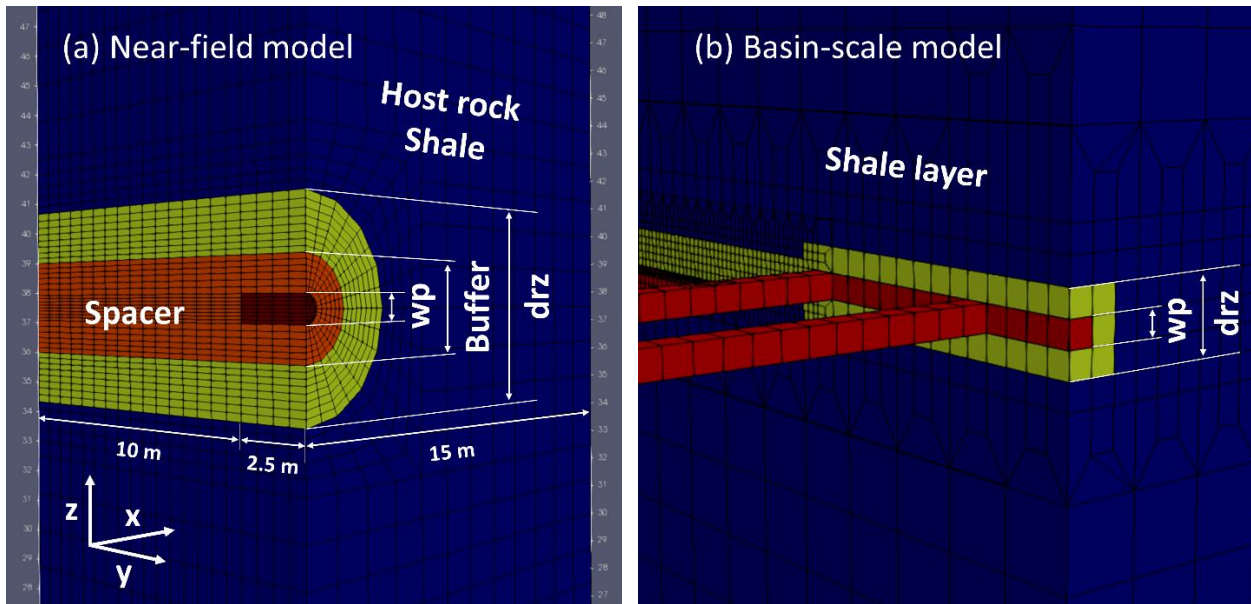Figure 6-8. Model domain with grids: (a) near-field model and (b) basin-scale model (refer to Mariner et al. 2017). [The color scheme represents each material.]

6.2.2 Model Material Properties

This near-field model focuses on a single waste package within a shale layer. The material properties are the same as those used in the previous basin-scale shale reference case model (Mariner et al. 2017), as shown here in Table 6-2.

Table 6-2. Material properties for the reference case.

	Waste package	Buffer/Spacer	DRZ	Host rock (shale)
Permeability (m²)	1×10⁻¹⁶	1×10⁻²⁰	1×10⁻¹⁸	1×10⁻¹⁹
Porosity	0.5	0.35	0.2	0.2
Effective diffusion coefficient (m²/s)	5×10⁻¹⁰	8.1×10⁻¹¹	2.2×10⁻¹¹	2.2×10⁻¹¹
Saturated thermal conductivity (W/m/K)	16.7	1.5	1.2	1.2
Heat capacity (J/kg/K)	466	830	830	830
Grain density (kg/m³)	5000	2700	2700	2700

When a waste package fails, radionuclides are exposed to pore fluid in the simulation and are thus available for transport. Advective transport through the failed waste package is quantified by defining a waste package permeability, which in the reference case simulations is defined as invariant at 1×10^{-16} m². A 12-PWR waste package is used in these simulations. The buffer/spacer is filled with a compacted mixture of 70% bentonite and 30% quartz sand. The DRZ is defined as the portion of the host rock adjacent to the engineered barrier system that experiences elevated permeability due to mining-induced perturbations in stress states.

6.2.3 Initial and Boundary Conditions

Initial pressure and temperature throughout the model domain are calculated by applying hydrostatic and geothermal gradients (10kPa/m and 0.025°C/m, respectively) in the vertical direction assuming a temperature of 18°C and atmospheric pressure at the land surface. The model includes the inventory of 18 radionuclides listed in Table 4-4 of Mariner et al. (2017), and initial concentrations of all radionuclides in all grid cells are 10^{-20} mol/L. Assuming that geometry and material properties of the rest of the repository system constitute a reflection of the current discretization about the x and y axes, symmetry boundary conditions are implemented at the side boundaries.

6.2.4 Effect of Refined Grids

The grid resolution has a considerable impact on the results of transient numerical simulations. The truncation error can be ignored in numerical simulation only if the change in calculated results is negligible with changing grid resolution in the model domain. In general, the truncation error will become smaller with refined grids.

For the basin-scale shale reference case model, gridding constraints limit the geometry and discretization of the repository system. The size of the waste package is $1.67 \times 1.67 \times 5$ m³, which is larger in volume that a single 12-PWR waste package is expected to be, and waste package discretization is not refined in *x* and *z* directions. The thickness of the DRZ surrounding the emplacement drifts is equal to one third the width of the drift (1.67 m).

On the other hand, this near-field model has refined grid cells within the waste package and also includes the buffer surrounding the waste package that has lower permeability, porosity, and heat conductivity. Unstructured grid cells are used within the waste package and shale, and radial grid

cells are applied within buffer/space and DRZ to discretize the cylinderical repository properly (Figure 6-8a).

The presence of refined grid cells within the waste package results in a non-uniform spatial distribution of temperature over time, as shown in Figure 6-9. The average temperature within the waste package reaches up to 180°C, which is higher than the maximum waste package temperature prediced from the basin-scale model ($T_{max} \approx 150$°C).
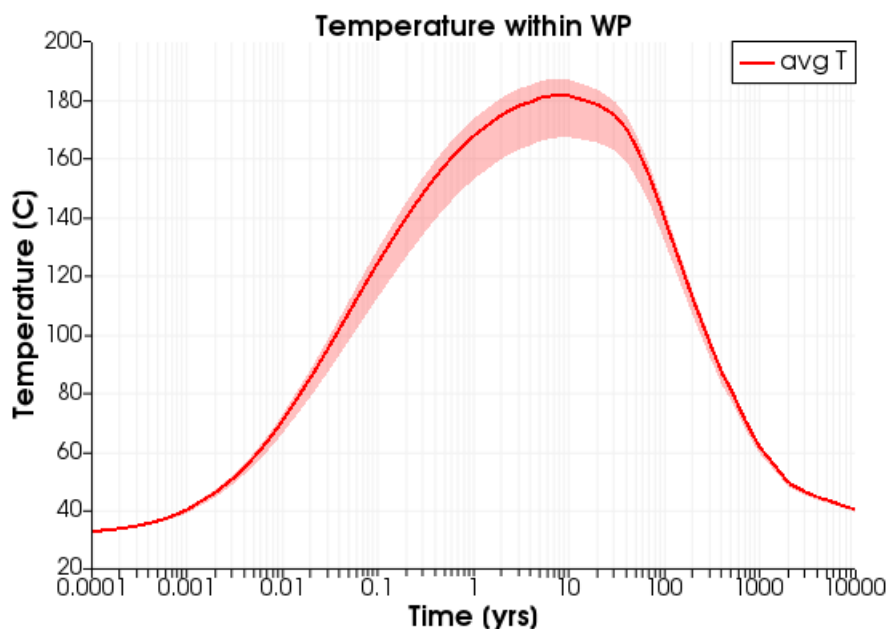
Figure 6-9. The minimum, maximum, and average temperature distribution within the waste package.

6.2.5 Sensitivity Test

A series of sensitivity tests were conducted to look into the effect of the permeability/porosity variation in the buffer and/or DRZ on the fluid flow and heat/solute transport. The engineered buffer system can vary its hydrogeological characteristics depending on the design of compacted mixtures, and thus, this sensitivity analysis can suggest the most efficient material composition for the system to achieve desirable thermal/mechanical properties.

6.2.5.1 *Permeability of Buffer and DRZ*

In the basin-scale reference case, the probabilistic simulations sampled on the permeability of buffer and DRZ using a uniform distribution over the ranges 10^{-20} to 10^{-16} m^2 and 10^{-18} to 10^{-16} m^2, respectively. In this study, we choose 10^{-16} m^2 for buffer and DRZ as an end-member case to see how higher permeability affects fluid flow, heat and solute transport.

Figure 6-10 shows temporal evolution of pressure and temperature within each repository feature: reference case (top), high permeability in buffer and DRZ (middle), and the difference (bottom). The high-permeability buffer and DRZ release pressure buildup out of the waste package faster than in the low permeability reference case. Note that low-permeability shale confines pressure within the repository even though buffer and DRZ have higher permeability ($\Delta P = 0$, magenta line). The presence of high-permeability buffer and DRZ results in more convective heat transfer

out of the waste package ($\Delta T < 0$, red line), which increases temperature within the shale ($\Delta T > 0$, magenta line).

Figure 6-10. Temporal evolution of pressure and temperature at each section: WP (red), Buffer (green), DRZ (blue), and shale (magenta). Pressure and temperature in the reference case (P1 and T1) are compared to the high permeability buffer/DRZ scenario (P2 and T2).

Figure 6-11 shows the concentrations of ^{129}I and ^{36}Cl collected at the cell of each section over time. Transport of both radionuclides away from the repository is diffusive but both are confined to the immediate vicinity of the breached waste package. The temporal evolution of ^{129}I and ^{36}Cl behaves quite similarly but the ^{36}Cl concentration is two orders of magnitude lower than the ^{129}I concentration due to lower release rate.

The high-permeability buffer and DRZ allows faster accumulation of ^{129}I and ^{36}Cl within the waste package (positive difference within the waste package until 1.5 years), and subsequently more ^{129}I and ^{36}Cl are leaked into buffer and DRZ over time (negative difference within the waste package, red lines). No significant amounts of ^{129}I and ^{36}Cl have breached into the host rock within 1000 years (magenta lines in Figure 6-11) as expected from the basin-scale reference model (refer to Figure 4-13 of Mariner et al. 2017).

Figure 6-12 shows temporal evolution of ^{237}Np concentration. As shown in the result of the basin-scale reference model (Section 4.5.1.5 of Mariner et al. 2017), ^{237}Np remain within the vicinity of the repository. For 1000 years, most of ^{237}Np is confined within the waste package. Higher permeability within buffer and DRZ results in faster accumulation of ^{237}Np within the waste package ($\Delta[^{237}$Np$] > 0$, red line).
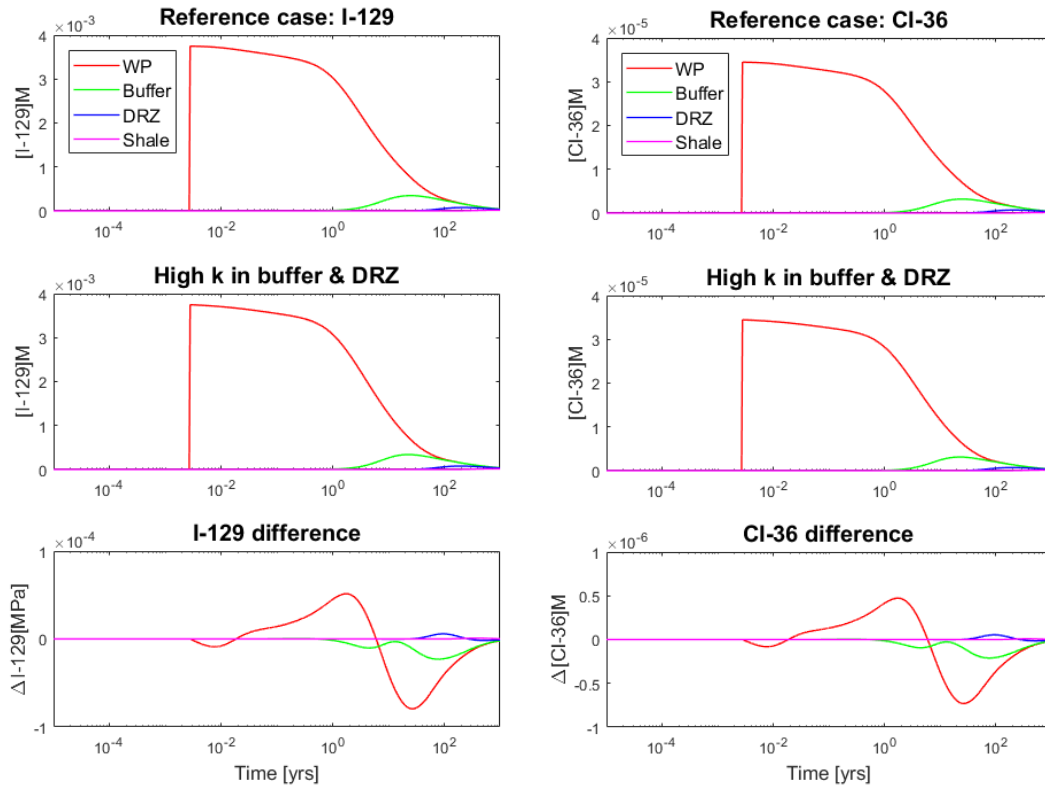
Figure 6-11. Temporal evolution of concentrations of ^{129}I and ^{36}Cl at each section: WP (red), Buffer (green), DRZ (blue), and shale (magenta).
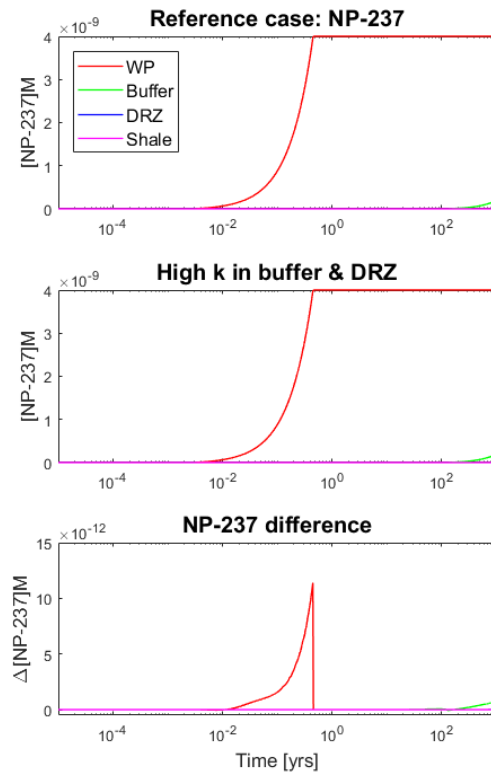
Figure 6-12. Temporal evolution of concentrations of ^{237}Np at each section.

6.2.5.2 Permeability and porosity of bentonite

The measured values of intrinsic permeability to water and gas flow as functions of porosity show a difference of about eight orders of magnitude in the permeability values for saturated or dry clay (Villar 2004) as shown in Figure 6-13 below.
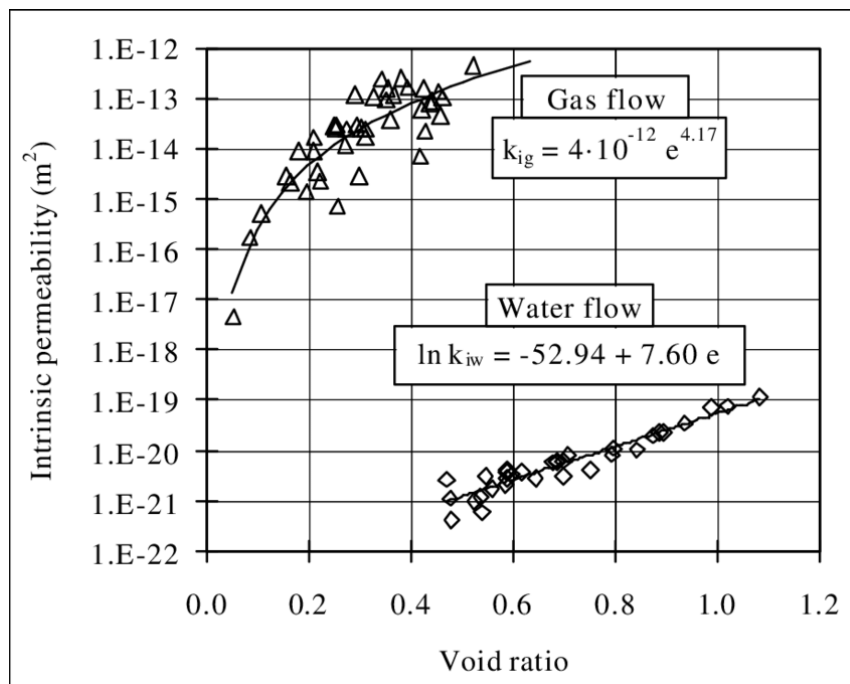
Figure 6-13. Intrinsic permeability and void ratio of compacted bentonite measured from water and gas flow tests (Villar 2004).

The swelling of deformable clay causes the variation in the microstructural arrangement of the saturated and unsaturated portions. The hydration of clay particles under constant volume reduces the pore size between the clay aggregates due to the swelling of the clay particles. Most of the water will be captured within the interlamellar space in addition to water bound to the clay mineral surfaces, which leave only narrow, tortous interparticle passages for water and solute transport (Villar 2004).

In this sensitivity study, we use the following relationship between intrinsic permeability and porosity of bentonite measured under saturated conditions (Villar and Lloret 2001):

$$\ln k = -52.94 + 7.6 \frac{\phi}{(1-\phi)} \tag{6-1}$$

where the porosity ϕ is converted from the void ratio e. The intrinsic permeability of bentonite is set to 10^{-16} m^2, and its corresponding porosity is calculated as 0.68 from the above equation, which applies to the buffer/spacer properties. The other material properties remain consistent with the reference case.
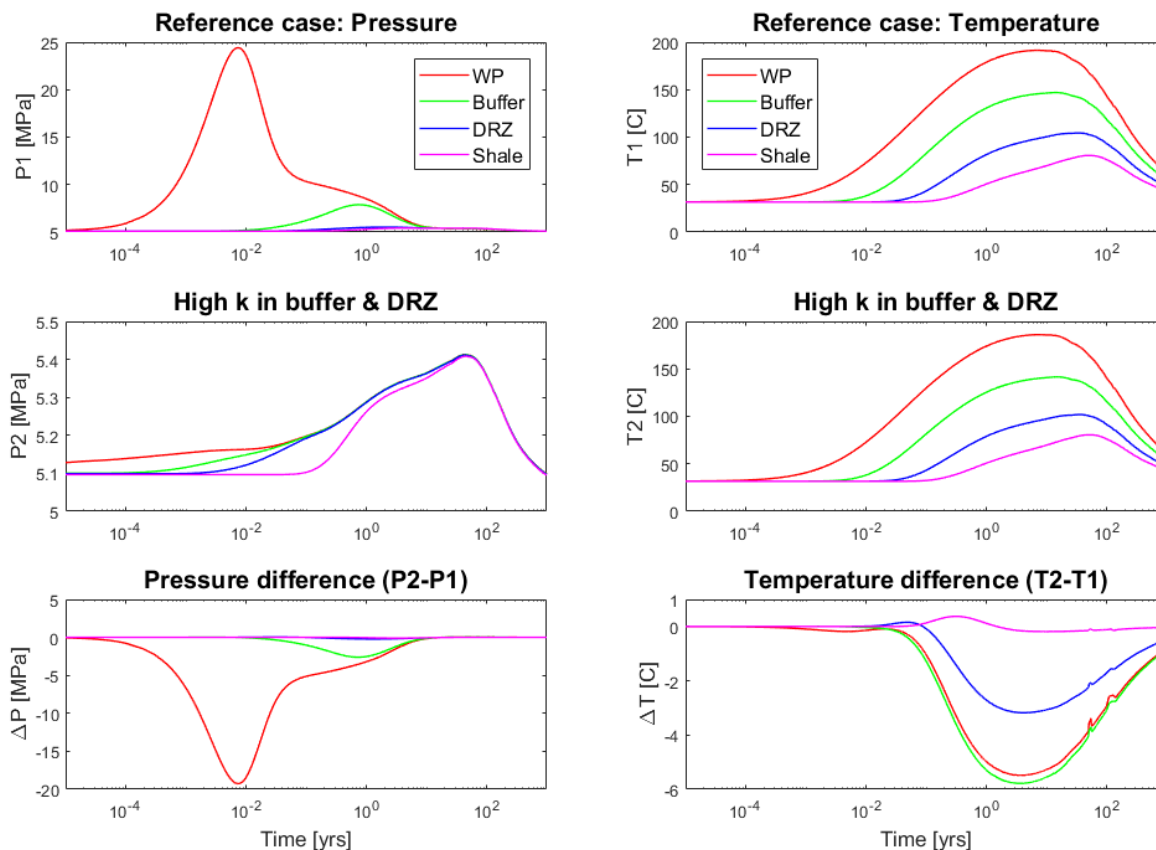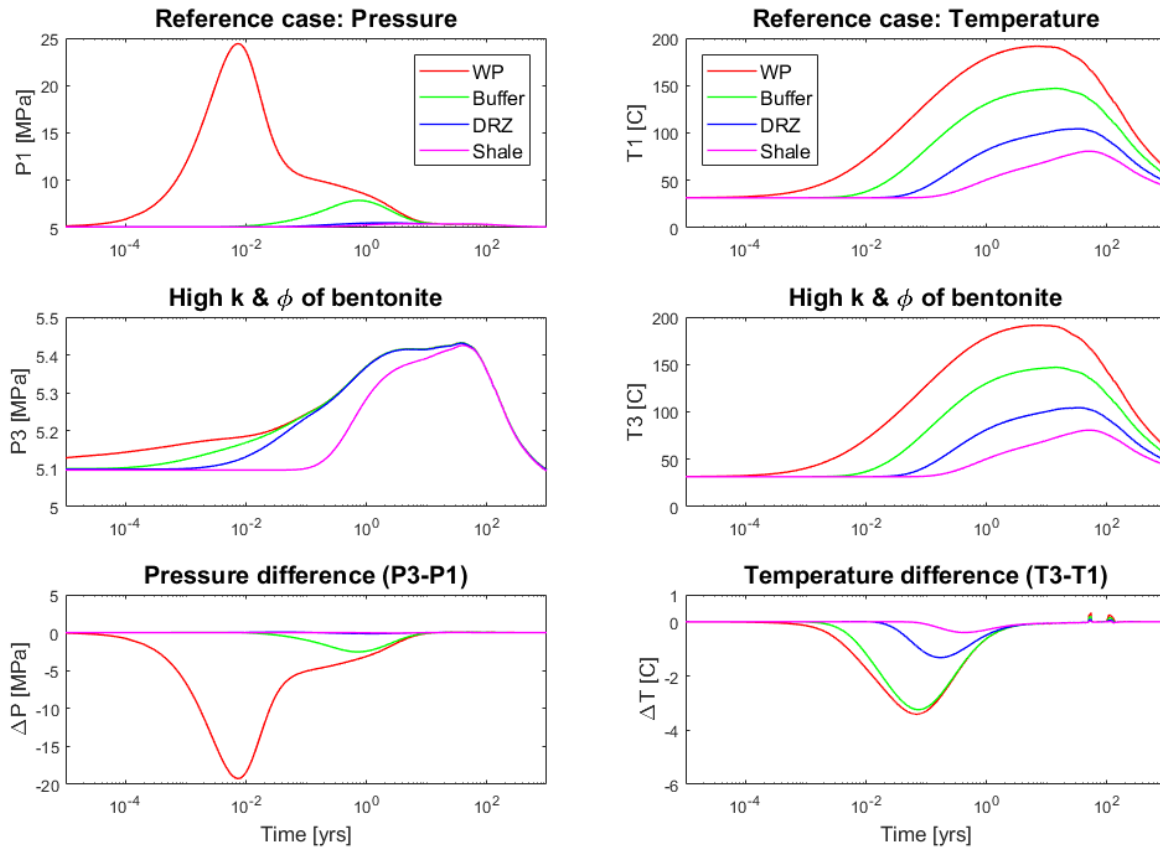
Figure 6-14. Temporal evolution of pressure and temperature at each section: WP (red), Buffer (green), DRZ (blue), and shale (magenta). [The figure scheme remains the same as used in the previous section. Pressure and temperature in the reference case (P1 and T1) are compared to the high permeability buffer/DRZ scenario (P3 and T3).]

Figure 6-14 shows temporal evolution of pressure and temperature within each near-field feature. Higher permeability and porosity within the buffer reduce pressure buildup within the waste package. The magnitude of temperature perturbation (ΔT) is smaller than the case of high-permeability buffer and DRZ because more pore spaces within the buffer/spacer (higher ϕ) absorb more heat and subsequently less heat within DRZ and shale.

Compared to the reference case buffer and DRZ properties (Figure 6-11), the high-permeability and -porosity buffer allows faster leakage of ^{129}I and ^{36}Cl out of the waste package (smaller positive change of $\Delta[^{129}$I$]$ and $\Delta[^{36}$Cl$]$ within the waste package, the red lines in Figure 6-15), and subsequently more ^{129}I and ^{36}Cl leak into buffer and DRZ with time (larger negative difference within the waste package).

Figure 6-16 shows temporal evolution of ^{237}Np concentration. Higher permeability and porosity within buffer results in slower accumulation of ^{237}Np within the waste package ($\Delta[^{237}$Np$] < 0$, red line), and also leak of ^{237}Np into the buffer is observed after 100 years ($\Delta[^{237}$Np$] > 0$, green line). These results show that high-permeability and -porosity bentonite will mitigate the pressure buildup and heat accumulation within the waste package at the expense of radionuclides breaching into the buffer/spacer.
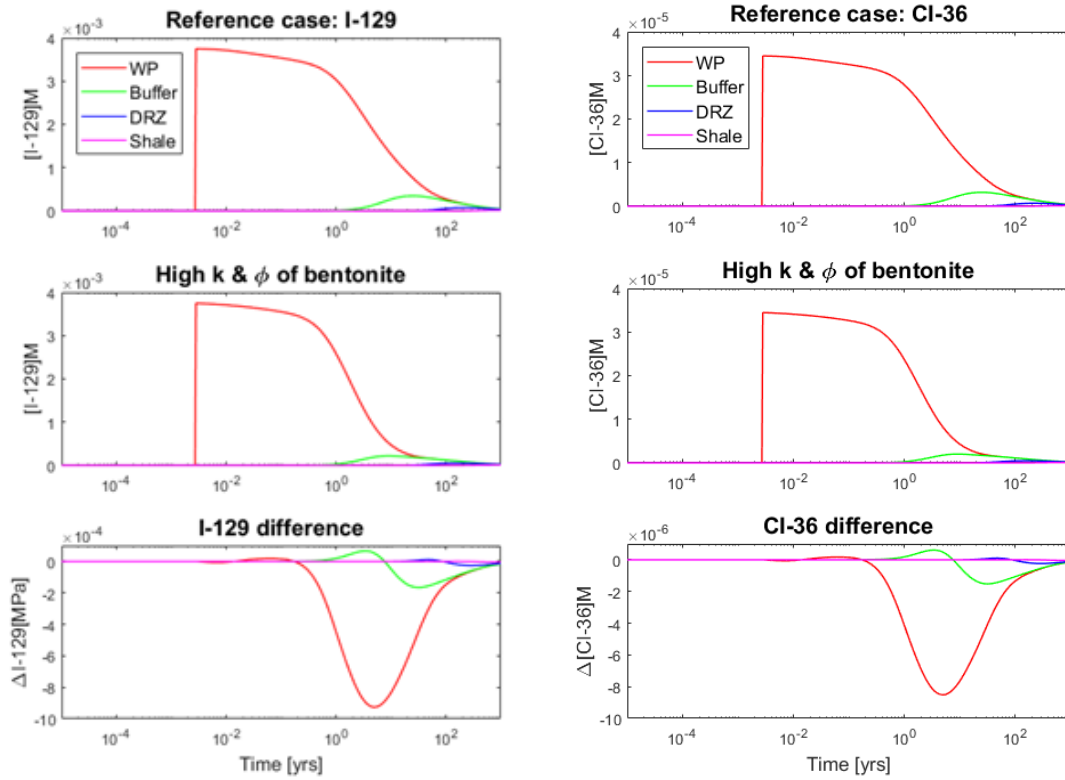
Figure 6-15. Temporal evolution of concentrations of ^{129}I and ^{36}Cl at each section.
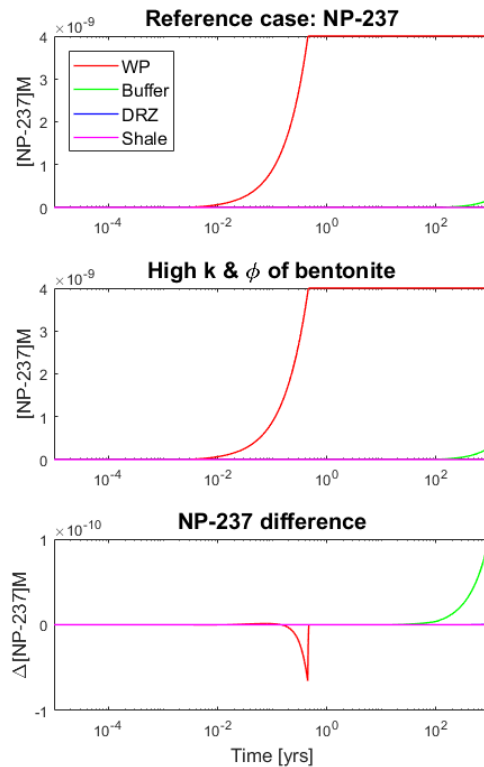
Figure 6-16. Temporal evolution of concentrations of ^{237}Np at each section.

6.2.6   Considerations for Future Work

Near-field thermal-hydrologic modeling of a geologic repository at finer discretization than comparable basin-scale models suggests more localization of thermal effects within a waste package in the high-resolution model as compared to a basin-scale model. Furthermore, when sampling on a range of permeabilities and porosities, local pressure buildup that is observed in the reference case is able to dissipate in scenarios with higher permeability buffer and DRZ material. The reference case and the high permeability system show little difference in ^{129}I or ^{36}Cl concentrations by the time at which the thermal pulse has subsided. These results could change though when considering mechanical impacts of temperature and pressure buildup on the pore system. Work will continue on this near-field model for the remainder of FY2019, with a goal of using this domain in a PA-GDSA model to represent near-field THM coupled process effects. Surrogate modeling will be used to couple a mechanical response to thermal loading by linking permeability and porosity with the pressure and temperature distribution in the near-field. The bentonite host rock will also be modeled as unsaturated, and associated changes in heat and radionuclide transport will be quantified. This is in support of R&D Activity A-4 in Sevougian et al. (2019).

6.3   Updated Shale Reference Case PA Model and Simulations

The current GDSA status on evaluation of the suitability of generic shale formations as potential hosts for a geological disposal repository is documented in Mariner et. al (2017) and includes studies presented in Mariner (2015) and Jove-Colon et al. (2014). This section presents status on the FY2019 proposed update to the GDSA Shale Reference Case described in Section 4 of Mariner et. al (2017). This work has only recently begun, so only a very preliminary update is provided here. The comprehensive report on the update will be reported in the September 27, 2019 Level 3 milestone for the FY19 GDSA Repository Systems Analysis work package (SF-18SN01030405), entitled *GDSA Repository Systems Analysis FY19 Update* (M3SF-19SN010304052).

The main tasks that will be undertaken in FY2019 are

(4) Inclusion of 24-PWR and 37-PWR DPC waste packages in the reference case simulations.

(5) An update to the stratigraphic model for a representative shale domain (Perry et al. 2014; Perry and Kelley 2017)—see Section 6.1 above.

(6) An update to the numerical model grids and formation properties (see Table 6-3) to incorporate changes to stratigraphy and repository design needed for DPC waste packages.

Table 6-3. Comparison of current (2019) GDSA simulations to 2017 shale reference case GDSA simulations. Inventory count (MTHM and number of waste packages) includes *the virtual inventory beyond the reflection boundary condition.*

	2019 GDSA 24-37-PWR	**2017 GDSA 12-PWR**
Waste Inventory	70,000 MTHM in 3150 24-PWR WPs and 2100 37-PWR WPs	21,000 MTHM in 4200 WPs
Waste Emplacement	In-drift axial emplacement 40-m drift spacing 42 emplacement drifts for 24-PWR 42 emplacement drifts for 37-PWR 20-m center-to-center WP spacing for 24-PWR 30-m center-to-center WP spacing for 37-PWR Bentonite buffer/backfill	In-drift axial emplacement 84 emplacement drifts 30-m drift spacing 20-m center-to-center WP spacing Bentonite buffer/backfill
Grid	Unstructured 10.68 million cells with refined drift 6.88 million cells without refined drift	Unstructured 7 million cells
Boundary and Initial Conditions	Regional head gradient Regional geothermal heat flux Fully saturated	Regional head gradient Regional geothermal heat flux Fully saturated
Natural Barrier	Shale (**550ᵃ m thick**) with high permeability interbeds Aquifer above and two below	Shale (585 m thick) with silty shale stratum Aquifer above and two below
Shafts and Seals	4 vertical shafts with high permeability DRZ $D_e = 8.1 \times 10^{-11}$	4 vertical shafts with high permeability DRZ $D_e = 8.1 \times 10^{-11}$
Radionuclides	18	18
TH Modeling	Coupled heat and water transport	Coupled heat and water transport
WP Degradation	WPs breach over time (sampled distribution)	WPs breach over time (sampled distribution)
WF Degradation and Radionuclide Release	Decay in waste form is accounted for in instantaneous releases and in releases due to WF dissolution	Decay in waste form is accounted for in instantaneous releases and in releases due to WF dissolution
Radionuclide Transport	Advection, diffusion, element-based solubility, medium-specific sorption, decay in all phases	Advection, diffusion, element-based solubility, medium-specific sorption, decay in all phases
Biosphere	Well water ingestion dose model	Well water ingestion dose model

ᵃ 550 m shale is from updated stratigraphic model
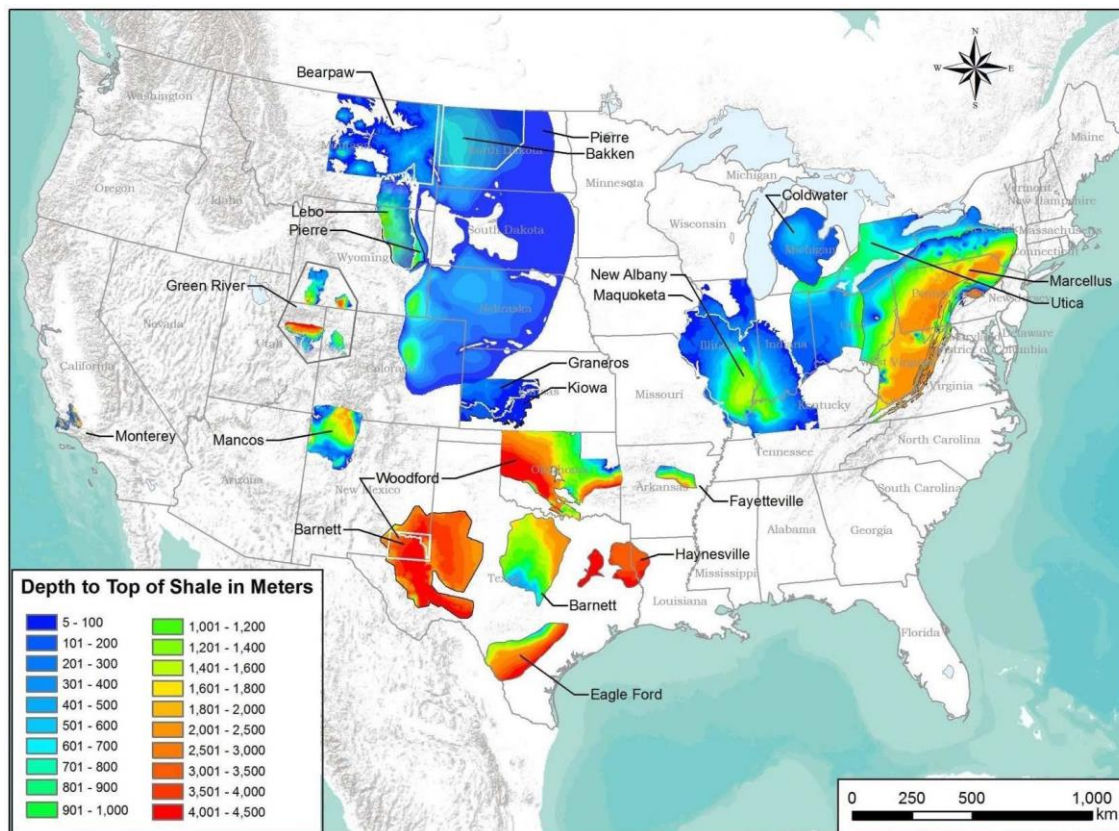
Figure 6-17. Locations of really extensive shale formations in the U.S. Shale formations of an appropriate depth are the darker shades of blue (Mariner et.al. 2017 Figure 4-1).

6.3.1 Engineered Barriers

6.3.1.1 Engineered Barrier Characteristics

The shale reference case assumes a mined repository located approximately 500 m below land surface, accessed by vertical shafts, and containing 70,000 MTHM of CSNF, 50% of which is in 24-PWR and 50% in 37-PWR DPC waste canisters. The total inventory of MTHM load is consistent with the maximum allowed by the Nuclear Waste Policy Act of 1983.

The 37-PWR inventory could be accommodated in 2100 waste packages (Table 6-4) in 42 1535-m long emplacement drifts, each containing 50 waste packages emplaced lengthwise and spaced 30 meters center-to-center. A 25-m long seal is placed at either end of each emplacement drift. Drifts are 4.5 m in diameter spaced 40 meters center-to-center.

The 24-PWR inventory could be accommodated in 3150 waste packages (Table 6-5) in 42 1535-m long emplacement drifts each containing 75 waste packages spaced 20 meters center-to-center. A 25-m long seal is placed at either end of each emplacement drift. Drifts are 4.5 m in diameter spaced 40 meters center-to-center.

PA simulations use a half-symmetry model domain, such that only 50% (35,000 MTHM) of the 70,000 MTHM inventory needs to be included in PA simulations. Dimensions used in the simulations (Tables 6-4 and 6-5) reflect the smaller inventory, as well as adjustments needed to facilitate gridding.

Table 6-4. Dimensions and counts for the 37-PWR repository layout.

Parameters	2019 GDSA Model Value	2017 GDSA Model Value (12-PWR)
Waste Package (WP)		
WP length (m)	5.00	5.00
WP outer diameter (m)	1.67 (5/3 on a side)	1.67 (5/3 on a side)
WP center-to-center spacing (m)	30.0	20
Inventory per WP (MTHM)	17.39	5.225
Number of WPs	2100	2100/4200
Emplacement Drift		
Drift diameter (m)	5.0 (on a side)	5.0 (on a side)
Drift center-to-center spacing (m)	40	30
Number of WPs per drift	50	50
Drift seal length (m)	25	25
Drift length, including seals (m)	1535	1035
Repository		
Repository Depth (m)	515	515
Number of drifts	21/42[b]	42/84[b]
Number of shafts	2/4[b]	2/4[b]
Shaft access size (m²)	5x10	5x10
Emplacement footprint (km²)	1.3/2.6[b]	1.3/2.6[b]

[b]Value in half-symmetry domain / Value with reflection

Table 6-5. Dimensions and counts for the 37-PWR repository layout.

Parameters	2019 GDSA Model Value	2017 GDSA Model Value (12-PWR)
Waste Package (WP)		
WP length (m)	5.00	5.00
WP outer diameter (m)	1.67 (5/3 on a side)	1.67 (5/3 on a side)
WP center-to-center spacing (m)	20.0	20
Inventory per WP (MTHM)	11.28	5.225
Number of WPs	1575/3150[c]	2100/4200
Emplacement Drift		
Drift diameter (m)	5.0 (on a side)	5.0 (on a side)
Drift center-to-center spacing (m)	40	30
Number of WPs per drift	75	50
Drift seal length (m)	1535	1035
Drift length, including seals (m)		
Repository	515	515
Repository Depth (m)	21/42	42/84
Number of drifts	2/4[c]	2/4[c]
Number of shafts	5 x 10	5x10
Shaft access size (m²)	1.3/2.6[c]	1.3/2.6[c]
Emplacement footprint (km²)	5.00	5.00

[c]Value in half-symmetry domain / Value with reflection

6.3.1.2 Inventory

PA simulations assume that the inventory consists entirely of 24-PWR and 37-PWR DPC assemblies. Each 37-PWR DPC assembly contains 17.39 MTHM and each 24-PWR DPC assembly contains 11.28 MTHM. An update of the radionuclide inventories in these DPC assembles to be used in all PA simulations is presented in Section 4.1.1 of this status report.

6.3.1.3 Waste Form

Same as Mariner et. al. (2017, Section 4.1.3).

6.3.1.4 Waste Package

The 2019 shale reference case considers two DPC waste package configurations: a 24-PWR waste package and a 37-PWR waste package. Both are assumed to consist of a stainless-steel canister and a stainless steel overpack. The waste package is 5 meters in length with a diameter of 2 m. Due to gridding considerations, the size of simulated waste packages is $1.67 \times 1.67 \times 5$ m^3, which is slightly smaller in volume than waste packages are expected to be.

Waste package porosity is set equal to the fraction of void space within the waste package, which is set at 50% (Mariner et al. 2016). Permeability is set several orders of magnitude higher than that of the surrounding materials, so that flow through waste packages is uninhibited. The waste package is given the thermal properties of stainless steel (Shelton 1934).

The shale reference case uses a temperature-dependent waste-package degradation rate with a truncated log normal distribution. The degradation rate distribution is such that 50% of the waste packages breach within a few tens of thousands of years (Mariner et al. 2017, Section 4.1.4).

6.3.1.5 Bentonite Buffer

Same as Mariner et. al. (2017, Section 4.1.3).

6.3.1.6 Other Materials

Same as Mariner et. al. (2017, Section 4.1.3).

6.3.2 Geosphere/Natural Barriers

6.3.2.1 Natural Barrier Characteristics

The natural barrier system (NBS) comprises the shale formation hosting the repository, the disturbed rock zone (DRZ) adjacent to the repository, and geological formations above and below the host formation. On the basis of stratigraphic sequences observed in sedimentary basins throughout the U.S. (Gonzales and Johnson 1985; Perry et al. 2014), the NBS is conceptualized as a thick (on the order of thousands of meters) marine depositional sequence created by transgression and regression of inland seas, and consisting of thick layers of low permeability sediments such as shales and marls alternating with thinner layers of high permeability sediments such as limestones and sandstones (Mariner et a.l 2017 Section 4.2.1).

The generic stratigraphic column for the shale reference case used in the 2017 GDSA reference case (Mariner et al. 2017, Section 4.2.1, Figure 4-5) is presented in Figure 6-18. This stratigraphy will form the basis of the initial GDSA 2019 shale reference case update. As additional data on

the updated stratigraphy of the representative shale formation become available (see Section 6.1 of this report), it will be incorporated and used in the final 2019 GDSA shale reference case.
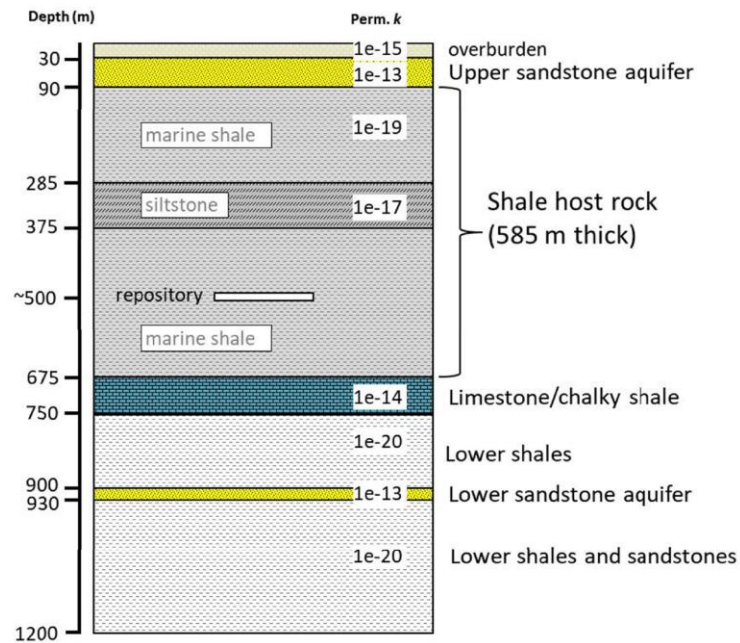
Figure 6-18. Generic stratigraphic column (Perry and Kelly 2017).

6.3.2.2 Shale Host Rock

Shale host rock properties as in Mariner et. al. 2017 Section 4.2.2, to be updated based on the revised stratigraphic information in Section 6.1.

6.3.2.3 Disturbed Rock Zone (DRZ)

For the finely gridded repository horizon, the grid resolution of 1.67 m (5/3 m) dictates the extent to which the DRZ can be explicitly modeled in the vicinity of the emplacement drifts. In the coarse grid, the entire repository drift element is assumed have the properties of DRZ and the DRZ is assigned higher permeability than the surrounding formations. In deterministic simulations, the permeability of the DRZ (10^{-18} m^2) is 10 times that of the undisturbed host rock. In probabilistic simulations the permeability of the DRZ is sampled from a log uniform uncertain distribution between 10^{-18} m^2 and 10^{-16} m^2.

6.3.2.4 Properties of Other Formations

The formations above and beneath the repository horizon will be patterned after Mariner et. al. (2017, Section 4.1.3), but with changes based on the new information in Section 6.1 above.

6.3.3 Post-Closure Performance Assessment

6.3.3.1 Conceptual Model

As in the 2017 Shale Reference Case, the conceptual the components of the conceptual model of the repository system are the engineered barrier, the natural barrier, and the biosphere in the

undisturbed scenario. The characteristics of and processes occurring in key components of each system are summarized in Table 6-6 from Mariner et al. (2017, Table 4-8).

Table 6-6. Conceptual representation of key components in PA.

Region	Component	Key characteristics	Key processes included in PA
Engineered Barrier	Waste Form	Commercial SNF (UO_2)	Radionuclide decay, instant release fraction, waste form dissolution
	Waste Package	Stainless steel	Degradation and breach
	Bentonite Buffer	Low permeability, high sorption capacity	Radionuclide advection, diffusion, sorption, decay
Natural Barrier	Shale Host Rock	Low permeability, high sorption capacity	Radionuclide advection, diffusion, sorption, decay
	DRZ	Enhanced permeability	Radionuclide advection, diffusion, sorption, decay
	Upper Sandstone Aquifer	High permeability, potable water	Radionuclide advection, diffusion, sorption, decay
Biosphere	Pumping Well	500 gallons/day	Well water extraction, adsorption enhancement, dose by well water ingestion

Simulations assume (1) a mined repository at 515 m depth; (2) a head gradient of −0.0013 m/m from west to east; (3) a regional heat flux of 60 mW/m^2 and a mean annual surface temperature of 10°C; and (4) a saturated model domain, with a hydrostatic gradient extending to the top of the model domain. Simulations that include the biosphere also assume a well located 5 km down gradient of the repository, screened in the 60-m thickness of the upper sandstone aquifer, and pumping 500 gallons/day. This pumping rate is similar to what a single rural family of six might use (van der Leeden et al. 1990).

Processes accounted for in the conceptual model include waste package degradation, waste form (UO_2) dissolution, equilibrium-controlled radionuclide sorption and precipitation/dissolution, radioactive decay and ingrowth in all phases (aqueous, adsorbed, precipitate), coupled heat and fluid flow, and radionuclide transport via advection and diffusion. Mechanical dispersion is conservatively neglected, because including it would result in earlier arrival of radionuclides at observation points, but lower peak concentrations than reported here (Mariner et al. 2017, Section 4.4.1).

6.3.3.2 *Numerical Implementation*

PA simulations shown here consist of one deterministic simulation for the grid with refined drifts and a repository loaded with 24-PWR and 37-PWR DPC waste packages.

The general layout of the model domain used for 2019 GDSA Shale Reference Case is shown in Figure 6-19. The half-symmetry model domain dimensions are 2265 m in width (*Y*) and 1200 m in height (*Z*) and 7155 m length (X). The domain is long enough to place an observation point 5000 m down-gradient of the repository (*X* direction). Two grids were generated using this domain. One has fine gridded repository drifts (Figures 6-20 to 6-22). The second is a coarse grid (Figure 6-23). The grids are mostly discretized into cells 15 m on a side. In the refined grid, emplacement 5m drift blocks are discretized into cells 1.67 m (5/3 m) on a side with the center cell representing a possible location for a waste package. Transitional zones from the 5/3 m cells are 5 m on the side. The refined grid contains 10,678,268 cells, of which approximately 4 million are

the smaller cells in and around the repository. In the coarse grid the repository drift is only discretized into 5 m blocks (Figure 6-23) and contains 6,877,604 cells, of which approximately 1 million are the smaller cells in and around the repository. The numerical grids and the grid refinement were generated using Cubit (Blacker et al. 2016, Version 15.3, 2018-09-20).

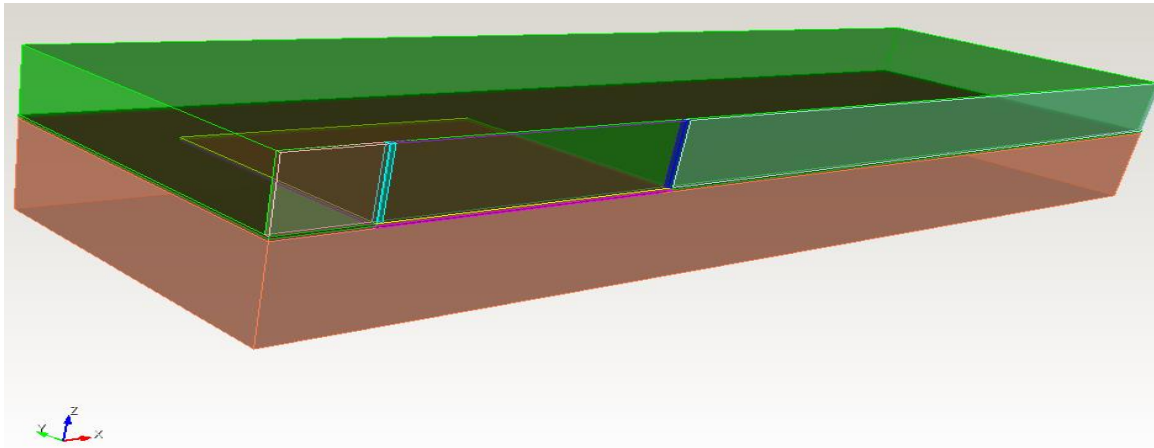Figure 6-19. General layout of the model domain for 2019 GDSA Shale Reference Case numerical grid.
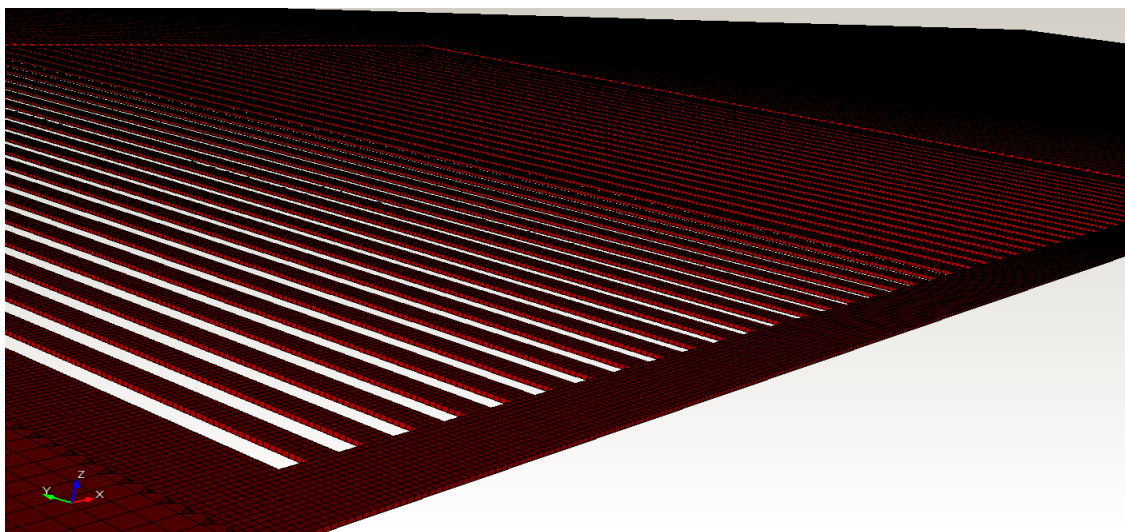

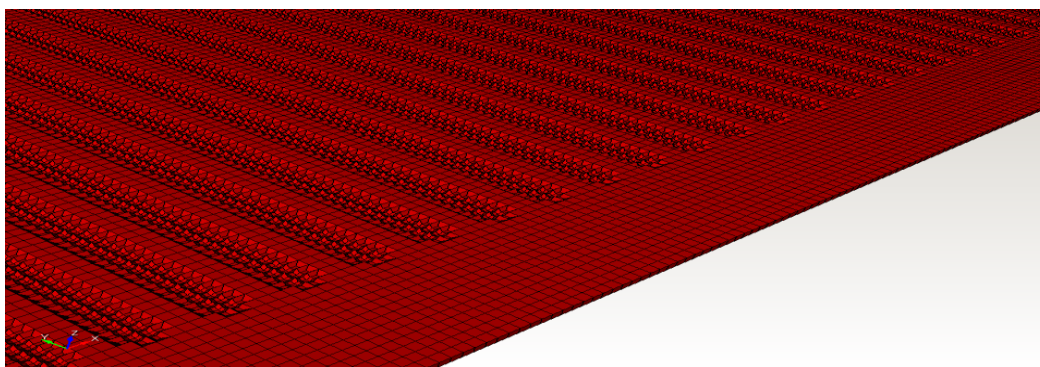Figure 6-20. Horizontal cross-section at the repository horizon.

Figure 6-21. Horizontal cross-section for the fine gridded repository horizon.
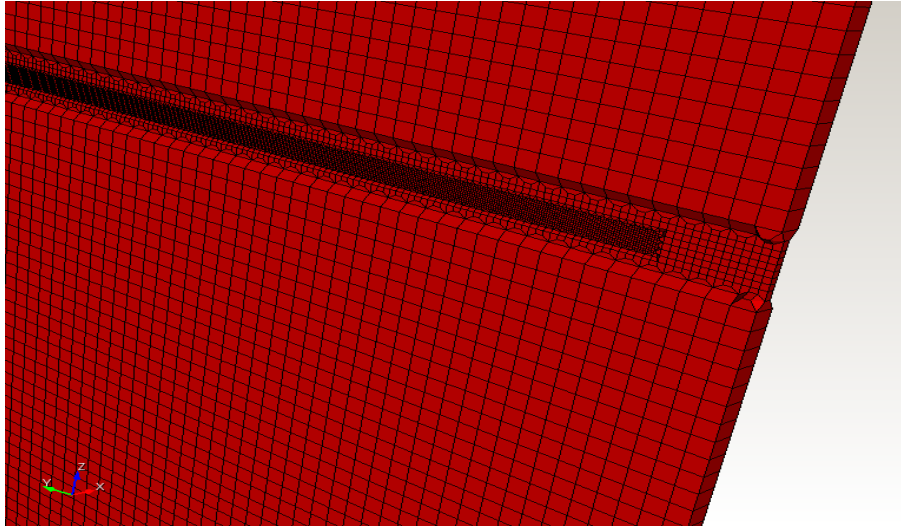
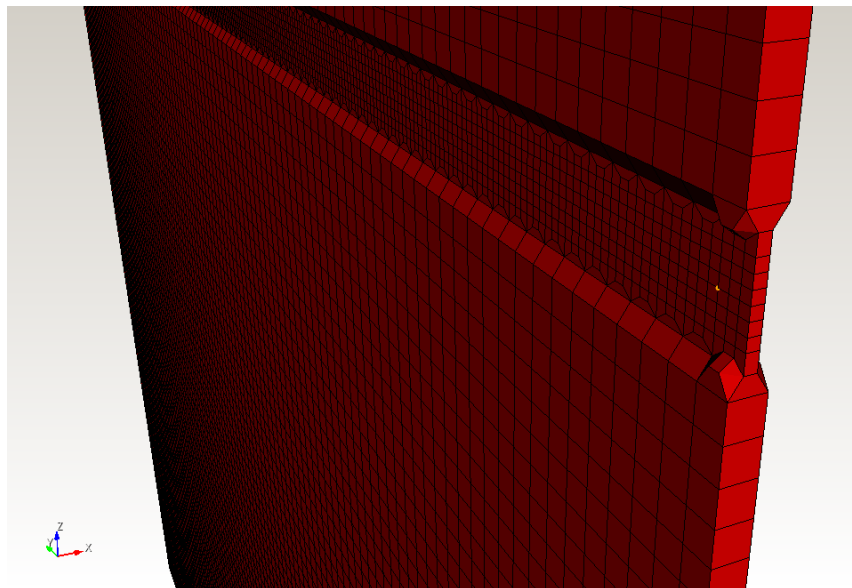Figure 6-22. Vertical cross-section for the fine gridded repository horizon.

Figure 6-23. Vertical cross-section for coarse grid repository horizon.

7 CONCLUSIONS AND RECOMMENDATIONS

The Spent Fuel and Waste Science and Technology (SFWST) Campaign of the U.S. Department of Energy Office of Nuclear Energy, Office of Spent Fuel and Waste Disposition (SFWD), has been conducting research and development on generic deep geologic disposal systems (i.e., geologic repositories). This report describes specific activities in fiscal year (FY) 2019 associated with FY19 Geologic Disposal Safety Assessment (GDSA) Repository Systems Analysis (RSA) work package within the SFWST Campaign. The overall objective of the GDSA RSA work package is to develop generic deep geologic repository concepts and system performance assessment (PA) models in several host-rock environments, and to simulate and analyze these generic repository concepts and models using the *GDSA Framework* toolkit, and other tools as needed. The specific objectives in FY2019 are to

- Develop and/or augment generic repository reference cases for three liquid-saturated host rock environments: crystalline (e.g., granite), argillaceous (e.g., typical shale or clay), and bedded salt host rocks; and a host rock environment in the unsaturated zone, such as alluvial valley fill.

- Ensure that reference cases include repository concepts and layouts for the disposal of DPC-canisterized pressurized water reactor (PWR) assemblies, including 37-PWR and 24-PWR waste packages, including the possible effects of criticality events on repository performance.

- Perform PA simulations (deterministic and probabilistic) with *GDSA Framework* for the foregoing reference case concepts and models. Analyze and plot the PA simulation results, including uncertainty and sensitivity analyses.

This report describes specific GDSA RSA accomplishments midway through FY 2019, with more comprehensive reference-case updates and PA simulation results to be reported at the end of the FY in a subsequent Level 3 milestone M3SF-19SN010304052, *GDSA Repository Systems Analysis FY19 Update*.

Improvements to the numerical solvers in PFLOTRAN, needed for modeling the high heat output from dual purpose canister (DPC) waste packages, particularly during two-phase flow, such as might occur in an unsaturated host-rock environment have been reported on in this report. The most significant of these involved refactoring of convergence criteria used during each iteration of the Newton-Raphson nonlinear solution search algorithm.

The major new piece of R&D initiated in this report is a technical basis and conceptual model for a reference-case repository located in unsaturated alluvial sediments, including initial simulations for a small-scale "sector" model (four disposal drifts each with four waste packages), as well as a "field-scale" repository model (27 drifts with 24 waste packages each). This model and associated simulations are a major update of the unsaturated zone alluvium reference case introduced preliminarily in Mariner et al. (2018), particularly related to the inclusion of DPC waste packages and their representative higher heat output per package, which results in more severe coupled process effects at early times after repository closure. Preliminary results indicate that even using a more coarsely discretized numerical grid with simplified two-phase flow parameters, computation time for flow and temperature in the field-scale simulation remains prohibitively long, perhaps due to numerical difficulties of the coupled thermal and fluid flow problem in unsaturated

rock. Several avenues will be explored during the remainder of the FY to investigate the long numerical simulation times:

- Have the development team assess whether any changes can be made to GENERAL mode to speed up simulations

- Divide the simulation workflow up into two separate <u>areal-cale</u> simulation models. In this concept:
    - The first model will be a finely gridded domain focusing on the smaller scale ("sector"), and will accurately capture heat, flow, and radionuclide transport near the waste packages.
    - The second model will have a relatively coarse and uniform mesh covering the full domain of interest for radionuclide transport. It will be used to assess transport in the subsurface but cannot accurately capture heat and fluid flow in and around the waste packages.

- Divide the simulation workflow up into two separate <u>time-scale</u> simulation models. In this concept the two modeling stages would be on the same mesh, the extent and discretization of which would be suitable for modeling both near repository heat and fluid flow and far field transport of radionuclides. In this concept:
    - The first model would run GENERAL flow mode to compute flow and temperature for the first several hundred years or until the waste packages are relatively cool.
    - The second model will restart at the end of the first and be used for radionuclide transport. After the waste packages are relatively cool it should be possible to simulate in RICHARDS mode without incurring much error. This will speed up the longer-term simulations enormously.

Also presented here is an update and adaptation of the bedded salt reference case documented in Sevougian et al. (2016) and other past bedded-salt reference-case simulations between 2012 and 2016, including some early simulation results for disposal of DPC waste packages. This update changes the repository design to accept 24- and 37-PWR DPC's, in a 50/50 split by weight of heavy metal for each canister size. This report details the preliminary simulations of a near-field repository model simulation that have been conducted in anticipation of a full-scale PA simulation that will be documented in a September 27, 2019 M3 deliverable (M3SF-19SN010304052).

An update to the generic shale reference case developed in Mariner et al. (2017) is also given here, with the introduction of a new Geologic Framework Model (GFM) for a representative shale environment. Construction of the GFM is the first step in developing a workflow that consists of constructing the GFM, exporting the relevant features of the GFM for meshing, and using the mesh for flow and transport modeling in PFLOTRAN. This discussion focuses on the mechanics of creating the GFM as the first step of the workflow. The shale GFM described here represents a relatively simple geologic environment of a horizontally layered sedimentary rock sequence consisting predominantly of shale formations interbedded with limestone and sandstone formations.

Another development presented here for the generic shale reference case is a set of near-field simulations with a highly discretized grid, as a precursor to coupling more detailed process models into *GDSA Framework*. The objective of this study is to investigate the near-field thermal-hydrologic behavior of pore fluids in a geologic repository located in a shale host rock. The focus

is on the impact of hydrogeological properties of the engineered buffer and disturbed rock zone (DRZ) on the near-field performance of a typical bentonite back-filled shale repository. Work will continue on this near-field model for the remainder of FY2019, with a goal of using this domain in a PA-GDSA model (i.e., *GDSA Framework*) to represent near-field thermal-hydrologic-mechanical coupled process effects. Surrogate modeling will be used to couple a mechanical response to thermal loading by linking permeability and porosity with the pressure and temperature distribution in the near-field.

Finally, some very early considerations for a site-scale shale-host-rock reference case that includes DPC disposal are presented at the end of this report. This will be an update to the GDSA Shale Reference Case described in Section 4 of Mariner et. al. (2017). This work has only recently begun, so only a very preliminary update is provided here. The comprehensive report on the update will be reported in the September 27, 2019 Level 3 milestone for the FY19 GDSA Repository Systems Analysis work package (SF-18SN01030405), entitled *GDSA Repository Systems Analysis FY19 Update* (M3SF-19SN010304052). The main tasks that will be undertaken in FY2019 are:

(1) Inclusion of 24-PWR and 37-PWR DPC waste packages in the reference case simulations.

(2) An update to the stratigraphic model for a representative shale domain (Perry et al. 2014; Perry and Kelley, 2017)—see Section 6.1.

(3) An update to the numerical model grids and formation properties to incorporate changes to stratigraphy and repository design needed for DPC waste.

This report fulfills the FY19 GDSA Repository Systems Analysis work package (SF-18SN01030405) Level 2 milestone *GDSA Repository Systems Analysis Progress Report* (M2SF-19SN010304051).

8 REFERENCES

Abdelkader, A., Bajaj, C.L., Ebeida, M.S., Mahmoud, A.H., Mitchell, S.A., Rushdi, A.A., & Owens, J.D. 2018. Sampling Conditions for Conforming Voronoi Meshing by the VoroCrust Algorithm. *LIPIcs : Leibniz international proceedings in informatics*, *99*, 10.4230/LIPIcs.SoCG.2018.1. doi:10.4230/LIPIcs.SoCG.2018.1

Blacker, T., S.J. Owen, M.L. Staten, R.W. Quador, B. Hanks, B. Clark, R.J. Meyers, C. Ernst, K. Merkley, R. Morris, C. McBride, C. Stimpson, M. Plooster, and S. Showman, 2016. *CUBIT Geometry and Mesh Generation Toolkit 15.2 User Documentation*, SAND2016-1649R, Sandia National Laboratories, Albuquerque, New Mexico.

Blackwell, D.D., M.C. Richards, Z.S. Frone, J.F. Batir, M.A. Williams, A.A. Ruzo, and R.K. Dingwall, 2011. "SMU Geothermal Laboratory Heat Flow Map of the Conterminous United States, 2011," Supported by Google.org. Available at http://www.smu.edu/geothermal Retrieved October 25, 2016.

Bourg, I.C., 2015. "Sealing Shales versus Brittle Shales: A Sharp Threshold in the Material Properties and Energy Technology Uses of Fine-Grained Sedimentary Rocks." *Environmental Science & Technology Letters, 2*(10), 255-259. doi: 10.1021/acs.estlett.5b00233

Bredehoeft, J.D., C.E. Neuzil, and P.C.D. Milly, 1983. *Regional Flow in the Dakota Aquifer: A Study of the Role of Confining Layers*. Water-Supply Paper 2237. United States Geological Survey, Alexandria, Virginia.

BSC, 2004, Heat Capacity Analysis Report: ANL-NBS-GS-000013 Rev 01, 100 p.

Carter, J.T., A.J. Luptak, J. Gastelum, C. Stockman, and A. Miller, 2013. *Fuel Cycle Potential Waste Inventory for Disposition*. FCRD-USED-2010-000031 Rev 6. Savannah River National Laboratory, Aiken, South Carolina.

Carter, J.T., Rodwell, P.O, Robinson, B., and B. Kehrman, 2012. *Defense Waste Salt Repository Study*, FCRD-UFD-2012-000113, May 5, 2012.

Clayton, D., G. Freeze, T. Hadgu, E. Hardin, J. Lee, J. Prouty, R. Rogers, W.M. Nutt, J. Birkholzer, H.H. Liu, L. Zheng, and S. Chu 2011. *Generic Disposal System Modeling – Fiscal Year 2011 Progress Report*. FCRD-USED-2011-000184, SAND2011-5828P. U.S. Department of Energy, Office of Nuclear Energy, Used Fuel Disposition Campaign, Washington, DC.

Clayton, D.J., J.G. Arguello Jr., E.L. Hardin, F.D. Hansen, and J.E. Bean 2012. "Thermal-Mechanical Modeling of a Generic High-Level Waste Salt Repository." In: SALTVII, 7th Conference on the Mechanical Behavior of Salt, Paris, France. April 16-19, 2012. (www.saltmech7.com), SAND2012-2741C.

Cochran, J.R, and 16 others, 2001. Compliance assessment document for the transuranic wastes in the greater confinement disposal boreholes at the Nevada Test Site, v. 2: Sandia National Laboratories, Albuquerque, New Mexico, SAND2001-2977, 811 p.

Croff, A.G. 1983. "ORIGEN2: A Versatile Computer Code for Calculating the Nuclide Compositions and Characteristics of Nuclear Materials," *Nuclear Technology*, 62(3), 335-352. doi: dx.doi.org/10.13182/NT83-1

DOE, 2009. *Waste Isolation Pilot Plant Compliance Recertification Application.* DOE 2009-24-34. March 2009.

DOE (U.S. Department of Energy) 2010. *Program and Project Management for the Acquisition of Capital Assets*, DOE O 413.3B, 11-29-2010, U.S. Department of Energy, Washington, D.C. 20585, available at https://www.directives.doe.gov/directives-documents/400-series/0413.3-BOrder-b

DOE (U.S. Department of Energy) 2012. Used Fuel Disposition Campaign Disposal Research and *Development Roadmap.* FCR&D-USED-2011-000065, REV 1, U.S. DOE Office of Nuclear Energy, Used Fuel Disposition, Washington, D.C., September 2012.

DOE (U.S. Department of Energy) 2014. Compliance Recertification Application 2014 for the Waste Isolation Pilot Plant: Appendix HYDRO-2014 Hydrological Investigations, DOE/WIPP-14–3503. Carlsbad, NM: US Department of Energy, Carlsbad Field Office. Available at http://www.wipp.energy.gov/library/cra/CRA-2014.html

Downey, J.S. and G.A. Dinwiddie, 1988. *The Regional Aquifer System Underlying the Northern Great Plains in Parts of Montana, North Dakota, South Dakota, and Wyoming - Summary*. Professional Paper 1402-A. United States Geological Survey, Washington, DC.

Drefke, C., Stegner, J., Dietrich, J., and I. Sass, 2015, Influence of the hydraulic properties of unconsolidated rocks and backfill materials on the change of the thermophysical characteristics by heat transfer: Proceedings of the World Geothermal Conference, Melbourne, Australia, 19-25 April 2015, 8 p.

Driscoll, D.G., Carter, J.M., Williamson, J.E., and Putnam, L.D., 2002. Hydrology of the Black Hills area, South Dakota: U.S. Geological Survey Water-Resources Investigations Report 02-4094, 150 p.

Estrella, R., S. Tyler, J. Chapman, and M. Miller, 1993. "Area 5 Site Characterization Project - Report of Hydraulic Property Analysis Through August 1993." *Water Resources Center Publication #45121*, Desert Research Institute, DOE/NV/10845-41.

Fahrenbach, M.D., Steece, F.V., Sawyer, J.F., McCormick, K.A., McGillivray, G.L., Schulz, L.D., and Redden, J.A., 2010, South Dakota Stratigraphic Correlation Chart: Oil and Gas Investigation 3, South Dakota Geological Survey.

Forster, A. and D. Merriam, 1997. "Heat Flow in the Cretaceous of Northwestern Kansas andImplications for Regional Hydrology." *Current Research in Earth Sciences*, 1997(Bulletin 240, part 1.).

Fox B., 2008. *Parameter Summary Report for CRA-2009, Revision 0*, WIPP:1.2.5:PA:QA-L:547488, Sandia National Laboratories, Carlsbad, New Mexico.

Fox, J.E., McCormick, K.A. and T.N. Hagger, 2009. Cross-Sections showing Geophysical Logs of Phanerozoic Rocks in South Dakota, South Dakota Department of Natural Resources Geological Survey, Oil and Gas Investigation 2, Structural Cross Sections D, E, F, G.

Freeze, G., P. Gardner, P. Vaughn, S.D. Sevougian, P. Mariner, V. Mousseau and G. Hammond, 2013a. *Enhancements to Generic Disposal System Modeling Capabilities.* FCRD-UFD-2014-000062. SAND2013-10532P. Sandia National Laboratories, Albuquerque, New Mexico.

Freeze, G., M. Voegele, P. Vaughn, J. Prouty, W.M. Nutt, E. Hardin and S.D. Sevougian, 2013b. *Generic Deep Geologic Disposal Safety Case.* FCRD-UFD-2012-000146 Rev. 1, SAND2013-0974P, August 2013, Sandia National Laboratories, Albuquerque, New Mexico.

Freeze, R.A. and J.A. Cherry 1979. *Groundwater*. Englewood Cliffs, New Jersey: Prentice Hall.

Gonzales, S. and K.S. Johnson, 1985. Shales and Other Argillaceous Strata in the United States. ORNL/Sub/84-64794/1. Oak Ridge National Laboratory, Oak Ridge, Tennessee.

Greene, E.A., 1993. Hydraulic Properties of the Madison Aquifer System in the Western Rapid City Area, South Dakota. *U.S. Geological Survey Water-Resources Investigations Report 93-4008*, 65 p.

Greene, S.R., Medford, J.S. and S.A. Macy, 2013. Storage and Transport Cask Data for Used Commercial Nuclear Fuel – 2013 U.S. Edition. ATI-TR-13047. Knoxville, Tennessee: Advanced Technology Insights, LLC; Oak Ridge, Tennessee: EnergX.

Gupta, S.C., Kang, D.H., and A. Ranaivosoon 2009, Hydraulic and mechanical properties of recycled materials: Final report to the Minnesota Department of Transportation, 219 p.

Hadgu, T., D. Clayton, and E. Hardin 2015. *Cavern/Vault Disposal Concepts and Thermal Calculations for Direct Disposal of 37-PWR Size DPCs*, FCRD-UFD-2015-000715, U.S. Department of Energy, Office of Used Nuclear Fuel Disposition, Washington, DC, February 2015.

Hammond, G.E., Lichtner, P.C. and R.T. Mills 2014. "Evaluating the performance of parallel subsurface simulators: An illustrative example with PFLOTRAN." *Water Resources Research*, 50(1), 208-228. doi: 10.1002/2012wr013483

Hansen F.D., S.J. Bauer, S.T. Broome, and G.D. Callahan 2012. *Coupled Thermal-Hydrological-Mechanical Processes in Salt: Hot Granular Salt Consolidation, Constitutive Model and Micromechanics,* FCRD-USED-2012-000422, U.S. Department of Energy, Office of Nuclear Energy, Office of Used Nuclear Fuel Disposition, Washington, DC. SAND2012-9893P, Albuquerque, New Mexico: Sandia National Laboratories. November 15, 2012.

Hansen, F.D. and C.D. Leigh 2011. *Salt Disposal of Heat-Generating Nuclear Waste*, SAND2011-0161, Sandia National Laboratories, Albuquerque, New Mexico.

Hansen, F.D., Hardin, E.L., Rechard, R.P., Freeze, G.A., Sassani, D.C., Brady, P.V. Stone, C.M., Martinez, M.J., Holland, J.F., Dewers, T., Gaither, K.N., Sobolik, S.R. and R. T. Cygan 2010. Shale Disposal of U. S. High-Level Radioactive Waste. SAND2010-2843. Sandia National Laboratories, Albuquerque, New Mexico.

Hansen, F.D., Hardin, E.L., Rechard, R.P., Freeze, G.A., Sassani, D.C., Brady, P.V., Stone, M., Martinez, M.J., Holland, J.F., Dewers, T., Gaither, K.N., Sobolik, S.R. and R.T. Cygan 2010. Shale Disposal of U.S. High-Level Radioactive Waste. Sandia National Laboratories report SAND2010-2843, 148 p.

Hardin, E. and E. Kalinina 2016. Cost Estimation Inputs for Spent Nuclear Fuel Geologic Disposal Concepts. SAND2016-0235. Sandia National Laboratories, Albuquerque, New Mexico.

Hardin, E. and M. Voegele 2013. *Alternative Concepts for Disposal of Dual-Purpose Canisters*. FCRD-USED-2013-000102, Rev.0. U.S. Department of Energy, Used Fuel Disposition R&D Campaign.

Hardin, E., Clayton, D., Howard, R., Scaglione, J.M., Pierce, E., Banerjee, K., Voegele, M.D., Greenberg, H., Wen, J., Buscheck, T.A., Carter, J.T., Severynse, T., and W.M. Nutt 2013. Preliminary Report on Dual-Purpose Canister Disposal Alternatives (FY13), August 2013, FCRD-UFD-2013-000171 Rev. 0.

Hardin, E., Hadgu, T., Clayton, D., Howard, R., Greenberg, H., Blink, J., Sharma, M., Sutton, M., Carter, J., Dupont, M. and P. Rodwell 2012. Repository Reference Disposal Concepts and Thermal Load Management Analysis. FCRD-UFD-2012-000219 Rev. 2, U.S. Department of Energy, Office of Used Nuclear Fuel Disposition, Washington, DC.

Hocking, C.M. 2013. Elevation Contour Map of the Inyan Kara Group: Butte, Meade, and Lawrence Counties, South Dakota, prepared by RESPEC, Rapid City, South Dakota, for Belle Fourche River Watershed Partnership, Belle Fourche, South Dakota.

Hjerpe, T. and R. Broed 2010. Radionuclide Transport and Dose Assessment Modelling in Biosphere Assessment 2009. Posiva Oy, Working Report 2010-79.

Hu, Q.H., Zavarin, M. and T.P. Rose 2008, Effect of reducing groundwater on the retardation of redox-sensitive radionuclides: Geochemical Transactions, v. 9, np. 12, 1-24.

IAEA (International Atomic Energy Agency) 2012. *The Safety Case and Safety Assessment for the Disposal of Radioactive Waste*, Specific Safety Guide, IAEA Safety Standards Series No. SSG-23, International Atomic Energy Agency, Vienna, 2012.

Isaacson, E. and H.B. Keller 2012. *Analysis of numerical methods*. Courier Corporation.

James S. and J. Stein 2002. *Analysis Plan for the Development of a Simplified Shaft Seal Model for the WIPP Performance Assessment*, AP-094 Rev. 0, December 11, 2002, Sandia National Laboratories, Carlsbad, New Mexico.

Jobmann, M. and G. Buntebarth 2009. "Influence of graphite and quartz addition on the thermo-physical properties of bentonite for sealing heat-generating radioactive waste." *Applied Clay Science*, 44(3-4), 206-210. doi: 10.1016/j.clay.2009.01.016

Johnson, L., Ferry, C., Poinssot, C. and P. Lovera 2005. "Spent Fuel Radionuclide Source-Term Model for Assessing Spent Fueld Perforamce in Geological Disposal. Part 1: Assessment of the Instant Release Fraction," *Journal of Nuclear Materials*, 346, pp. 56-65

Jones, B.F. 1982, Mineralogy of fine grained alluvium from borehole U11G, Expl. 1, northern Frenchman Flat area, Nevada Test Site: U.S. Geological Survey Open File Report 82-765, 13 p.

Jove-Colon, C. F., P. F. Weck, D. C. Sassani, L. Zheng, J. Rutqvist, C. I. Steefel, K. Kim, S. Nakagawa, J. Houseworth, J. Birkholzer, F. A. Caporuscio, M. Cheshire, M. S. Rearick, M. K. McCarney, M. Zavarin, A. Benedicto-Cordoba, A. B. Kersting, M. Sutton, J. L. Jerden, K. E. Frey, J. M. Copple and W. L. Ebert 2014. *Evaluation of Used Fuel Disposition in Clay-Bearing Rock*, FCRD-UFD-2014-000056, SAND2014-18303 R. Sandia National Laboratories, Albuquerque, New Mexico.

Judge, A. 2013, Measurement of the hydraulic conductivity of gravels using a laboratory permeameter and silty sands using field testing with observation wells: University of Massachusetts, Amherst [Ph. D. dissertation], 109 p.

Kilroy, K.C. 1992. Aquifer storage characteristics of Paleozoic carbonate rocks in southeastern Nevada estimated from harmonic analysis of water-level fluctuations: University of Nevada at Reno, PhD Dissertation, 84 p.

Konikow, L.F. and C.E. Neuzil 2007. "A method to estimate groundwater depletion from confining layers". *Water Resources Research*, 43(7). doi: 10.1029/2006wr005597

Kwicklis, E.M., Wolfsberg, A.V., Stauffer, P.H., Walvoord, M.A. and M.J. Sully 2006, Multiphase, multicomponent parameter estimation for liquid and vapor fluxes in deep arid systems using hydrologic data and natural environmental tracers: *Vadose Zone Journal*, v. 5, p. 934-950.

Langenheim, V.E. 2000, Constraints on the structure of Crater Flat, southwest Nevada, derived gravity and magnetic data, *in*, Whitney, J.W. and Keefer, W.R., Geologic and Geophysical Characterization Studies of Yucca Mountain, Nevada, a potential high-level radioactive-waste repository: U.S. Geological Survey Data Series 58, 11 p.

Li, Y.H. and S. Gregory 1974. "Diffusion of ions in sea-water and in deep-sea sediments," *Geochimica et Cosmochimica Acta*, **38**(5):703-714.

Lide, D.R., ed. 1999. CRC Handbook of Chemistry and Physics, CRC Press, Boca Raton, Florida.

Mariner, P.E., Gardner, W.P., Hammond, G.E., Sevougian, S.D. and E.R. Stein 2015. *Application of Generic Disposal System Models*. SAND2015-10037R; FCRD-UFD-2015-000126. Sandia National Laboratories, Albuquerque, New Mexico.

Mariner, P.E., Stein, E.R., Frederick, J.M., S. D. Sevougian, G. E. Hammond, and D. G. Fascitelli 2016. *Advances in Geologic Disposal System Modeling and Application to Crystalline Rock*, FCRD-UFD-2016-000440, SAND2016-96107R. Sandia National Laboratories, Albuquerque, NM, September 22, 2016.

Mariner, P. E., E. R. Stein, Frederick, J.M., Sevougian, S.D. and G. E. Hammond 2017. *Advances in Geologic Disposal System Modeling and Shale Reference Cases,* SFWD-SFWST-2017-000044 SAND2017-10304 R, Sandia National Laboratories, Albuquerque, New Mexico.

Mariner, P.E., Stein, E.R., Sevougian, S.D., Cunningham, L.J., Frederick, J.M., Hammond, G.E., Lowry, T.S., Jordan, S. and E. Basurto 2018. *Advances in Geologic Disposal Safety Assessment and an Unsaturated Alluvium Reference Case*, SFWD-SFWST-2018-000509, SAND2018-11858R, 130 p.

Martin, J.E., Sawyer, J.F., Fahrenbach, M.D., Tomhave, D.W. and L.D. Schulz 2004, Geologic Map of South Dakota: South Dakota Geological Survey. GIS data downloaded from https://mrdata.usgs.gov/geology/state/state.php?state=SD

Matteo et al. 2019. Evaluation of Engineered Barrier System Mid-Year Status Report, M2SF-19SN010308042, U.S. Department of Energy, Spent Fuel and Waste Science and Technology Campaign, Office of Used Nuclear Fuel Disposition, Washington, DC, June 30, 2019.

McCormick, K.A. 2010. Elevation Contour Map of the Precambrian Surface of South Dakota. South Dakota Geological Survey. Available online at http://www.sdgs.usd.edu/publications/index.html.

Neuzil, C.E. 1993. Low fluid pressure within the Pierre Shale: A transient response to erosion, *Water Resources. Research*, 29 (7), 2007–2020.

Neuzil, C.E. 1986. Groundwater Flow in Low-Permeability Environments. *Water Resources Research*, 22 (8), 1163-1195.

Neuzil, C.E. 1994. How permeable are clays and shales? *Water Resources Research*, 30(2), 145-150.

Nopola, J. R. 2013. Preliminary Evaluation of the Pierre Shale as a Nuclear Waste Repository. (Master of Science), South Dakota School of Mines and Technology, Rapid City, South Dakota, 115 p.

Perry, F.V., R.E. Kelley, P.F. Dobson and J.E. Houseworth 2014. *Regional Geology: A GIS Database for Alternative Host Rocks and Potential Siting Guidelines*. LA-UR-14-20368, FCRD-UFD-2014-000068. Los Alamos National Laboratory, Los Alamos, New Mexico.

Perry, F.V. and R.E. Kelley 2017. *Regional Geologic Evaluations for Disposal of HLW and SNF: The Pierre Shale of the Northern Great Plains*. SFWD-SFWST-2017-000119. U.S. Department of Energy, Spent Fuel and Waste Technology. Los Alamos Unlimited Release LA-UR-17-27829. 31 p.

Peters, E. J. 2012. *Advanced Petrophysics: Volume 1: Geology, Porosity, Absolute Permeability, Heterogeneity and Geostatistics*. Live Oak Book Co., Austin, Texas.

Price, L.L., Alsaed, A.A., Brady, P.V., Gross, M.B., Hardon, E.L., Nole, M., Prouty, J.L., Banerjee, K., and G.G. Davidson 2019, *Postclosure Criticality Consequence Analysis - Scoping Phase*, SAND2019- , 65 p.

Sassani, D.C., Jové Colón, C.F., Weck, P., Jerden, J.L., Frey, K.E., Cruse, T., Ebert, W.L., Buck, E.C., Wittman, R.S., Skomurski, F.N., Cantrell, K.J., McNamara, B.K. and C.Z. Soderquist 2012. Integration of EBS Models with Generic Disposal System Models (FCRD-UFD-2012-000277), U.S. Department of Energy: Washington DC.

Sassani, D.C., Jang, J.-H., Mariner, P., Price, L., Rechard, R.P., Rigali, M., Rogers, R., Stein, E.R., Walkow, W. and P.F. Weck 2016. *The On-line Waste Library (OWL): Usage and Inventory Status Report*. SAND2016-9485 R; FCRD-UFD-2016-000080. Sandia National Laboratories, Albuquerque, New Mexico.

Sevougian, S.D., Freeze, G.A., Gross, M.B., Lee, J., Leigh, C.D., Mariner, P., MacKinnon, R.J. and P. Vaughn 2012. *TSPA Model Development and Sensitivity Analysis of Processes Affecting Performance of a Salt Repository for Disposal of Heat-Generating Nuclear Waste*. FCRD-UFD-2012-000320 Rev. 0, U.S. Department of Energy, Office of Used Nuclear Fuel Disposition, Washington, DC.

Sevougian, S.D., Freeze, G.A., Vaughn, P., Mariner, P. and W.P. Gardner 2013. *Update to the Salt R&D Reference Case*. FCRD-UFD-2013-000368, SAND2013-8255P. Sandia National Laboratories, Albuquerque, New Mexico.

Sevougian, S.D., Freeze, G.A., Gardner, W.P., Hammond, G.E. and P. Mariner 2014. *Performance Assessment Modeling and Sensitivity Analyses of Generic Disposal System Concepts*. FCRD-UFD-2014-000320, SAND2014-17658. Sandia National Laboratories, Albuquerque, New Mexico, September 12, 2014.

Sevougian, S.D., Stein, E.R., Gross, M.B., Hammond, G.E., Frederick, J.M. and P.E. Mariner 2016. *Status of Progress Made Toward Safety Analysis and Technical Site Evaluations for DOE Managed HLW and SNF,* SAND2016-11232 R; FCRD-UFD-2016-000082, Rev. 1. Sandia National Laboratories, Albuquerque, New Mexico.

Sevougian, S.D., Mariner, P.E., Connolly, L.A., MacKinnon, R.J., Rogers, R.D., Dobson, D.C. and J. L. Prouty 2019. *DOE SFWST Campaign R&D Roadmap Update*, M2SF-19SN010304042, U.S. Department of Energy, Spent Fuel and Waste Science and Technology Campaign, Office of Used Nuclear Fuel Disposition, Washington, DC, April 30, 2019.

Shelton, S.M. 1934. "Thermal conductivity of some irons and steels over the temperature range 100 to 500 C," *Bureau of Standards Journal of Research, 12*(4/6), 441-450.

Shurr, G.W. 1977. The Pierre Shale, Northern Great Plains: A Potential Isolation Medium for Radioactive Waste. Open-File Report 77-776. *United States Geological Survey*, Reston, Virginia.

Smyth, J.R., Crowe, B.M., Halleck, P.M. and A.W. Reed 1979. A preliminary evaluation of the radioactive waste isolation potential of the alluvium-filled valleys of the great basin. Informal Report LA-7962-MS, Los Alamos National Laboratory.

Thomas, J.M., Welch, A.H. and M.D. Dettinger 1996. Geochemistry of isotope hydrology of representative aquifers in the Great Basin region of Nevada, Utah, and adjacent states: U.S. Geological Survey Professional Paper 1409-C, 110 p.

Thorne, M., Walker, R. and D. Roberts 2016. Downscaling of Climate Modelling Results for Application to Potential Sites for a Geological Disposal Facility. Quintessa and AMEC Report to RWM, AMEC/200041/002; QRS-1667A-2.

Tyler, S.W., Kranz, S., Parlange, M.B., Albertson, J., Katul, C.G., Cochran, G.F., Lyles, B.A., and G. Holder 1997. Estimation of groundwater evaporation and salt flux from Owens Lake, California, USA: *Journal of Hydrology*, v. 200, p. 110-135.

van der Leeden, F., Troise, F.L. and D. K. Todd 1990. *The Water Encyclopedia*. Chelsea, Michigan, Lewis Publishers.

van Genuchten, M.T. 1982. "A comparison of numerical solutions of the one-dimensional unsaturated-saturated flow and mass transport equations." *Advances in Water Resources*, **5**(1), 47-55. doi: 10.1016/0309-1708(82)90028-8

van Loon, L.R. and J. Mibus 2015. "A modified version of Archie's law to estimate effective diffusion coefficients of radionuclides in argillaceous rocks and its application in safety analysis studies." *Applied Geochemistry*, **59**, 85-94. doi: 10.1016/j.apgeochem.2015.04.002

Vaughn, P., Sevougian, S.D., Hardin, E.L., Mariner, P. and M.B. Gross 2013. "Reference Case for Generic Disposal of HLW and SNF in Salt," in *Proceedings of the 2013 International High-Level Radioactive Waste Management Conference*, Albuquerque, NM, April 28 – May 2, 2013, American Nuclear Society, La Grange Park, Illinois. (www.ans.org)

Villar, M.V. 2004. "Thermo-Hydro-Mechanical Characteristics and Processes in the Clay Barrier of a High Level Radioactive Waste Repository." *State of Art Report. Infomes Tecnicos Ciemat*, pp. 75.

Villar, M.V. and A. Lloret 2001. "Variation of the intrinsic permeability of expansive clays upon saturation." In: Adachi, K & M. Fukue (eds.) *Clay Science for Engineering*. Balkema, Rotterdam. 259-266.

Wagner, W., Cooper, J.R., Dittmann, A., Kijima, J., Kretzschmar, H.J., Kruse, A., ... and O. Sifner 2000. The IAPWS industrial formulation 1997 for the thermodynamic properties of water and steam. *Journal of Engineering jor Gas Turbines and Power*, *122*(1), 150-184.

Wang, Y., E. Matteo, J. Rutqvist, J. Davis, L. Zheng, J. Houseworth, J. Birkholzer, T. Dittrich, C. W. Gable, S. Karra, N. Makedonska, S. Chu, D. Harp, S. L. Painter, P. Reimus, F. V. Perry, P. Zhao, J. B. Begg, M. Zavarin, S. J. Tumey, Z. R. Dai, A. B. Kersting, J. Jerden, K. E. Frey, J. M. Copple and W. Ebert (2014). *Used Fuel Disposal in Crystalline Rocks: Status and FY14 Progress*, FCRD-UFD-2014-000060, SAND2014-17992R. Sandia National Laboratories, Albuquerque, New Mexico.Wang, Y. and J.H. Lee 2010. *Generic Disposal System Environment Modeling - Fiscal Year 2010 Progress Report*. SAND2010-8202P. Sandia National Laboratories, Albuquerque, New Mexico.

Weast, R. C. and M. J. Astle, Eds. (1981). *CRC Handbook of Chemistry and Physics*. Boca Raton, Florida, CRC Press, Inc.

Wilson, T. P. and D. T. Long 1993. "Geochemistry and isotope chemistry of Michigan Basin brines: Devonian formations," *Applied Geochemistry,* Vol. 8, pp. 81-100.